The machining process of Zircaloy-4 nuclear fuel rod end-caps

PJ Steyn

Orcid.org/0000-0001-9239-6898

Dissertation accepted in partial fulfilment of the requirements for the degree *Master of Engineering in Nuclear Engineering* at the North-West University

Supervisor: Prof J Markgraaff

Co-Supervisor: Mr DG Zimolong

Graduation: June 2021

Student number: 22840036

Private Bag X1290, Potchefstroom
South Africa 2520

North-West University Engineering Research
Ethics Committee (NWU-ENG-REC)

Tel: 018 299-2645
Email: ENG-REC@nwu.ac.za

8/28/2019

ETHICS APPROVAL LETTER OF STUDY

Based on approval by the North-West University Engineering Research Ethics Committee (NWU-ENG-REC) on 2019, the NWU-ENG-REC hereby approves your study as indicated below. This implies that the NWU-ENG-REC grants its permission that, provided the general and specific conditions specified below are met and pending any other authorisation that may be necessary, the study may be initiated, using the ethics number below.

Study title:
Economic feasibility of a high precision, high volume nuclear fuel component production facility

Principal Investigator/Study Supervisor/Researcher: AC Cilliers

Student: Petrus Jacobus Steyn (PETRUS.STEYN1@ICLOUD.COM)
Ethics number: NWU-00278-19-A1
Institution-Study Number-Year-Status

Status: S = Submission; R = Re-Submission; P = Provisional Authorisation; A = Authorisation

Application Type: Single
Approval date: 2019
Expiry date: 8/23/2020

Risk: Low

Approval of the study is provided for a year, after which continuation of the study is dependent on receipt and review of annual monitoring report and the concomitant issuing of a letter of continuation.

General conditions:

While this ethics approval is subject to all declarations, undertakings and agreements incorporated and signed in the application form, the following general terms and conditions will apply:

- *The principal investigator/study supervisor/researcher must report in the prescribed format to the NWU-ENG-REC:*
  - *Annually on the monitoring of the study, whereby a letter of continuation will be provided annually, and upon completion of the study; and*
  - *without any delay in case of any adverse event or incident (or any matter that interrupts sound ethical principles) during the course of the study.*
- *The approval applies strictly to the proposal as stipulated in the application form. Should any amendments to the proposal be deemed necessary during the course of the study, the principal investigator/study supervisor/researcher must apply for approval of these amendments at the NWU-ENG-REC, prior to implementation. Should there be any deviations from the study proposal without the necessary approval of such amendments, the ethics approval is immediately and automatically forfeited.*
- *Annually a number of studies may be randomly selected for active monitoring.*
- *The date of approval indicates the first date that the study may be started.*
- *In the interest of ethical responsibility, the NWU-ENG-REC reserves the right to:*

22840036:The_machining_of_Zircaloy-4_Nuclear_Fuel_Rod_Endcaps_PS_Vers6.docx

ORIGINALITY REPORT

7%	5%	3%	2%
SIMILARITY INDEX	INTERNET SOURCES	PUBLICATIONS	STUDENT PAPERS

MATCH ALL SOURCES (ONLY SELECTED SOURCE PRINTED)

1%

★ archive.org

Internet Source

Exclude quotes	On	Exclude matches	Off
Exclude bibliography	On		

ABSTRACT

Zirconium alloy 4 (Zry-4) is one of the most used materials inside a water-cooled reactor's fuel assembly (Schemel, 1977). The reasons for the extensive use of this material inside the fuel assembly, are its high corrosion resistance at elevated temperatures of 340 °C, and its low thermal neutron absorption cross-section (Schemel, 1977). One of the largest numbers of components manufactured from this material is endcaps, which are welded to the fuel rods to secure the UO_2 inside the Zry-4 tubes.

Zry-4 is a very ductile material which makes it great for forming using manufacturing procedures such as extrusion and rolling, but the challenge comes in when the material is machined using methods such as single point cutting procedures (turning) at high speeds. A side-effect of high speed-machining of ductile materials is galling. If tight dimensional tolerances are required, this issue can result in parts not meeting specifications. Furthermore, an added challenge of Zry-4 is that it has a high probability to ignite during machining if special care is not taken with the chips. Thus, it is especially important to have a predetermined and controlled machining setup combined with the correct inline measurement procedures, as well as a good final batch release procedure to ensure that the components satisfy the strict nuclear plant specifications for nuclear fuel assemblies.

The aim of this study was

- to review applicable cutting-tool principles and rotational machinability of ductile materials, with special reference to Zry-4, with the view
- to find and apply the best possible cutting parameters to machine Zry-4 nuclear fuel rod endcaps in high volume production to circumvent galling, and
- to measure the resulting dimensions and calculate the ensuing tolerances verified by using standard and numerical methods.

Machining parameters that were investigated in this study, were the rotational speed, the cutting depth, the feed rate, and the cutting insert design. The machining was done, making use of different shaped ceramic tool inserts, such as the ISCAR PENTA TiAlN+TiN coated inserts, VCMT shaped TiCN+Al_2O_3+TiN coated inserts and VCGT shaped uncoated inserts. During consecutive machining procedures, using the VCGT inserts, the rotational speed, and feed rate was set at 1000 rpm and 0,25 mm/rev, respectively, with a cutting depth of 0,80 mm for the roughing cut. For the finishing cut, the cutting depth was set at 0,03 mm with a rotational speed of 2500 rpm and a feed rate of 0,09 mm/rev.

Dimensional tolerances of machined endcaps were evaluated using conventional measuring techniques, such as micrometre dimensional measuring and profiling. The results obtained from this measurement procedure were compared with the measurements obtained from using the state-of-the-art DEA GLOBAL CMM, Zeiss Duramax, and the Zeiss O-Inspect coordinate measuring

systems. These machines use a probe to measure the components either by line scanning or point scanning.

After measuring all the components using the equipment available for this study it was found that the components could be machined with a 35% success rate. However, it is possible to increase this capability when measuring machines such as the multi-sensor CMM is being used, as these machines do have a higher repeatability rate than that of the conventional methods used in this study, with an added benefit of reduced cycle time.

Acknowledgements

Hereby I would like to thank the following people and entities to make the Master's in Nuclear Engineering a possibility:

- The Department of Science and Innovation (DSI), through their Advance Metals Initiative (AMI) for the opportunity to do this study at the Nuclear Energy Corporation of South Africa (Necsa).
- Dr Johan T. Nel
- Dr Anthonie Cilliers
- Mr Dieter G. Zimolong for all the technical support, the support to find sponsors and all the knowledge that he shared with me to make the project a success.
- The Technology Localisation Implementation Unit (TLIU) for funding the project.
- The Institute of Advance Tooling at the Tshwane University of Technology (TUT) at Soshanguve South Campus.
    - Mr Jefferey Makhubela for helping to coordinate this project in collaboration with TLIU
    - Mr Siviwe Mruasi
    - Mrs Ntaoleng Tshabalala and Mrs Rabelani Nveholoro
- Mr Michael Barnard at ISCAR Tooling South Africa, thank you very much for all the support in terms of cutting parameters and all the tools you sponsored towards the project.
- Mr Manuel da Silva and Mr Arthur van Jaarsveld of Carl Zeiss, thank you for supporting us in the measurements of the components using state-of-the-art equipment.
- Mr Oelof Kruger and Mr Poloko Kuduntwane of the National Metrology Institute of South Africa (NMISA)
- Necsa's personnel
- Mr Ian Pretorius at Necsa's Metrology Lab
- Mr Charl Botha from Necsa
- Mr Sylvester Mudaly, my manager at Johnson Matthey South Africa, thank you for your support and for giving me the relevant times off, which helped me in the completion of my Master's.
- Prof. Johan Markgraaff, for helping me finalize my Master's and allowing me to complete and submit it.
- My parents for allowing me to study, the support to succeed in my studies and the motivational speeches during the cause of my Master's. Even though it might not have seemed that I appreciate it at times, it always helped - especially when I lost momentum.
- My sister for all her support during my studies.
- My wife, Esta Steyn, thank you for all your support, kindness, patience, and help you gave me in the last two years of this study.

TABLE OF CONTENTS

List of Figures

List of Tables

List of Abbreviations

Abbreviation	Definition
°C	Degree Celcius
Al-6005-T6	Aluminium
AQL	Acceptance Quality Level
ASTM	American Society for Testing and Materials
BEC	Bottom Endcap
BRA	Back Rake Angle
BUE	Built-up Edge
BWR	Boiling Water Reactor
CANDU	Canadian Deuterium Uranium
CNC	Computer numerical controls
d	Depth of cut
ECEA	End Cutting Edge Angle
ERA	End Relief Angle
f	Feed rate
HPC	High-Pressure Cooling
IAT	The Institute for Advanced Tooling
mm	Millimetres
mm/rev	Millimetres per revolution
MTCVD	Medium temperature chemical vapour deposition
N	Rotational/Specific speed
Nb	Niobium
Necsa	The South African Nuclear Energy Corporation
NR	Nose Radius
PCD	Polycrystalline diamond
PVD	Physical Vapor Deposition
PWR	Pressurised Water Reactor
QC	Quality Control
RA	Side Rake Angle
rpm	Revolutions per minute
SCEA	Side Cutting Edge Angle
SEM	Scanning Electron Microscope
SRA	Side Rake Angle
SS316	Stainless Steel 316
TEC	Top Endcap
TLIU	The Technology Localisation Implementation Unit
TUT	The Tshwane University of Technology
UO2	Uranium Oxide
Zr	Zirconium
Zry-2	Zirconium alloy 2
Zry-4	Zirconium alloy 4

1. INTRODUCTION

1.1. BACKGROUND

Zirconium alloy 4 (Zircalloy-4 and used herein abbreviated form, Zry-4) is one of the most commonly used materials in fuel assemblies for commercial nuclear power reactors, such as Pressurised Water Reactors (PWR), due to its high corrosion resistance at elevated coolant temperatures (up to 340 °C) and its low thermal neutron absorption cross-section (Schemel, 1977). A PWR fuel assembly is illustrated in Figure 1-1(a). These assemblies are constructed of various sub-assemblies enclosing fuel rods consisting of Zircaloy tubes (Figure 1-1b) that contain uranium oxide (UO_2) fuel pellets. The fuel rods are capped by Zry-4 endcaps (Figure 1-2) and are affixed by using high-pressure laser welding to the Zircaloy tubes to keep the UO_2 pellets secured within the fuel rods.

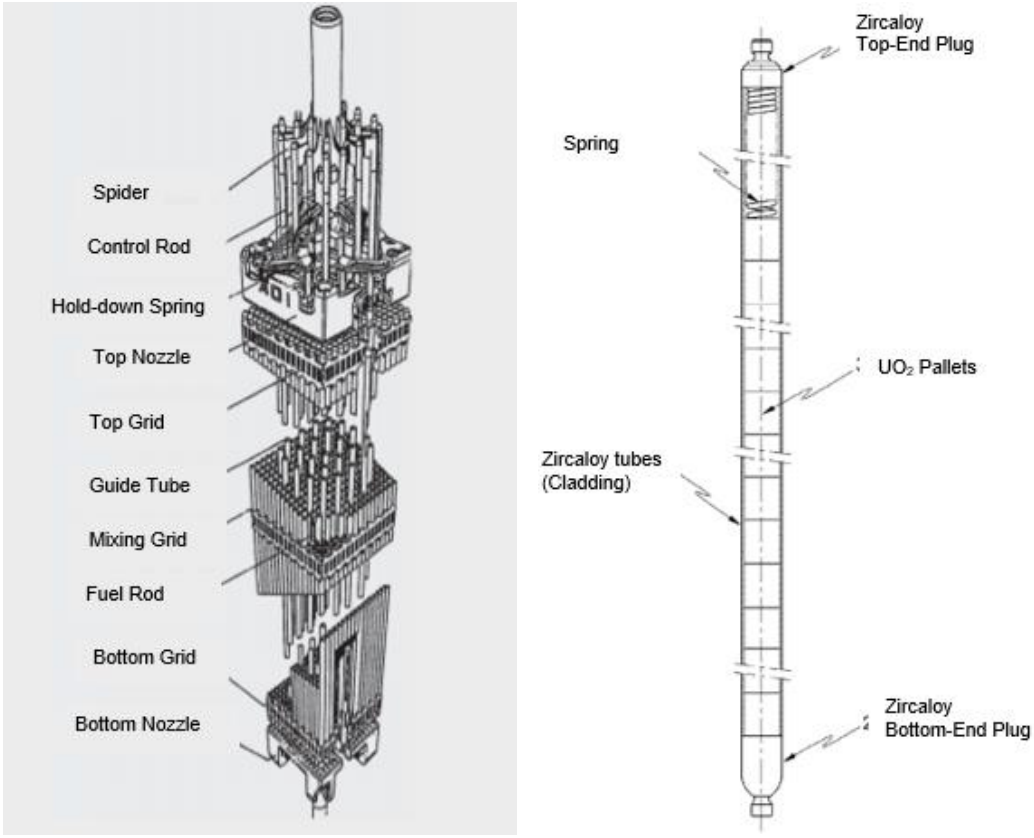

(a) (b)

Figure 1-1 – (a) Schematic view of PWR Fuel Assembly, modified after Parisot & France (2009a) and (b) Schematic view of a PWR fuel rod assembly, modified after Lee et al. (2009)

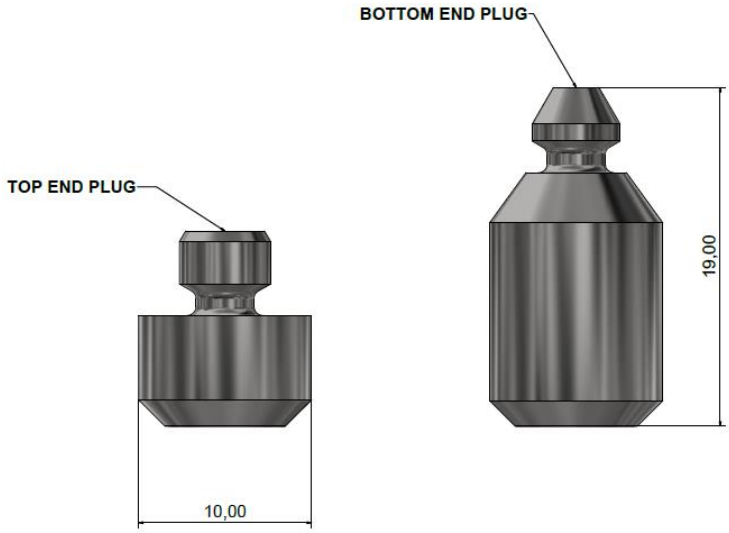

Figure 1-2 – Side view models of two nuclear fuel rod endcaps, illustrated in Figure 1-1. Dimensions are in mm.

The endcaps are generally manufactured using conventional cutting procedures such as turning. This procedure is largely dependent on the machinability of the material, as a cutting tool is used to cut into the material to obtain the desired shapes and sizes required by the customer. The endcap specifications require tolerances ranging from ±0,025mm to a diameter of approximately 10,00mm. These tight tolerances are generally easily achieved when doing high-speed machining using materials with good machinability, but it becomes more challenging when machining ductile materials, such as Zry-4 (Reid, 2011, and personal communication with D.G. Zimolong, Necsa).

Ductile materials tend to gall when they are being machined, resulting in dimensions different from the required set machining dimensions (Podgornik & Jerina, 2012). Galling happens gradually as the work material build-up increases during repeated cutting cycles on the cutting tool (Podgornik & Jerina, 2012). Galling has a direct impact on the quality of the part, especially on the surface quality and integrity. As the wear of the cutting tool continues, the dimensional size of the components is increasingly affected.

The effect of wear can be monitored by using dimensional inspection methods to evaluate whether the component satisfies the client's dimensional specifications presented on the component drawing. Quality control (QC) systems, such as statistical process control and final batch release, must also be implemented to ensure that the batch meets the client’s batch specification, for example, a 95/95 release specification. This batch specification is calculated using Acceptable Quality Levels (AQL) that are set and used by the client to evaluate whether the batch complies with the batch standards linked to the high-quality standards for nuclear fuel fabrication processes.

1.2. PROBLEM STATEMENT AND AIM

As mentioned above, the machining of a ductile material, such as Zry-4, is not easy as the material tends to gall, and work-harden during the machining process. These properties affect the quality of the component in terms of attaining dimensional tolerances that are necessary for nuclear fuel assemblies and required by strict nuclear plant specifications and quality control.

The aim of this study was.

- to review applicable cutting-tool principles and rotational machinability of ductile materials, with special reference to Zry-4, with the view
- to find and apply the best possible cutting parameters to machine Zry-4 nuclear fuel rod endcaps in high volume production to circumvent galling, and
- to measure the resulting dimensions and calculate the ensuing tolerances verified by using standard and numerical methods.

2. LITERATURE STUDY

2.1. INTRODUCTION

Zry-4 mainly consisting of zirconium (Zr) is a shiny greyish white refractory metal that has excellent corrosion resistance combined with good mechanical properties and can be manufactured using standard fabrication techniques (Reid, 2014). Zr is commonly used as the base metal for some components in nuclear reactors (as mentioned in Section 1.1), it is generally alloyed into one of the following three alloys Zry-2, Zry-4 or Zr-2.5Nb (Muntean & Inţă, 2013). There are also two Zr-based non-nuclear grade metals commonly used in the chemical process plants, ASTM R60702 (Zr 702) which is unalloyed metal with a maximum hafnium content of 4.5% and ASTM R60705 (Zr 705) which is alloyed with 2.0% to 3.0% niobium.

Zry-2 is predominantly used in Boiling Water Reactors (BWR) and as the calandria tubing in Canadian Deuterium Uranium (CANDU) reactors.

Zry-4 is a very expensive nuclear grade alloy, used in most of the Generation 3 reactors currently under operation (Schemel, 1977). It has a high corrosion resistance at elevated coolant temperatures (up to 340 °C), a low thermal neutron absorption cross-section and good mechanical properties (Reid, 2014; Schemel, 1977). It also has a similar chemical composition as Zry-2, except for the nickel that was removed and the amount of iron that was increased to ensure a lower amount of hydrogen uptake in certain reactor conditions, as presented in Table 2-1. It is commonly used as fuel cladding in PWR and CANDU reactors. The homogeneous refinement of the ingot helps with tighter control of the alloy elements as specified by the American Society for Testing and Materials (ASTM). Eighty per cent of fuel fabrication material costs go into Zry-4 as it is used in various forms such as endcaps, fuel tubes, grid assemblies, control rod guide thimble tubes and the instrumentation tube. The oxidation kinetics of zirconium alloys is one of the prominent reasons for the use of Zry-4 in PWR fuel. Another advantage of using Zry-4 as a cladding material in a nuclear reactor is its low oxidation transition thickness of approximately 1,7 µm, whereas other zirconium alloys have an oxidation transition thickness of approximately 3,1 µm (Parisot & France, 2009).

Zr-2.5Nb is a binary alloy with Nb to increase the material strength and is generally used for the pressure tubes in the CANDU reactors, as presented in Table 2-1.

One of the long-term advantages of using Zr as a base metal for nuclear components is that it is good for long-term nuclear waste disposal, as Zr has excellent radiation stability and is 100% compatible with existing Zircaloy fuel cladding, easing any concerns of galvanic corrosion.

Table 2-1 – Composition of Zr-base alloys used in nuclear reactor fuel rods (Weight %) (Reid, 2014)

Name	Zry-2	Zry-4	Zr-2.5Nb
UNS Grade	R60802	R60804	R60904
Tin (Sn)	1.20 – 1.70	1.20 – 1.70	-
Iron (Fe)	0.07 – 0.20	0.18 – 0.24	-
Chromium (Cr)	0.05 – 0.15	0.07 – 0.13	-
Nickel (Ni)	0.03 – 0.08	-	-
Niobium (Nb)	-	-	2.40 – 2.80
Oxygen (O_2)	Per P.O.	Per P.O.	Per P.O.
Fe + Cr + Ni	0.18 – 0.38	-	-
Fe + Cr	-	0.28 – 0.37	-

There are a few challenges when it comes to the machining of Zr, as it is a very ductile material, which is good for forming processes, however, leads to galling when being machined using processes like single-point cutting and milling. However, there are a few special considerations to be kept in mind when machining Zr-alloys using cutting operations, such as the attainment of specified dimensions due to undercutting. Zr is also a highly oxidising material and it is subjected to spontaneous ignitions when it is exposed to high and uncontrolled temperatures, for instance during machining.

Machining is defined by Kalpakjian & Schmid (2006) as “a group of processes that consists of the removal of material and modification of the surfaces of a workpiece after it has been produced by various methods”.

Figure 2-1 divides the various machining processes into two main groups, namely traditional and non-traditional machining processes, however, the traditional machining processes can be divided further into subcategories as illustrated.

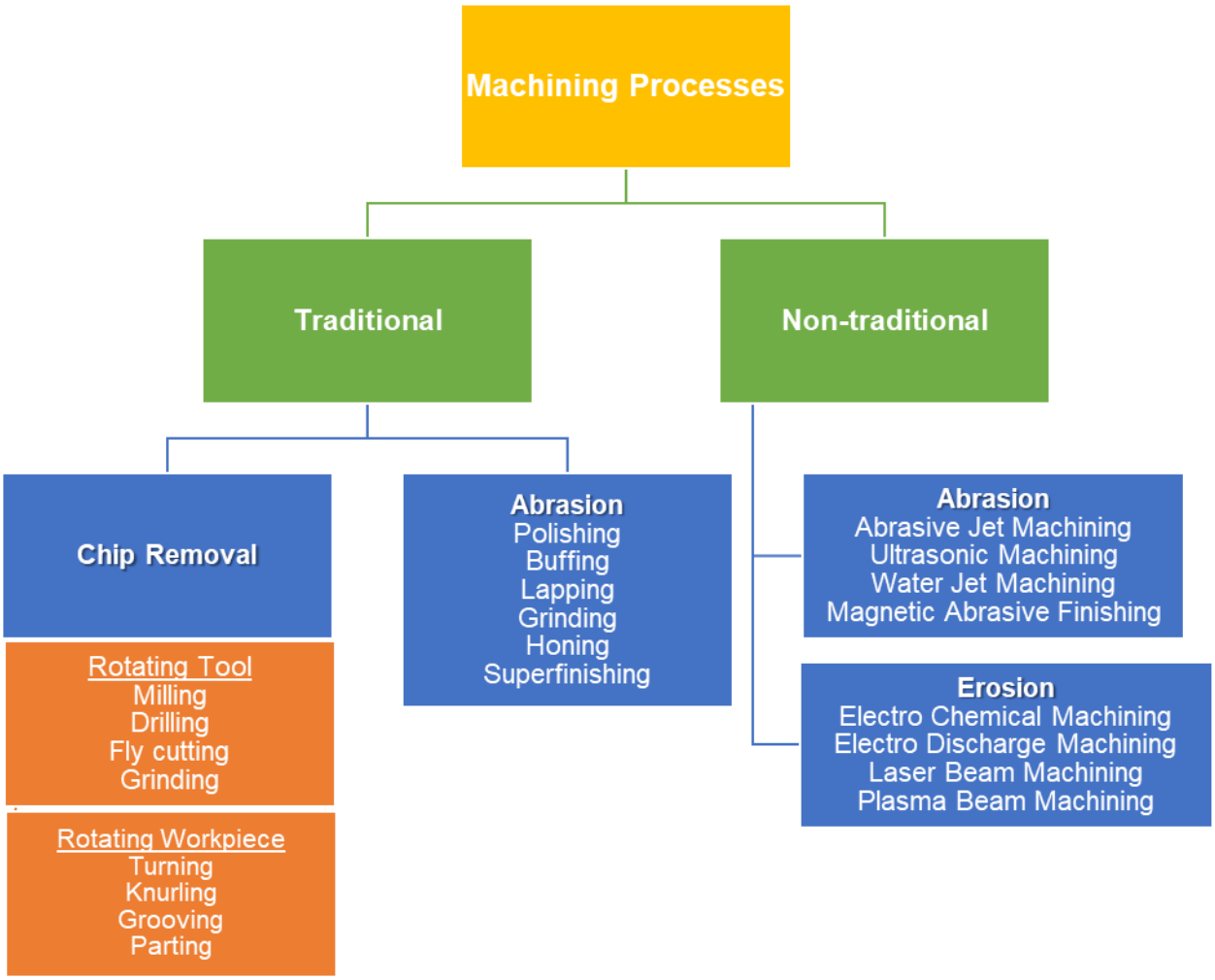

Figure 2-1 – Schematic of various machining processes that could be used to shape a workpiece material into the desired shape.

- **Chip Removal Processes** are processes that shape a piece of material into the desired form, by removing material from the surface of the material and produces chips as it machines the material (Kalpakjian & Schmid, 2006). Chip removal processes can be divided further into two categories, namely:
    - **Rotary tool chip removal processes** - when the workpiece is mounted in a fixed position on a working table and the cutting tool rotates, cutting the material on a specific plane as illustrated in Figure 2-2. These systems generally consist of more than one cutting edge, the face milling cutter, illustrated in Figure 2-3, is an example thereof.

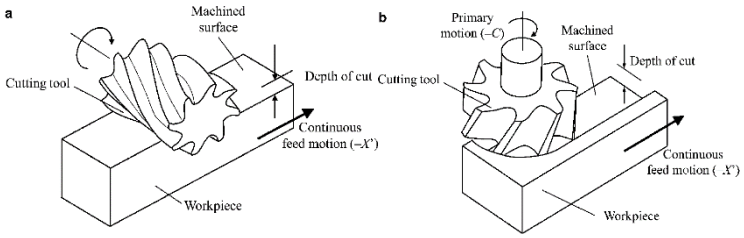

Figure 2-2 – Rotary tool chip removal processes. a) peripheral milling processes. b) face milling process.

Figure 2-3 –Model of a face milling cutting tool with 11 cutting edges.

- **Rotary workpiece chip removal processes** (or single-point cutting processes) - when the workpiece material is rotating, and the cutting tool is fed into the material to shape the material into the desired shape.

- **Abrasion Machining** uses small, hard particles with sharp edges and irregular shapes capable of removing small amounts of material from the surface of a workpiece, by producing tiny chips as it cuts the surface. The traditional process generally uses extremely hard materials such as aluminium oxide or silicon carbides in the form of tiny particles and particle-wheels or cutting blades, with water or other cutting fluids (Figure 2-4). Non-traditional abrasion machining processes use particles with various technologies to generally achieve better surface finishes and tolerances.

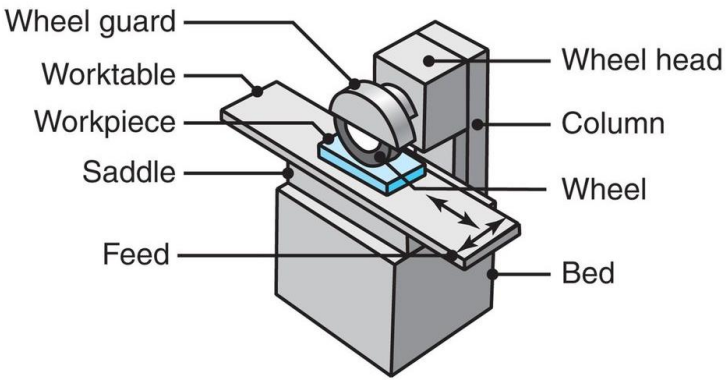

Figure 2-4 –Building blocks of a horizontal-spindle surface grinder (Kalpakjian & Schmid, 2006)

- **Erosion Machining** is a non-traditional machining process, generally used to cut shapes into sheet metals by breaking down the material, using one of the following: chemical reactions with the workpiece, electric erosive discharge on the surface of the workpiece, or laser cutting into the material.

The selection of the appropriate machining process, or more often the series of processes, depends on the shape of the part which needs to be produced, including the dimensional tolerance and surface texture requirements, as well as on numerous factors associated with the workpiece material and its manufacturing properties (Kalpakjian & Schmid, 2006). As mentioned in Section 1.1, a nuclear fuel assembly consists of various components, as illustrated in Figure 1-1, and each of these components is manufactured using a different machining process, for example, the bottom and top nozzle can be formed by using milling processes due to the shape of the components, whereas the endcaps are circular and can only be manufactured using a single-point cutting process.

2.2. SINGLE POINT CUTTING PRINCIPLES

The single point cutting process is generally used to produce straight, conical, curved, or grooved components, such as pins, shafts, spindles etc. (Kalpakjian & Schmid, 2006). The shape is achieved by clamping the workpiece material (Zry-4) to a chuck and rotating it at a specific speed (N). The cutting tool is feeding into the material with a horizontal/vertical movement at a specific feed rate (f) to remove a certain amount of material. The amount of material removed is defined as the depth of cut (d) It is the depth at which the cutting tool enters the cutting process, or stated differently, the difference between the initial diameter and the diameter after the cut, measured in mm per cut. This is usually less than 50% of the inscribed circle of the insert. These parameters are also known as the **cutting parameters** of the single point cutting process. The basic working setup of the single point cutting process is illustrated in Figure 2-5.

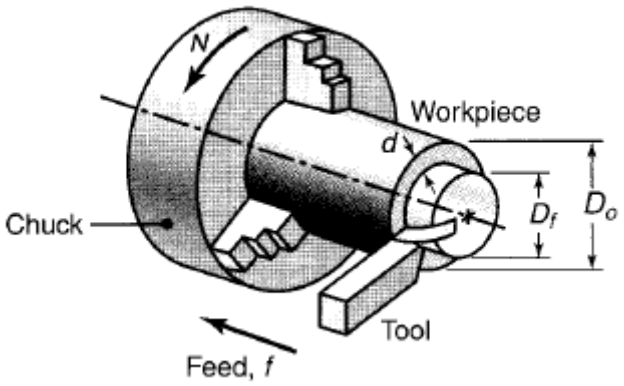

Figure 2-5 –Basic working setup of a single point cutting process – rotary workpiece chip removal (modified after Kalpakjian & Schmid, 2006)

The cutting tool used for the process, generally only has a single cutting edge. Hence the name single-point cutting. The cutting tool is the heart of the single point cutting process and there are three types of cutting tools that can be used for this cutting process, namely:

- Solid type cutting tools - Figure 2-6(a) - are the conventional cutting tools, normally constructed out of high-speed steels or carbon steel, shaped in one piece and ground into various geometries, depending on the angle needed for the material being machined. The one disadvantage of these tools is that once the cutting edges become dull, the tool needs to be removed from the lathe and it needs to be ground again, which is a time-consuming process when looking at a high-volume production facility.
- Brazed insert cutting tools - Figure 2-6(b) - are constructed of two different materials brazed together. The cutting portion of these tools are constructed from a good cutting tool material, whereas the shank part of the tool does not have any cutting ability, however, it is constructed of tough material. Tungsten carbide is generally used as the cutting material brazed to the shank.
- Mechanically clamped insert cutting tools - Figure 2-6 (c) - normally consist of a shank made of tough steel, and insert tips consisting of the various materials. The advantage of using a mechanically clamped insert cutting tool is that after a cutting edge is worn, another edge is available for the cutting process (Kalpakjian & Schmid, 2006). This makes the process more time- and cost-effective, whereas the solid type and brazed type tools must be removed from the turret to be reground.

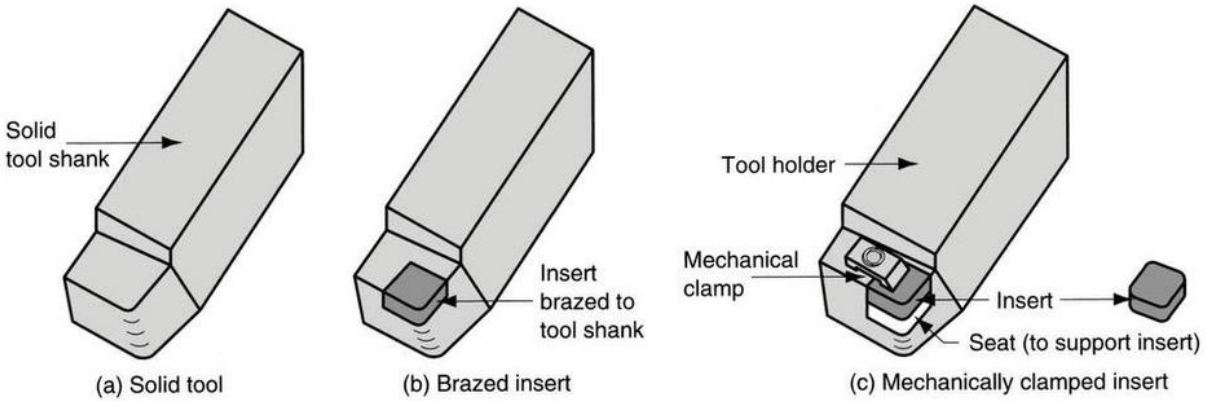

Figure 2-6 – Illustration showing a) a Solid Type b) a Brazed insert tool and c) a Mechanically clamped insert.

The most important features of the cutting tool are its **tool angles** and **tool material**. Furthermore, the cutting angles, especially the back-rake angle, influences the flow direction of the chips formed, as well as the resistance to tool wear and chipping. The following factors are influenced by changing the tool angles and material (Kalpakjian & Schmid, 2006):

- Type of chips produced.
- Force and energy dissipated during cutting.
- Rise in workpiece, tool, and chip temperatures
- Tool wear and failure
- Workpiece surface finish and integrity

Figure 2-7 is an illustration of the five major angle groups on a cutting tool, with additional elements on the cutting tool. Each of these angles has an important function in the machining operations and is measured in a coordinate system, consisting of the 3 major axes on the tool shank.

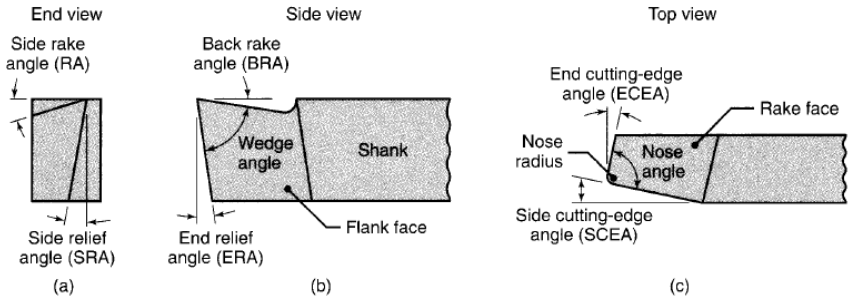

Figure 2-7 – An illustration of the elements a single-point cutting insert is constructed off (Kalpakjian & Schmid, 2006)

- **Back Rake Angle (BRA):** The rake angle controls the direction in which the chips flow and determines the strength of the cutting insert. A positive rake angle improves the cutting operation by reducing the cutting forces and temperatures, however, it can also result in a small, included angle, which can lead to premature tool chipping and failure.
- **Side Rake Angle (RA):** The RA is more important than the BRA, even though the latter usually controls the direction of chip flow. The RA usually ranges between -5° and 5° for metal cutting, using carbide inserts.
- **End – (ERA) and Side Relief Angles (SRA):** These angles control the interference and rubbing between the tool and the workpiece. If these angles are too big, the tooltip may chip off, and if these angles are too small, it may lead to excessive flank wear. The relief angles are typically 5°.
- **Side – (SCEA) and End Cutting Edge Angle (ECEA):** These angles influence the chip formation, tool strength and cutting forces to various degrees, and are typically around 15°.
- **Nose Radius (NR):** The NR influences the surface finish of the component and the tool-tip strength of an insert. If the NR is small, it can lead to rougher surface finishes and weaker tool-tip strength, and if the NR is too big, it may lead to tool chatter.

Another important element of a cutting tool is the chip breaker. This controls the chip disposal during a single-point cutting process (Groover, 2010). Long and continuous chips are undesirable because they tend to get tangled up between the part and the cutting tool during the single point cutting

process, and then it affects the quality of the final component (Kalpakjian & Schmid, 2006). A chip breaker is frequently installed on the cutting tool, forcing the chips to curl more tightly than they naturally would, leading to premature fractures in the curls (Groover, 2010). Figure 2-8 illustrates two methods by which a chip breaker is incorporated into the cutting tool:

- The groove type chip breaker - Figure 2-8 (a) - is designed into the tool itself (Groover, 2010). The groove is just after the cutting edge of the insert, and the groove radius is specifically formed for the type of workpiece material machined.
- The obstruction type chip breaker - Figure 2-8 (b) - is an extra device installed on the rake face of the tool, and the chip breaker distance can be adjusted for different cutting conditions. (Groover, 2010).

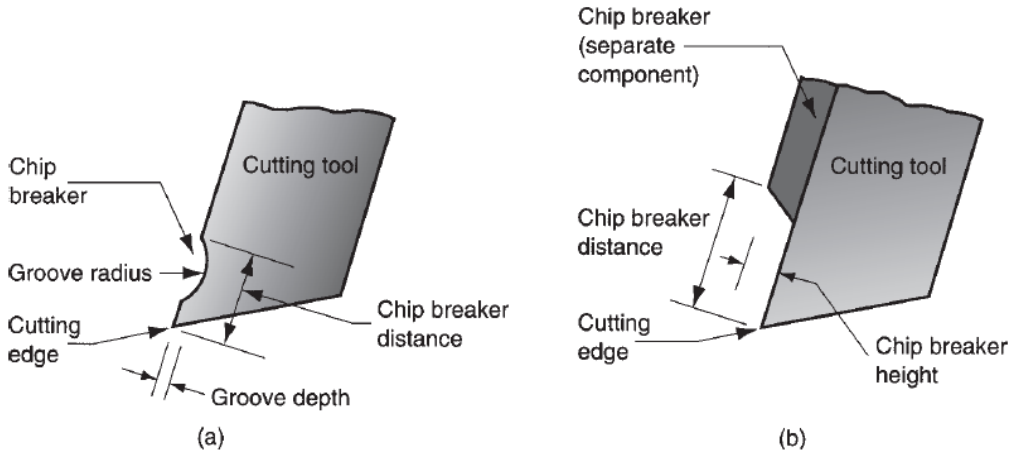

Figure 2-8 – Illustrations of Chip Break Designs for single-point cutting inserts – (a) groove-type and (b) obstruction-type (Groover, 2010)

There are three types of chips that can form during the cutting process:

- **Continuous chip formation** is when a chip never breaks during a single cut. This is normally a result of ductile workpiece material, a cutting speed that is too high, a small feed rate and cutting depth, a sharp cutting edge, or low tool-chip friction. A good surface finish is a result of continuous chip formation, however, it makes the disposal of chips more challenging, as it is difficult to handle long chips.
- **Built-up edge (BUE)** is when a layer of the workpiece material is deposited onto the cutting edge of a tooltip. BUE formation generally leads to poor surface finishes and integrity and it can be reduced by doing one or more of the following:
    - Increase cutting speed.
    - Decrease the depth of cut.
    - Increase the tool rake angle.
    - Use a sharp tool.
    - Apply an effective cutting fluid.
    - Use a cutting tool material that has a lower chemical attraction to the workpiece material.

- **Discontinuous chips** generally consist of chip segments that may be attached loosely or firmly to one another. These chips are desired for their ease of disposal. This creates fluctuations in the cutting forces that could affect the surface finish and lead to vibration and chatter. It is found that the ideal discontinuous chips are chips that form the entire letter C or the number 9 and fits inside a 25 mm square space (Kalpakjian & Schmid, 2006). Discontinuous chips are generally formed under these conditions:
    - Brittle workpiece material
    - Workpiece materials with hard inclusions and impurities
    - Extremely low or extremely high cutting speeds
    - Large depth of cut
    - Low rake angles
    - Lack of effective cutting fluid
    - Low stiffness of the tool holder or machining tool, allowing chatter to occur.

During the chipping process, the temperature of the cutting tool and workpiece can increase significantly when there is a high amount of friction at the cutting zone, due to non-ideal cutting parameters. It has a direct influence on the tool life, and it introduces crater wear on the cutting surface, affecting the dimensional accuracy of the workpiece. Furthermore, it can lead to thermal damage on the surface of the workpiece. The best way to manage the temperature rises at the cutting zone is by the application of cutting fluid. Cutting fluid is defined as any liquid or gas that can be applied directly at the cutting edge of a cutting tool when cutting material. This is used to improve cutting performance (Groover, 2010). The use of cutting fluids adds the following advantages to the single-point cutting process (Groover, 2010; Kalpakjian & Schmid, 2006):

- It removes chips from the cutting zone.
- It reduces the final component heat for easy handling after cutting.
- It reduces the friction at the cutting zone.
- It reduces the required cutting power.
- It improves dimensional stability.
- It improves the surface finish.
- It improves tool life.
- It protects the machined surface from environmental corrosion.

At the end of the process, the main purpose of all the single point cutting principles is to reduce the tool wear and to improve the machinability of the workpiece material. Tool wear is the process where the cutting tool starts losing dimension and sharpness during the cutting process, influencing the surface finish and integrity of the component, as well as the dimensional accuracy. It also increases the cutting temperature, cutting forces, and power required for the cutting process. Machinability

refers to the easiness to shape the workpiece material. It is usually defined in terms of the following factors:

- Surface finish and integrity of the machined part
- Tool life
- Required cutting force and power.
- The level of difficulty in chip control

This whole process is packaged into one machine called a lathe. Engine lathes (Figure 2-9) require skilled labour to machine components, but has a low production rate, as the operator cuts the component using the tool post. Automatic machines or turret lathe (Figure 2-10) generally uses a turret tool system, has a medium to high production rate and requires less skilled labour, as these machines use computer numerical controls (CNC) to cut the components (Groover, 2010).

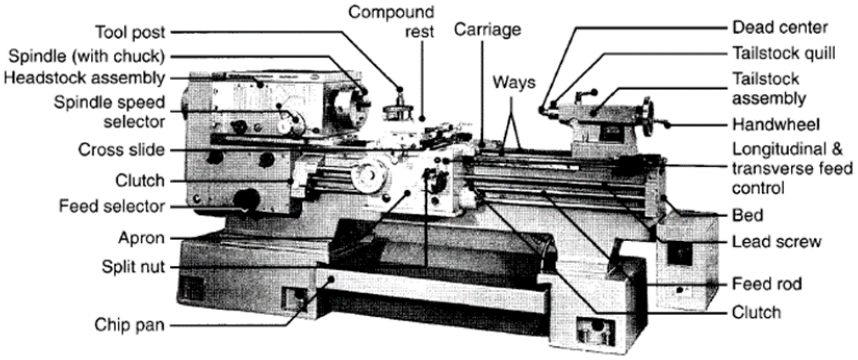

Figure 2-9 – Illustration of the typical setup of an engine lathe (Kalpakjian & Schmid, 2006)

Figure 2-10 – DMG Ecoline CTX 310 eco Turret Lathe

2.2.1. Cutting tool material & tool shapes

There are various insert shapes and sizes which can be used for single-point cutting, depending on the type of cutting operation needed - as illustrated in Figure 2-11. Various cutting operations can

be performed using only one cutting tool insert, depending on the shape and flow of the component. Looking at the nuclear fuel endcaps in question, it is noted that the endcaps can be machined using two types of inserts, namely a forming insert and a parting insert. The first four boxed operations as illustrated in Figure 2-11, straight turning - Figure 2-11(a) -, taper turning - Figure 2-11(b) -, turning and external grooving - Figure 2-11(d) - and facing - Figure 2-11(e) -, can normally be combined into one tool for the profile of the endcap, whereas the cutting off or parting operation - Figure 2-11(j) - of the endcap will need a separate tool. Each of these inserts will have its specified tool angles, chip-breaker design, insert design and insert material.

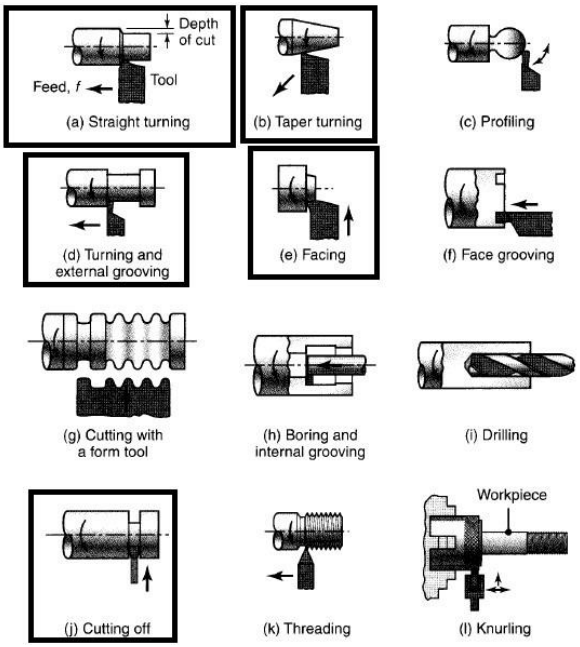

Figure 2-11 – Various cutting operations that could be performed using a lathe, modified after Kalpakjian & Schmid (2006)

Figure 2-12 illustrates the range of the common insert shapes that can be used for the cutting operation. The shapes shown in Figure 2-12, are as follows:

a. Round Insert
b. Square Insert
c. Rhombus Insert with two 80°-point angles.
d. Hexagonal Insert with three 80°-point angles
e. Triangular (Equilateral) Insert
f. Rhombus Insert with two 55°-point angles.
g. Rhombus Insert with two 35°-point angles.

The insert shape depends on the type of operation required and the cutting tool material. Besides, Figure 2-12 ranges the inserts by versatility from left to right and in strength from right to left. A round insert - Figure 2-12 (a) - is a lot stronger than a Rhombus insert with two 35°-point angles - Figure 2-12 (g) -, and is usually used for parting operations, whereas the Rhombus inserts are a lot

more versatile than the round insert, and used for operations such as straight turning - Figure 2-11(a) -, taper turning - Figure 2-11(b), - etc. A Rhombus insert - Figure 2-12 (g) - is usually honed, chamfered or produced with a negative land to improve the strength of the cutting edge and to prevent chipping (Kalpakjian & Schmid, 2006).

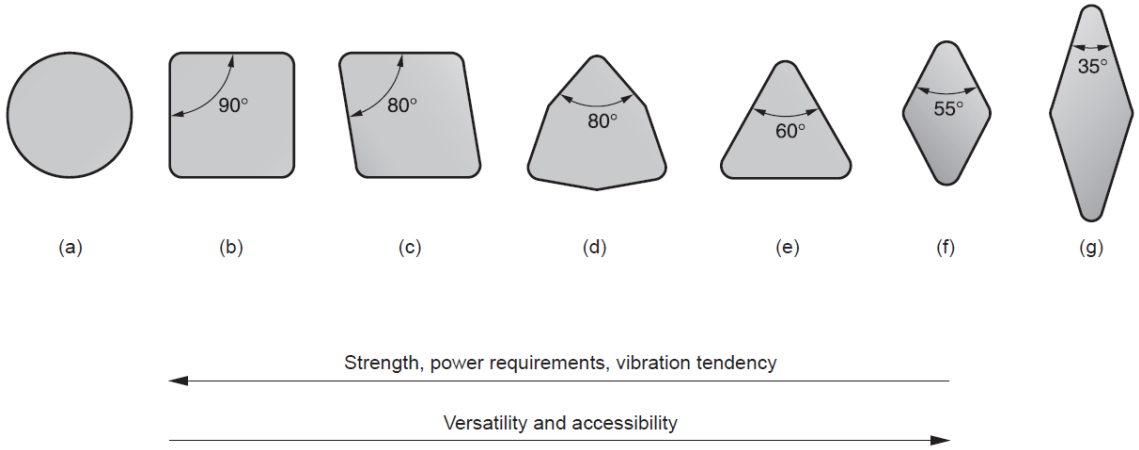

Figure 2-12 – Common Insert Shapes illustrating different rake angles used for single-point cutting processes (Groover, 2010)

Turning inserts are defined by their ANSI insert designation, which is a shorthand method that indicates an insert's shape and size as well as other important parameters (Shum & MachiningCloud Inc., 2016a).

Cutting insert material

The insert material selection is an essential part of the insert selection process, as it is directly dependent on the workpiece material and the cutting inserts shape requirements. Some workpiece materials are not compatible with certain insert materials and some insert materials cannot be shaped into certain forms. There are five main material groups from which tool inserts are made, namely:

- high-speed steel, carbon steel, and low alloy steels
- cast cobalt alloys.
- cemented carbides, cermet, and coated carbides
- ceramics and
- synthetic diamond and cubic boron nitride (Groover, 2010).

The cutting speeds and tool life can be increased by coating the insert with a protective layer (Shum & MachiningCloud Inc., 2016b). Cutting tools are commonly subjected to a) elevated temperatures, b) high contact stresses, and c) rubbing between cutting edge and workpieces surfaces (Kalpakjian & Schmid, 2006). The following properties are important when selecting insert material:

- Toughness
- Shock resistance

- Hot hardness
- Wear resistance
- Thermal shock resistance
- Chemical stability and inertness

The toughness of an insert is defined as the material's capability to absorb energy without failing and is usually characterised as a combination of the material strength and ductility (Groover, 2010). It is also a necessary property of the insert, to prevent fracture failure (Kalpakjian & Schmid, 2006). Mechanical shock resistance is the ability of the insert to withstand impact forces that are encountered during interrupted cutting operations, or forces due to vibration and chatter (Kalpakjian & Schmid, 2006).

Hot hardness is the material's ability to retain its hardness, strength and wear resistance at elevated temperatures (Groover, 2010; Kalpakjian & Schmid, 2006). This property ensures that the insert does not experience any plastic deformation, keeping its shape and sharpness when experiencing high temperatures during the cutting process (Kalpakjian & Schmid, 2006). Figure 2-13 is an illustration of the relationship between the hardness of the various insert materials and the cutting temperatures. From Figure 2-13 it is visible that an insert using a ceramic tip has a high hardness when exposed to high cutting temperatures, whereas an insert made of carbon tool steel loses it hardness very quickly as the cutting temperature increases.

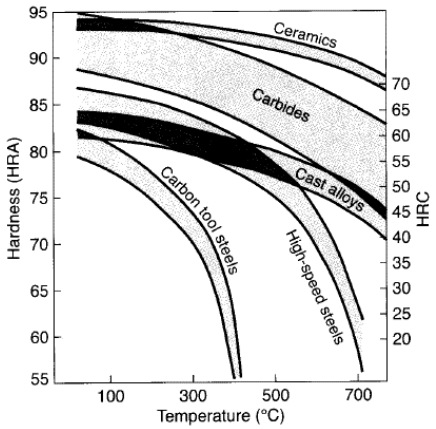

Figure 2-13 – Insert material hardness as a function of temperature (Kalpakjian & Schmid, 2006)

The insert material hardness is also the single most important property in the prevention of abrasive wear (Groover, 2010). The cutting tool's wear resistance depends on more than just the insert hardness. Other tool wear mechanisms that are influencing the life span of an insert, include the insert surface finish, the insert and workpiece chemical composition, and the use of coolant that could affect the wear resistance of an insert (Groover, 2010). In addition to the wear resistance of the insert material, Figure 2-14 illustrates the relationship between an insert material's strength and its wear resistance capability. For example, inserts made with a diamond or cubic boron nitride has a remarkably high wear resistance and hot hardness, meaning that it can be exposed to elevated

cutting temperatures without being subjected to tool wear, however, the insert's strength and toughness are very low, meaning that can break easily when not taken care off.

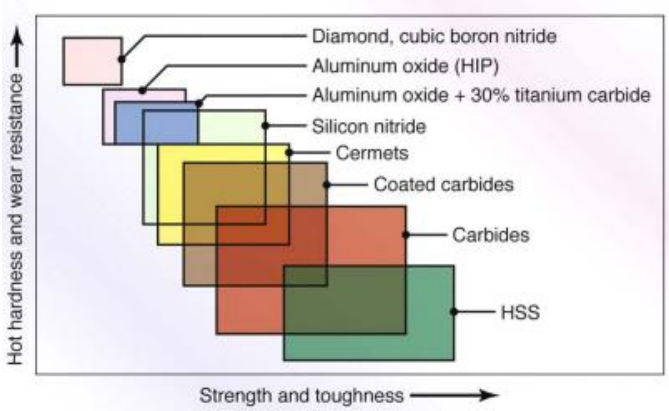

Figure 2-14 – Mechanical properties for various groups of insert materials (Kalpakjian & Schmid, 2006)

Thermal shock resistance is the material's ability to withstand rapid temperature changes when the cutting process is interrupted (Kalpakjian & Schmid, 2006). Chemical stability and inertness refer to any adverse reactions that can be experienced between the cutting insert material and the workpiece material, which could lead to adhesion or tool-chip diffusion between the insert and the workpiece. This contributes to rapid tool wear and must be avoided, or at least be minimised, during the cutting process (Kalpakjian & Schmid, 2006).

Figure 2-15 is an illustration of the range of the appropriate cutting speed and the feed rate associated with the specific type of insert material. The combination of Figure 2-14 and Figure 2-15 has a direct effect on the productivity of the machining process. For example, even though diamond inserts have high wear resistance and the capability to operate at high cutting speeds, the feed rate and strength and toughness associated with the tips are generally low, and the variety of shapes in which the diamond inserts are available is extremely limited.

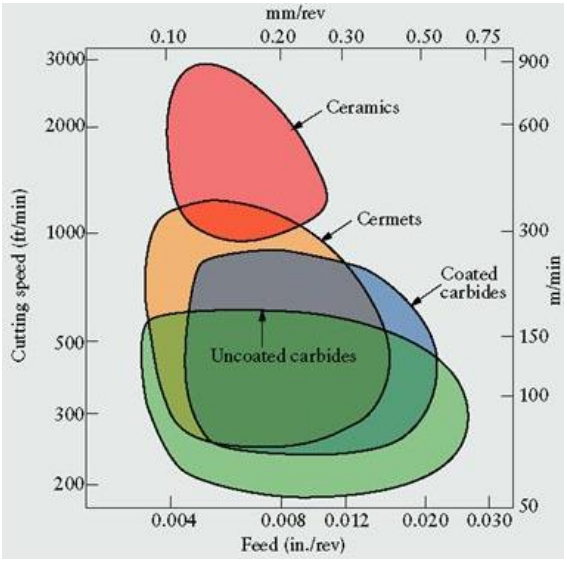

Figure 2-15 – The range of acceptable cutting speeds and feeds rates for various cutting insert materials (Kalpakjian & Schmid, 2006)

2.2.2. Cutting process lubrication

As mentioned at the beginning of this section, cutting fluids are a particularly important part of the cutting process as it is used to control the cutting temperature. It also improves the overall performance of the single point cutting process. Depending on the cutting operation, the cutting fluid required may be a coolant, a lubricant or both (Kalpakjian & Schmid, 2006). Cutting fluids are used to address two main problems experienced during single-point cutting operations (Groover, 2010), namely:

- Heat-generation at the shear and friction zones
- Friction between the cutting-edge and the cutting-surface

These two problems experienced during the single point cutting process has a direct effect on the quality of the part. If the heat generated on the surface is too excessive, the material's surface hardness increases which can lead to galling, or expansion of both the workpiece material and the cutting insert (thermal expansion), leading to bigger cuts that will have a direct effect on the dimensional size of the components. If the friction at the cutting zone is not minimized, the tool wear will start to get excessive, meaning that the tool starts to get smaller and removes less material when cutting. This would then have a direct effect on the dimensional sizes of the component, as the workpiece is now bigger than the programmed size. Wear also damages the surface finish of the component, since it will increasingly worsen as the cutting edge wears out.

The effectiveness of using a cutting fluid depends on various factors, such as type of machine operations, tool and workpiece materials, cutting speed, method of application, and how well the two problems mentioned are balanced during the cutting process (Kalpakjian & Schmid, 2006).

Water can effectively reduce high temperatures developed in the cutting zone, however, it does not lubricate the cutting point effectively, thus it cannot reduce the friction of the single-point cutting process (Kalpakjian & Schmid, 2006). Another problem experienced by using water as a cutting fluid is the high probability that it can promote oxidisation during the single-point cutting process in the cutting zone, due to the heat generated between the surface of the workpiece and the edge of the cutting tool (Kalpakjian & Schmid, 2006).

The necessity for the use of a lubricant depends on the severity of the machining process, and is dependent on the following (Kalpakjian & Schmid, 2006):

- The level of temperatures and forces encountered by the tool and its ability to withstand it
- The tendency of chip build-up on the edge of the cutting insert
- The ease at which the chips can be removed from the cutting zone.
- How effectively the fluid can be applied to the tool-chip interface.

There are various types of lubricant that could be used to control the severity of the machining process. Kalpakjian & Schmid (2006) divides the cutting lubricants into four groups, namely:

- Oils / Straight Oils: It is typically used for low-speed operations where there is no significant increase in cutting temperatures. These oils include mineral, animal, vegetable, compounded and synthetic oils.
- Emulsion / Soluble Oils: It is a combination of oil, water, and additives. This is generally used for high-speed operations where the temperature rise is significant. The presence of the water makes it a highly effective coolant and the presence of the oil reduces or eliminates the water's tendency to cause oxidation.
- Synthetics Fluids: These are chemicals with additives. It is diluted with water and does not contain any oils. The advantage of these fluids is that it has an incredibly good cooling capability, good lubrication properties, good stability in hard water, good corrosion protection, low mist and easy handling, cleaning, and maintenance. However, the disadvantages are that it has some toxicity, it is easily contaminated by foreign oils and it is relatively expensive.
- Semisynthetic Fluids: This is a chemical emulsion, containing a little mineral oil that is diluted in water. It also contains an additive that reduces the size of the oil particles, making it more effective. The advantage of using semisynthetic fluid is that it possesses better corrosion protection than synthetic fluids and better cooling and wetting capabilities. It is also easier to handle and maintain than mineral emulsions. The disadvantages, on the other hand, are misting, relatively poor stability in hard water, contamination by foreign oils, and that it has some levels of toxicity.

Various methods can be used to apply the lubricant to the cutting zone during the single point cutting process. Figure 2-16 illustrates the common methods used for cooling and lubrication for single-point cutting processes.

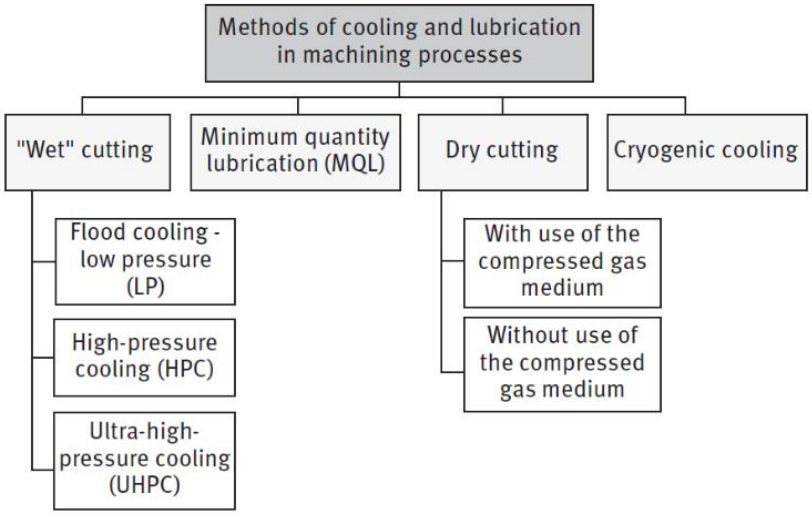

Figure 2-16 – Methods of cooling and lubrication in machining processes (Habrat *et al.*, 2016)

<u>Wet-cutting</u>

Wet cutting is the most common method used for applying lubricants to the cutting zone of a single point cutting process (Kalpakjian & Schmid, 2006). It uses a steady stream of cutting fluid, directed at the tool-work or tool-chip interface of a cutting operation (Groover, 2010). The typical flow rate for a single-point cutting tool starts at 10 L/min (Kalpakjian & Schmid, 2006). Figure 2-17 is an illustration of good and poor practice when applying the cutting fluid to the cutting zone, using flooding.

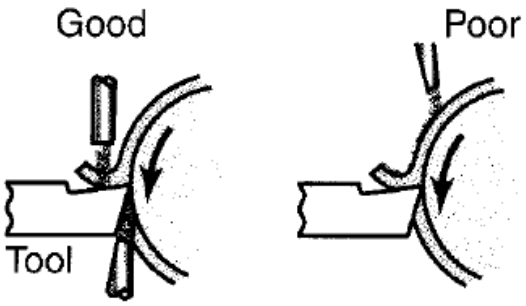

Figure 2-17 – Good and poor flooding practice for turning operations (Kalpakjian & Schmid, 2006)

Heat generation becomes a more significant factor in high-speed machining, as the cutting speeds and required power increases, using modern CNC lathe machines (Kalpakjian & Schmid, 2006). The effective application of the cutting fluid into the cutting zone is hindered by the creation of vapour near the cutting zone, which is due to the heat generated because of the large amount of friction experienced when cutting at high speeds (Habrat *et al.*, 2016).

The temperature in the cutting zone becomes increasingly problematic, thus it is advised to reassess the traditional application of lubricant, and to look at other possibilities to reduce the friction and temperature at the cutting zone.

The next option that needs to be investigated, is a high-pressure refrigerated coolant system (HPC) for high-speed machining. HPC uses a powerful jet of coolant which is delivered to the heat zone by a specially designed nozzle that is very effective in removing heat from the cutting zone, as illustrated in Figure 2-18(b) and (c) (Kalpakjian & Schmid, 2006).

When comparing the various types of wet-cutting applications illustrated in Figure 2-18(a), it is noticeable that the temperature zone at the cutting edge of the cutting insert is a lot bigger than the heat zone in Figure 2-18(c). The reason for this noticeable change is that the application method used in Figure 2-18(c) is much more localised and directed to the cutting zone than that of Figure 2-18(a). Furthermore, the application method of Figure 2-18(c) has an additional advantage, namely an increased level of chip removal. There is a higher probability that long, continuous chips - Figure 2-19(a) - would have been formed during the single point cutting process using the conventional coolant application of Figure 2-18(a), whereas the HPC adds a chip breaking feature as the pressure of the coolant jet ranges from 5.5 to 35 MPa (Kalpakjian & Schmid, 2006), as is illustrated in Figure 2-19(b).

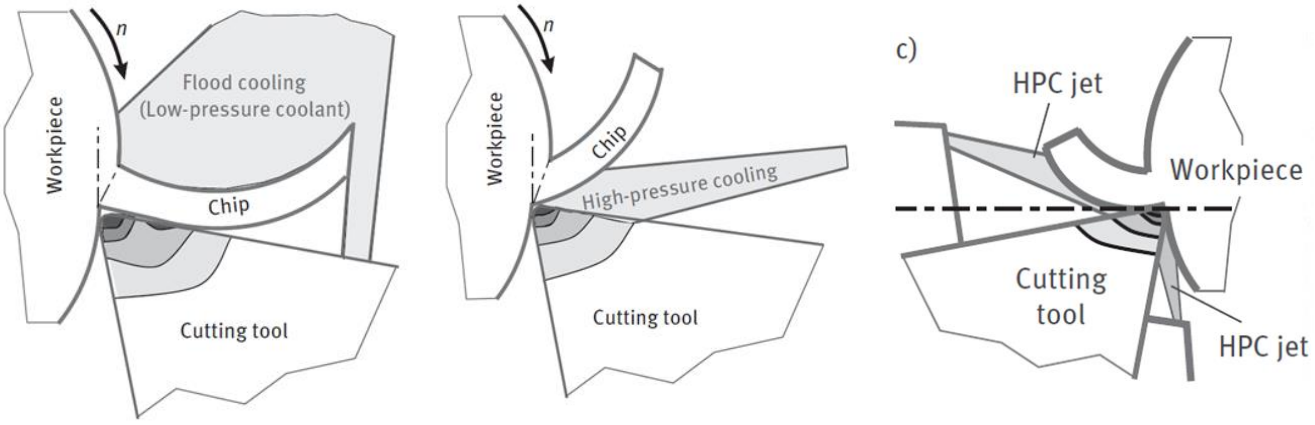

(a) (b) (c)

Figure 2-18 – Illustration of the three methods of applying lubricant to cutting zone, using flooding. (a) Lower Pressure Flooding (b) High-Pressure Cooling (c) Through Tool Cooling (Habrat et al., 2016)

There is a visible difference in the types of chips formed using the two different application techniques while machining Ti-6Al-4V. The long continuous ringlets - Figure 2-19(a) - can interfere with the cutting process by increasing the friction and temperature at the cutting zone. It also tends to interfere with the cutting edge of the insert, whereas the short, small chips - Figure 2-19(b) - are easily washed

away by the jet of coolant and therefore they do not interfere with the cutting process, making the cooling and lubricating effect of the lubricant even more efficient.

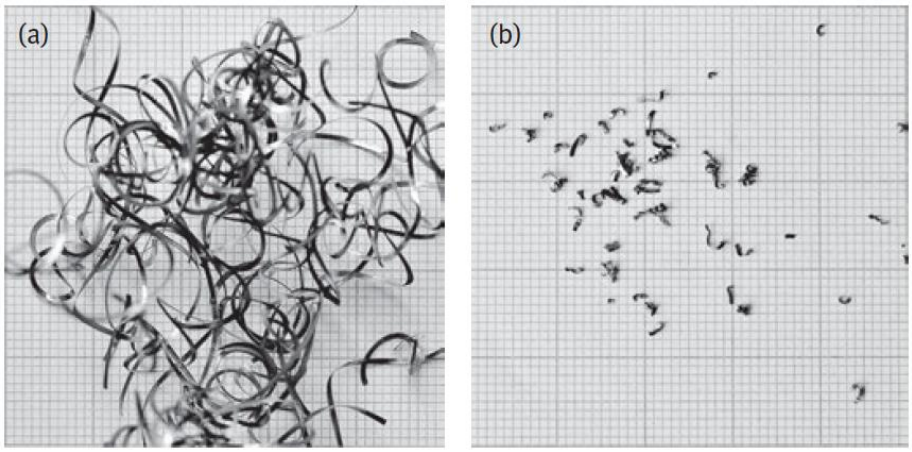

Figure 2-19 – Chips generated during machining of Ti-6Al-4V a) Flooding and b) HPC (Habrat et al., 2016)

The implementation of an HPC system has the following advantages (Habrat *et al.*, 2016):

- Improvement in tool life
- Reduction in cutting temperatures.
- Reduction in the number of chips welded to the workpiece during machining.
- Reduced tool-chip contact length
- Great chip evacuation from the cutting zone.

However, a special focus must be given to the contaminant size in the coolant. It must not exceed 20 µm, to avoid workpiece damage by the impact of the particles inside the coolant. Thus proper and continuous filtering must be done to maintain the quality (Kalpakjian & Schmid, 2006).

According to Kalpakjian & Schmid (2006), it was found that by using cutting fluids the chip formed may get *curlier* and thus cause the heat to get more concentrated closer to the tool-tip. This will lead to a reduction of the tool life. The increasing of the economic and environmental costs, and the health hazards associated with conventional cooling due to the reduction of tool life, makes dry machining or near-dry machining more favourable (Jayal & Balaji, 2009; Kalpakjian & Schmid, 2006).

Mist cutting

The next possibility of lubricant applied to the cutting zone is a middle ground between dry cutting and wet cutting, known as a mist or near-dry cutting (Kalpakjian & Schmid, 2006). The lubricant is directed at the cutting zone in the form of high-speed mist, carried by a pressurised air stream (Groover, 2010). The best way to describe it is that the method is similar to the principle used by an aerosol can (Kalpakjian & Schmid, 2006). This method supplies lubricant through the spindle of the tool to the cutting zone, the coolant tends to reach areas that are inaccessible by flooding (Kalpakjian & Schmid, 2006). It is most effective with water-based fluids at air pressures between 70 and 600 kPa and it uses flow rates between 1 and 100 cc/hr. The coolant is 1/10000 of that used in flooding (Kalpakjian & Schmid, 2006). According to the two handbooks, Kalpakjian & Schmid (2006) and Groover (2010), this method does not have the same cooling capacity as that of flooding, however according to a study conducted by Hasib *et al.* (2010), the mist application can reduce the average

chip-tool interface temperature by up to 40% -

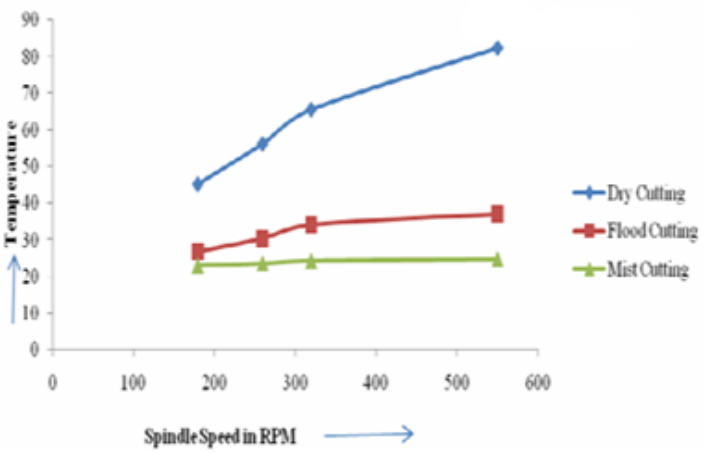

Figure 2-21 – Chip-Tool interface temperature vs. spindle speed for Depth of Cut 0.4 mm at a spindle speed of 120 rpm, machining medium carbon steel (after Hasib et al., 2010).

- more than the conventional flooding application, depending on the cutting conditions. The mist application with the technique presented by Hasib *et al.* (2010), as presented in Figure 2-20, has substantially reduced flank wear and thus improved the tool life, as illustrated in Figure 2-22. The one caution that needs to be kept in mind when using mist cutting is the fluid particles that can go airborne, therefore the facility requires adequate ventilation to reduce the health risk to the operator (Kalpakjian & Schmid, 2006).

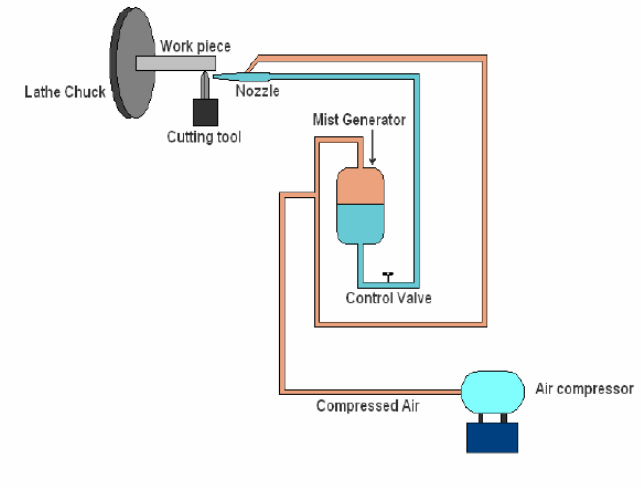

Figure 2-20 – Schematic of a mist application set-up and method used for the Hasib *et al.* (2010) study.

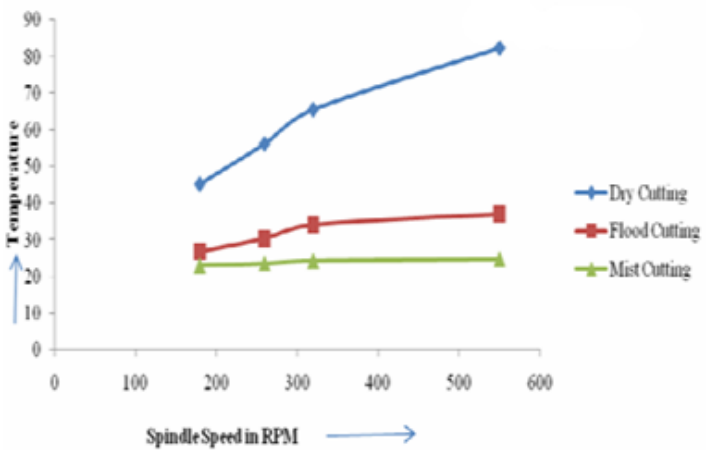

Figure 2-21 – Chip-Tool interface temperature vs. spindle speed for Depth of Cut 0.4 mm at a spindle speed of 120 rpm, machining medium carbon steel (after Hasib et al., 2010).

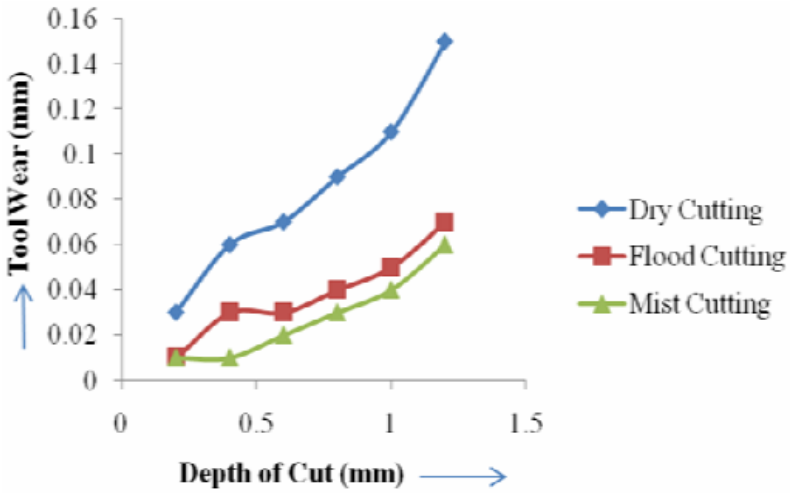

Figure 2-22 – Tool wear related to the depth of cut for a single point cutting process, at a spindle speed of 120 rpm, machining medium carbon steel (after Hasib et al., 2010)

Dry-cutting

Dry cutting is when no cutting fluid is used during the single-point cutting process (Groover, 2010). According to Habrat *et al* (2016) dry cutting have the following advantages:

- It limits the dangers to operator health.
- Reduced pollution
- Reduction in the effects of thermal shock
- Reduces operating cost.

However, according to Groover (2010) dry cutting has the following disadvantages as well:

- Overheating of the tool
- Lower cutting speeds and production rates to prolong tool life.
- Absence of chip removal benefits

As previously mentioned, one of the main purposes of cutting fluids is to flush chips away from the cutting zone (Kalpakjian & Schmid, 2006). This is a problem when using dry cutting, as mentioned in the disadvantages, but there are tools developed that allow the application of pressurised air through the tool shank, to blow the chips away (Kalpakjian & Schmid, 2006). However, the problem with this is that the thermal conductivity of air is a lot lower than that of water and even lower than that of water combined with cutting fluid. The pressured air also does not serve as a lubricant, and it increases the friction and the required power for the cutting process (Kalpakjian & Schmid, 2006).

Cryogenic cooling

As mentioned earlier, various types of coolants and lubricants can be applied to the cutting zone to lower the cutting temperatures and to reduce friction during the cutting process. However, some of these lubricants have negative environmental effects that drive up the cost of manufacturing. Furthermore, environmental acts and sustainability measures are important evaluation factors for companies nowadays, and this forces the industry to look at other innovative, and environmentally friendly ways to do manufacturing (Stefánsson, 2014). Cryogenic cooling is both an environmentally friendly and sustainable method used for cooling and lubricating the cutting zone of a single-point cutting process (Stefánsson, 2014). Cryogenic gasses such as liquid nitrogen or carbon dioxide are generally used as a coolant for a single point cutting process. These liquids are usually around a temperature of -200 °C and can be applied to the cutting zone in one of two methods, either through the internal or through the external supply (Kalpakjian & Schmid, 2006).

For the internal supply, the cryogenic liquid is supplied to the metal cutting zone in the nearest proximity to the tool-chip interface, using a specially designed cutting tool, as illustrated in Figure 2-23 (Jadhav, 2019; Stefánsson, 2014). Special considerations need to be taken when using internal cryogenic supply through the spindle, as simple bearings and rotary feeds are not designed for the extremely low temperatures of cryogenic liquids (Stefánsson, 2014). Special vacuum-insulated conduits must be installed on the spindle and special rotary feed-through has to be used to allow the cryogenic liquid to be carried through the channels (Stefánsson, 2014).

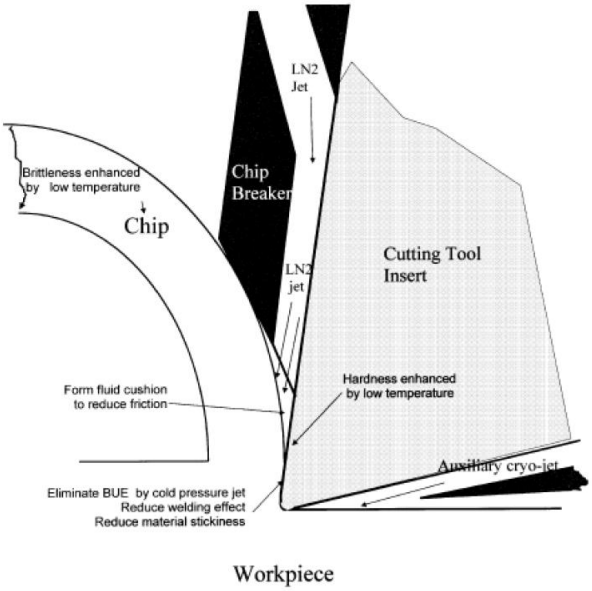

Figure 2-23 – Schematic illustration of an internal supply of a cryogenic liquid to the chip-tool interface of a single point cutting process (Stefánsson, 2014)

Two methods could be used for the external supply of the cryogenic liquid. The first method is the injection of the liquid into the cutting zone, using a small-diameter nozzle directed at the cutting zone (Kalpakjian & Schmid, 2006; Stefánsson, 2014), as illustrated in Figure 2-24. The second method uses a cap-like reservoir that is integrated on top of the cutting tool, as illustrated in Figure 2-24.

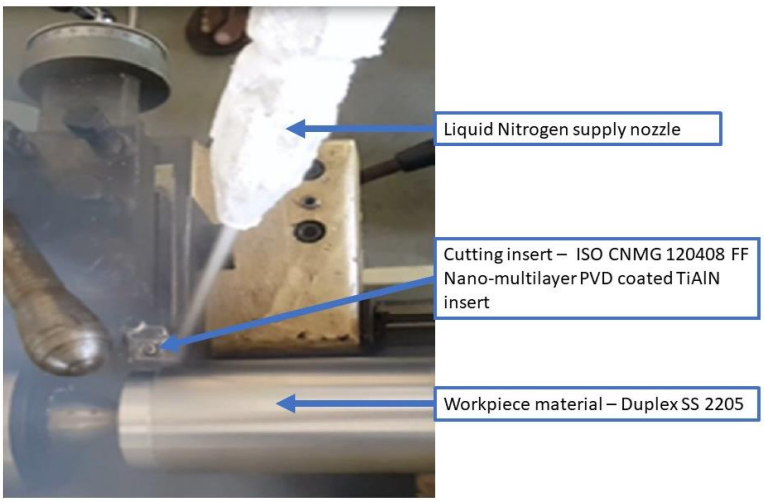

Figure 2-24 – Illustration of the external cryogenic cooling application in a single point cutting process used by Dhananchezian *et al.* (2018), illustrating the liquid nitrogen supply nozzle directed at the cutting zone between the insert and the workpiece material

The best way to take advantage and increase the efficiency of the cooling effect of cryogenic liquids is to have the supply as close as possible to the cutting zone of the cutting process, exposing the liquid to the highest temperature of the cutting process (Stefánsson, 2014). It can also be aimed at the workpiece in cases where it is ideal to change or improve the material characteristics (Stefánsson, 2014).

If the supply is too far away from the cutting zone, the required liquid flow rate is a lot higher, as the liquid evaporates as soon as it is exposed to atmospheric pressure and it could also lead to the cooling of machine components and other unwanted components (Stefánsson, 2014).

Due to the reduced temperature, the workpiece material hardness is maintained and the tool life is increased, allowing higher cutting speeds (Kalpakjian & Schmid, 2006). The chips are also very brittle, increasing the machinability of the workpiece material (Kalpakjian & Schmid, 2006). On the plus side, liquid nitrogen evaporates quickly leaving no environmental hazards (Kalpakjian & Schmid, 2006).

One concern regarding cryogenic cooling is the reduction of the integrity of the cutting tool during the single point cutting process. The reason for this concern is that if the cryogenic gas is not directed to the correct point of the process, the cutting tool's ductile-to-brittle transition point can be shifted, and the tool can become unstable for nicks and bumps during the cutting process. This can lead to a fatal injury if the tool breaks when cutting at high speeds.

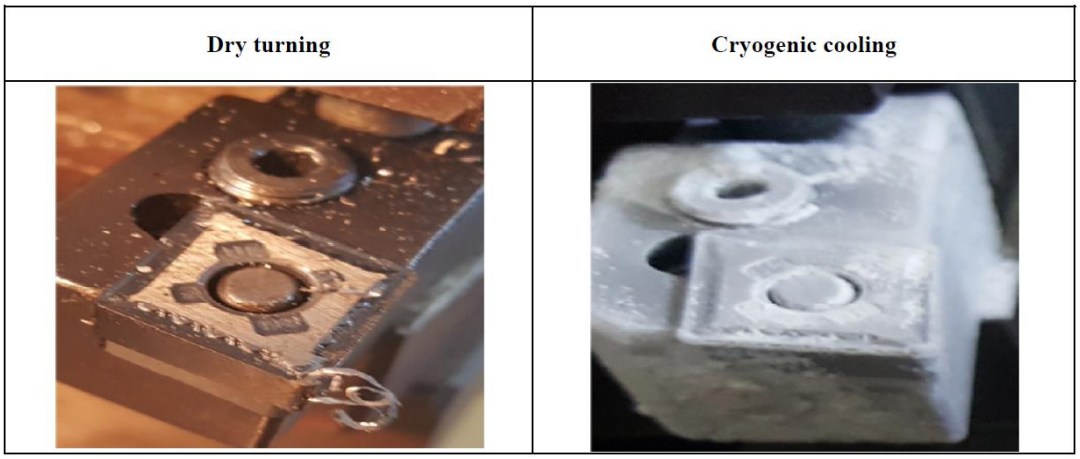

Figure 2-25 – Micrograph of a Dry Cutting tool vs. a Cryogenic Cutting tool, showing ice crystals formed while using liquid nitrogen as cutting fluid (Dhananchezian et al., 2018)

2.2.3. Single point cutting relationships.

As per the discussion in this section, many machining principles need to be considered when optimizing a single-point cutting process, as all the variables could have a direct impact on the result of a component's dimensions. Figure 2-26 categorises the various principles of single point cutting into three basic groups of variables, independent, interdependent, and dependent variables (ASM Handbook Committee & ASM International, 1978). The balance of these variables needs to be correct, as it has a direct effect on the quality of the component. The word "Quality" in this dissertation is defined as how well the dimensional size of the machined component matches the dimensional sizes specified by the client.

- **Independent (Input) variables:** These are variables such as the dimensional sizes, batch size, workpiece material and the surface finish specified by the client.
- **Interdependent variables:** These are those variables that have a relation to a specific input variable but could be independently changed for the machining process, for example, the cutting tool insert shape and material, cutting speeds (N), feed rate (f), depth-of-cut (d) and the cutting fluid.
- **Dependant (Output) variables:** These variables are the result of the machining process, for example, the cutting force experienced by the component that is machined and the power required, resulting in tool wear and potential rate of failure, cycle time, and component size deviation.

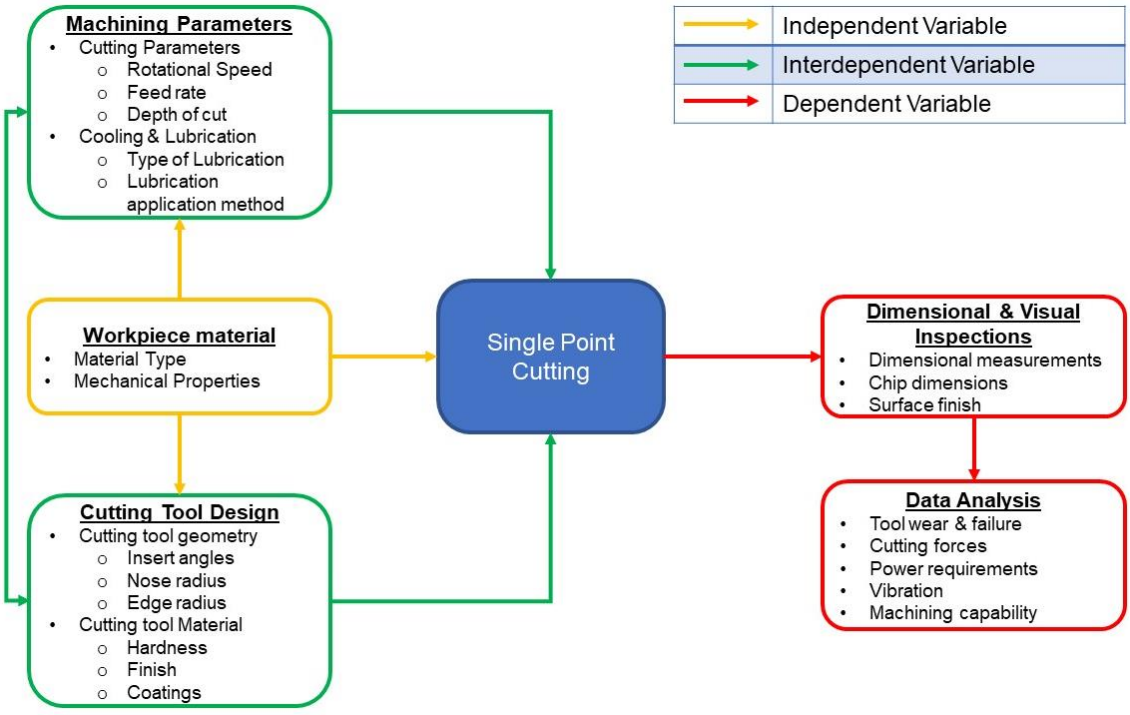

Figure 2-26 – Schematic of the variety of input parameters in Metal Machining relating to the output parameters (modified after ASM Handbook Committee & ASM International, 1978).

The interdependent variables of a single point cutting process must be selected in such a way that it complements the cutting process of the workpiece, as it has a direct impact on the dimensional size and surface finish of the component. These variables could be balanced by doing a series of machining trials before mass production occurs.

Table 2-2 quantifies the interdependent relationships found in the single point cutting process. The rotational speed (N) is the speed at which the workpiece material rotates, measured in revolutions per minute (rpm). The cutting depth (d) is the depth at which the cutting tool enters the cutting process or, stated differently, the difference between the initial diameter and the diameter after the cut measured in millimetres (mm) per cut - this is usually less than 50% of the inscribed circle of the insert, and the feed rate (f) is the speed at which the cutting tool moves over the workpiece material given in millimetre per revolution (mm/rev).

Table 2-2 –Single point cutting parameters and formulas indicating the interdependent relationship of the various variables (Kalpakjian & Schmid, 2006)

Symbol	Description	Calculation	Unit
N	Rotational speed of the workpiece		rpm
f	Feed		mm/rev
v	Feed rate / linear speed of the tool along workpiece length	$= f * N$	mm/min
V	Surface speed of the workpiece	$= \pi * D_o * N$ – Maximum speed $= \pi * D_{avg} * N$ – Average speed	m/min
l	Length of Cut		mm
D_o	Original workpiece diameter		mm
D_f	Final workpiece diameter		mm
D_{avg}	Average workpiece diameter	$= \frac{D_o + D_f}{2}$	mm
d	Depth of cut	$= \frac{D_o - D_f}{2}$	mm
t	Cutting time	$= \frac{l}{f * N}$	s or min
MRR	Material Removal Rate	$= \pi * D_{avg} * d * f * N$	mm^3/min
τ	Torque	$= \frac{F_c * D_{avg}}{2}$ F_c – Cutting Force [N/mm^2 or MPa]	N.m
P	Power	$= \tau * \omega$ $\omega = 2 * \pi * N\ (rad/min)$	kW / hp

If the depth of the cut is too big, the temperature in the cutting zone will increase due to the amount of friction it is exposed to, leading to an increased tool wear rate. This also has a direct influence on the torque and power required to machine the component. The required torque of a single point cutting process depends on the cutting force and the average diameter between the start and the finish of a cut. The cutting force is directly dependant on the shear strength of the workpiece material. The higher the shear strength of the workpiece material the smaller the cutting depth must be to keep the required power as low as possible, maintaining a proper machining efficiency.

If the cutting speed, the feed and the cutting depth are not balanced correctly, the temperature will increase during the cutting process and that would cause the part to be machined in its plastic deformation region instead of the elastic deformation region. This has a direct effect on the dimensional size of the component, because both the insert and workpiece material sizes increase due to thermal expansion, causing the insert to remove much more material than it was programmed for - leading to the component failing the lower tolerance of the component specification. Over time the tool wear will start to take effect and then the component will be manufactured larger than the programmed size. This is due to the size change of the insert because of the wear. Furthermore, the surface finish would also be affected, as there is now an imbalance between the cutting speed and the feed rate, because of the change in cutting depth.

According to Aggarwal & Singh (2005), the manufacturing industry has long depended on the inputs from machinists for optimising cutting tools and conditions, but there is still a considerable amount of handbook-based conservative cutting tool and condition selection on the planning level. However, the influences on the planning level are not always very scientific, which could lead to a reduction in the production rate, as the conditions selected are sub-optimal (Aggarwal & Singh, 2005). According to Aggarwal & Singh (2005), the biggest obstacle to the successful implementation of optimisation is the unavailability of the required technological performance equations. This problem is found due to the expensiveness of the extensive testing required to generate an empirical performance equation for each tool coating-workpiece-material combination for a given machining operation (Aggarwal & Singh, 2005). In their research, Aggarwal & Singh's (2005) found that there are several modern optimisation techniques, such as fuzzy logic, genetic algorithm, scatter search, Taguchi technique and response surface methodology, that could be used for the optimisation of the cutting process.

2.3. MACHINING ZRY-4 USING SINGLE POINT CUTTING

As discussed in Section 2.2.2, cooling and lubrication of cutting operations are extremely important for machining operations, as this reduces the cutting forces and keeps the cutting zone temperatures relatively low. According to Schemel (1977), it is possible to use mist generators where better visibility is needed during the cutting process, and dry cutting is also possible in some cases. However, if dry cutting is selected for Zr, then the cutting speed must be reduced, and great care must be taken to avoid fires (Schemel, 1977).

Before discussing the cutting parameters, the first thing that needs to be defined is the angle of the cutting insert that will be used to machine the components. According to Schemel (1977), the best-suited cutting insert that could be used to machine Zry-4 has the angles as presented in Table 2-3.

Table 2-3 – Zirconium Cutting Tool Geometry (Schemel, 1977)

Tool Element Name	Value
Back rake angle (BRA)	15°
Rake angle (RA)	10°
End relieve angle (ERA)	10°
Nose radius (NR)	0.8 mm

After identifying the best angle for the insert, the next question which needs answering is what type of material is best suited for the machining of Zry-4, and according to Reid (2011), both carbide and high-speed steel tools could be used for single-point machining operations. Carbide tooltips would generally allow higher productivity and give better surface finishes, and the performance of the single point cutting process could be greatly enhanced when the tools are kept sharp (Reid, 2011). Table 2-4 summarises the appropriate cutting parameters, that need to be used when cutting Zr using either carbide or high-speed steel inserts. Furthermore, Table 2-5 tabulates the feed rate required to the cutting tool used for the cut-off and forming process, as well as the feed rate to the width of the specific tool, for example, if the cut-off tool uses a carbide insert with an insert width of 1,5 mm, the cutting speed should be 58 mm/min, and the feed rate should be 0,05 mm/rev.

Table 2-4 – Cutting parameters of Zirconium metal using Carbide and High-speed steel as cutting tool materials (Reid, 2011)

	Carbide Inserts			High-Speed Steel		
Cutting Depth [mm]	Tool Material ISO	Cutting Speed [m/min]	Feed Rate mm/rev	Tool Material ISO	Cutting Speed [m/min]	Feed Rate [mm/rev]
1.0	K20/M20	84 – 100	0.18	S4 / S5	46	0.18
4.0	K20/M20	69 – 81	0.40	S4 / S5	30	0.40
8.0	K20/M20	53 – 60	0.50	S4 / S5	24	0.50

Table 2-5 – Cut-off and general forming tool feed rate (mm/rev) related to tool widths and cutting speed (Reid, 2011)

Tool ISO	Cutting Speed [m/min]	Cut-off Tool Width [mm]			Form Tool Width [mm]				
		1.5	3	6	12	18	25	35	50
S9 / S11	20	0.050	0.063	0.075	0.075	0.063	0.063	0.050	0.050
K40 / M40	58	0.050	0.063	0.075	0.075	0.063	0.063	0.050	0.050

Now that the shape of the cutting insert is known, as well as the material and the cutting parameter of those materials, the next focus should be on the cooling aspect of the cutting process. However, there is little information on the cooling effect of Zry-4 during a single-point cutting process. The only information that was found, were recommendations from Kalpakjian & Schmid (2006), that either dry cutting, emulsion oils or chemicals/synthetic oils could be used as cutting fluids for Zr. For this reason, the focus will be shifted to the cooling effect of the machining of ductile materials in general and assumptions will be made towards the machining of Zry-4.

The reason for looking at the best type of lubrication/cooling during the single point cutting process when machining Zry-4, is to control the cutting temperatures, to prevent the possibility of the exothermic oxidisation reaction that is found when machining Zry-4 under the wrong conditions. According to a fire protection evaluation conducted by the United States Nuclear Regulatory Commission (NRC, 2001), it was found that Zry-4 does not ignite at temperatures below 1600 °C. The NRC (2001) also reported that the ignition of metal could only occur if the metal was exposed to an oxidising environment. The oxidising temperature of zirconium is much lower than the ignition temperature, ranging between 850 – 950 °C. It was also found that the probability increases for spontaneous ignition of Zr when the particles are below 10 µm, however, the exact relationship between the particle size, size distribution, temperature, pressure, humidity, and surface characteristics is not well defined for Zr ignition. Furthermore, in a study conducted by Doyle *et al.* (1958), using thermodynamic data, it was calculated that the combustion temperature of Zr in oxygen is 4930 K (~ 4656,85 °C) at one atmospheric pressure, making it one of the highest temperatures obtained during metal combustion.

Table 2-3 is a summary of the physical properties of various ductile materials that has a direct influence on the cutting insert selection. From Table 2-3, few properties of Zry-4 relate to that of Ti6Al4V, as well as to that of Stainless Steel 316 (SS316). However, the most important property for the single point cutting process is the shear modulus of a material. From the comparison of the shear modulus, it is clear that the shear modulus of Zry-4 lies between that of aluminium (Al-6005-T5) and Ti6Al4V. For this reason, it is expected that Zry-4 might react similarly.

Table 2-6 – Physical properties of various ductile alloys, SS316, Al 6005-T5, Ti6Al4V and Zry-4 (ASM Aerospace Specification Metals Inc., 2020a,b; matweb.com, 2017a,b)

	Thermal Expansion	Thermal Conductivity	Shear Modulus	Tensile Strenght	Yield Strength
Unit	µm/(m.K)	W/(m.K)	GPa	MPa	MPa
Zry-4	6.0	21.5	36.2	413	241
SS316	16.0	16.3	74-82	550	240
Al-6005-T5	25.2	167	26	310	276
Ti-6Al-4V	8.6	6.7	44	1170	1100

In a study conducted by Naves *et al.* (2013), a comparison was made between the maximum flank wear associated with dry cutting, traditional flooding and HPC at various pressures, as illustrated in Figure 2-27. Austenitic stainless steel was used as the workpiece material and a cemented carbide cutting insert coated with TiN, Al_2O_3 and Ti(C, N) as the cutting tool. The machining parameters were set as follow: a cutting depth of 0,5 mm, a feed rate of 0,2 mm/rev and a cutting speed of 300 m/min. The cutting fluid that was selected for the test was an emulsion of vegetable oil at concentrations of 5% and 10%. Five experiments were conducted. First, dry cutting, then conventional flooding at 0,03 MPa and a flow rate of 4,3 l/min and then three high-pressure experiments at 10 MPa, 15 MPa and 20 MPa. The experiments were repeated over five different machined lengths, 540 mm, 1080 mm, 1620 mm, 2160 mm, and 2700 mm. In conclusion, Naves *et al.* (2013) found that there was a reduction in the maximum flank wear when using HPC at 20 MPa during single point cutting of austenitic stainless steel, as illustrated in Figure 2-27. This leads to an increased tool life of the cutting insert, which means that cutting productivity can be increased for the same tool wear cycle.

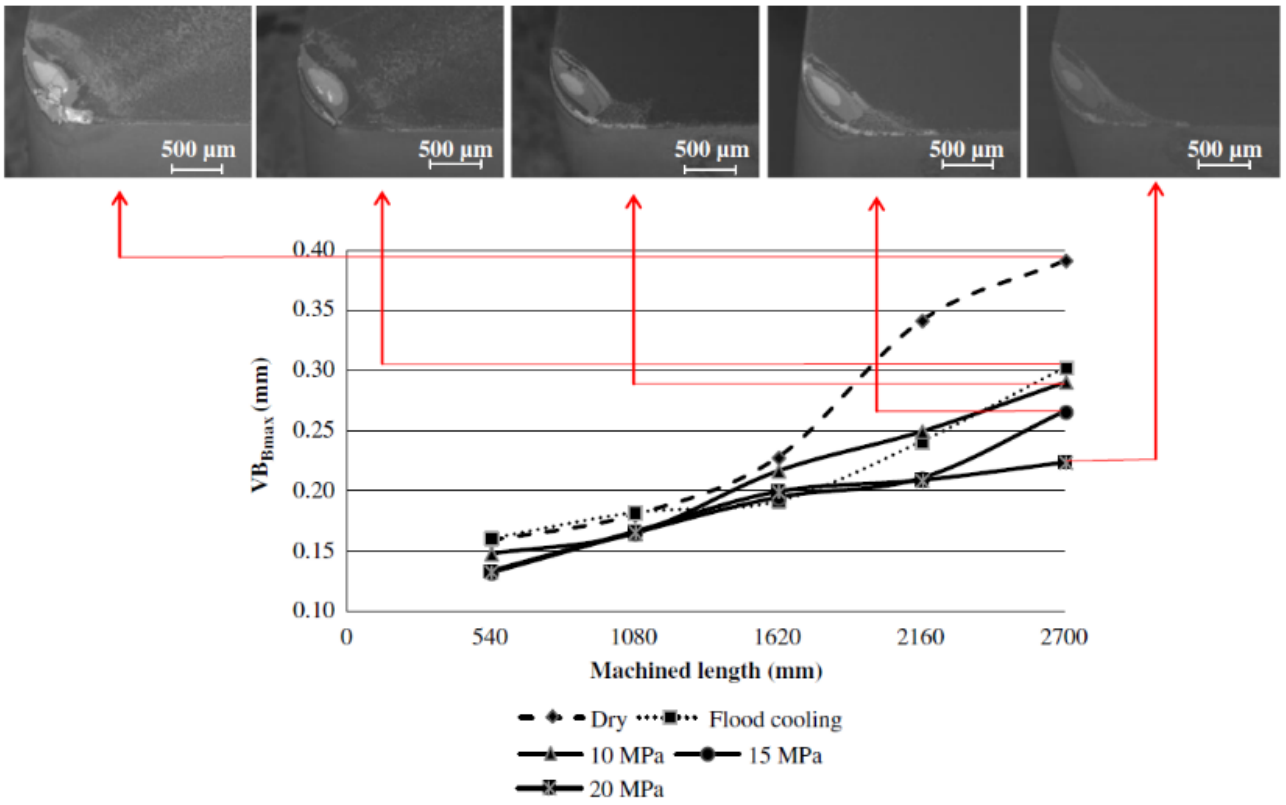

Figure 2-27 – Scanning electron microscope photos related to cutting tool insert (cemented carbide with TiN, Al2O3 and Ti (C, N) MTCVD coated layers) flank wear (VB) after machining SS316 with cutting fluid at different pressures (Naves *et al.*, 2013)

In another study conducted by da Silva *et al.* (2013), the investigation was done on the tool life in high-speed machining of Ti6Al4V, using PCD tools under various coolant pressures (conventional cooling, 7,0 MPa, 11 MPa and 20,3 MPa). The coolant used for this study was also emulsion based cutting fluid, a 6% concentration applied using two methods, namely the conventional cooling method and the high-pressure method. For the conventional method, a flow rate of 2,7 L/min was used and the flow direction A in Figure 2-29. For the high-pressure application, the pressures were set at 7 MPa, 11 MPa and 20,3 MPa at flow rates of 16,9 L/min, 18,5 L/min and 20,3 L/min, respectively, using the flow direction B in Figure 2-29. The cutting parameters were set as follow:

- Cutting speed – m/min – 175, 200, 230 and 250
- f – 0,15 mm/rev
- d – 0,5 mm

In conclusion, da Silva *et al.* (2013) found that there was a substantial improvement in the tool life when applying high-pressure cooling to the cutting zone of Ti6Al4V, using a Polycrystalline diamond (PCD) insert, as illustrated in Figure 2-28.

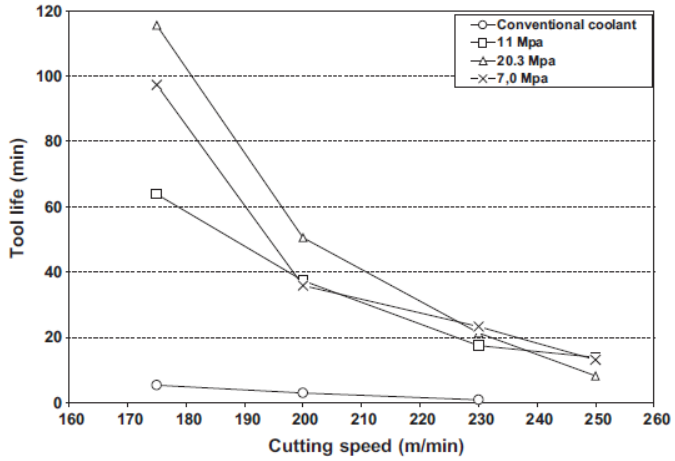

Figure 2-28 – Tool life results of a PCD insert after cutting Ti6Al4V at various cutting speeds, applying cutting fluids and using different pressures (Da Silva *et al.* 2013)

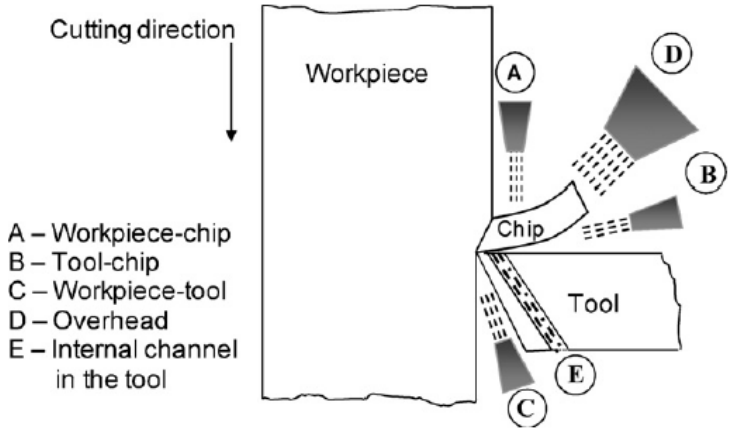

Figure 2-29 – Schematic illustration of the experimental setup used by da Silva *et al.* (2013), indicating various flow directions of the cutting fluid

Dhananchezian *et al.* (2018) conducted a study investigating the effect of cryogenic cooling using liquid nitrogen as cooling liquid on the single point cutting of duplex stainless steel 2205 and comparing it to dry cutting using a Physical Vapor Deposition (PVD) coated nano multilayer TiAlN cutting insert. The cutting parameters were set as follow:

- d – 1 mm
- f – 0,111 mm/rev
- Cutting speed – mm/min – 72, 119, 197

From the study it was concluded, it was found that the cutting temperature was reduced by 53–58 % - Figure 2-30 (b) -, the cutting forces were decreased by 30–43 % - Figure 2-30 (a) - and the surface roughness was improved by 18–23 %. This is proof that the machinability of the duplex stainless steel can be improved using liquid nitrogen as a cooling liquid. Furthermore, it is also visible in Figure 2-25 that chips tend to weld onto the insert during the dry cutting process, influencing

the quality of the part, while when using the cryogenic process, the chips are not interfering with the cutting process, hence the improvement of the surface roughness.

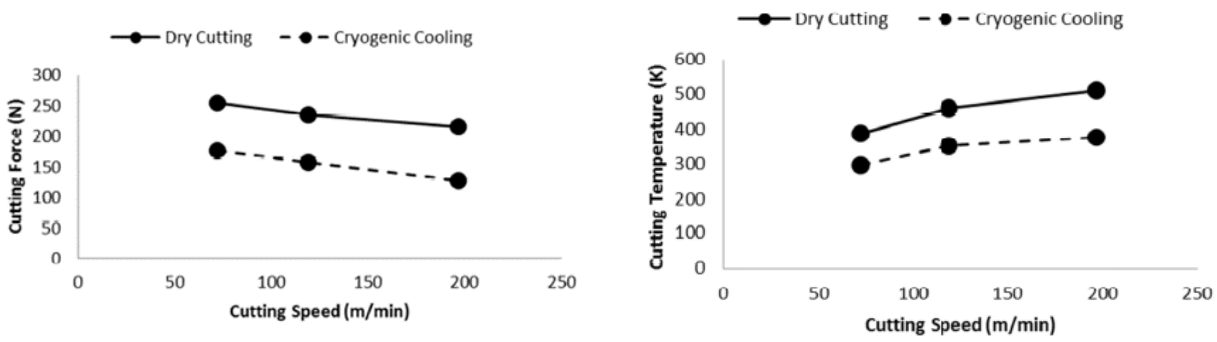

(a) (b)

Figure 2-30 – a) Comparison of the cutting forces (y-axis) of dry cutting and cryogenic cutting over three cutting speeds (x-axis), b) Comparison of the cutting temperatures (y-axis) of dry cutting and cryogenic cutting over three cutting speeds (x-axis) after machining duplex SS 2205, using a cemented carbide insert with a PVD coated TiAlN layer (Dhananchezian *et al.*, 2018)

By comparing Figure 2-31(a) and Figure 2-31(b) with each other, it is clear that the dry cutting is already showing signs of flank wear after 100 mm machining in dry conditions, whereas the cryogenic cutting does not show any signs of early wear.

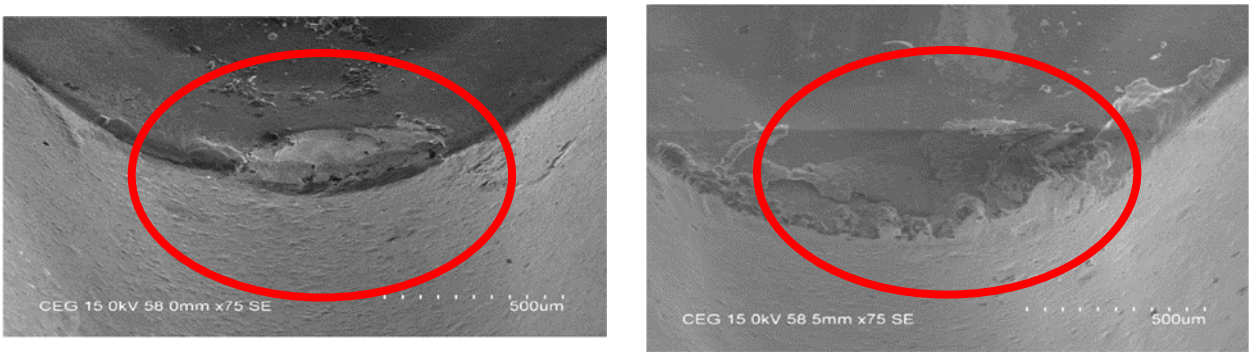

(a) (b)

Figure 2-31 – Scanning Electron Microscope (SEM) images of the cutting tool flank on the edge of the insert after (a) dry cutting and (b) cryogenic cutting at a speed of 197 m/min, f=0,111 mm/rev, and d=1 mm for a cutting length of 100 mm, showing a crater on the edge of the insert after using conventional cooling, compared to no crater on the edge of the insert after using cryogenic cooling.

To detect the wear of an insert, continuous monitoring of the cutting process is required. This could be done through dimensional inspection of the machined component. If the diameter starts to increase on the component, there is a possibility of tool wear. Tool wear could be detected using statistical process control (SPC). SPC is a statistical approach used to advise the operator to take

certain measures at a specific time to avoid components being rejected (Kalpakjian & Schmid, 2006). In parallel with SPC, there is another method to evaluate the batch performance and that is by using acceptance sampling. Acceptance sampling is widely used and is very valuable for high-production-rate facilities where 100% inspection can become too costly (Kalpakjian & Schmid, 2006), however, in some instances, 100% inspection is required, such as with the manufacturing of pacemakers, space shuttle components and prosthetics.

2.4. ACCEPTANCE SAMPLING

Acceptance sampling consists of selecting a sample of random components from a lot and inspecting them to evaluate the characteristics of the lot and to see whether the lot complies with the quality requirements set by the client (Kalpakjian & Schmid, 2006). By using this method, the probability of acceptance could be obtained from the various operating characteristics curve (Figure 2-32). This probability must also comply with the acceptance quality level (AQL).

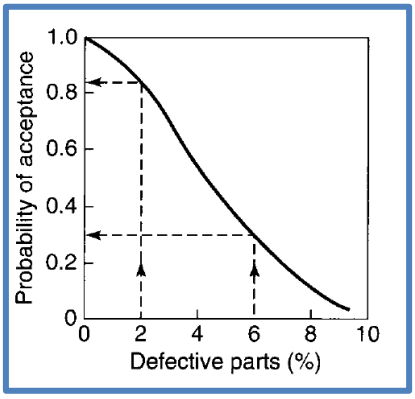

Figure 2-32 – Typical operating-characteristics curve (Kalpakjian & Schmid, 2006)

Some acceptance sampling plans have been prepared for both the military and national standards - based on an acceptable, predetermined and limiting percentage of nonconforming parts in the sample (Kalpakjian & Schmid, 2006). If the percentage of nonconformity exceeds the specified percentage, the entire lot is rejected and reworked (if economically feasible) (Kalpakjian & Schmid, 2006).

The greater the number of samples taken from a lot, the greater the chances are for a nonconforming part and the lower the probability of the lot's acceptance becomes (Kalpakjian & Schmid, 2006).

AQL is defined as the maximum percentage of defective components in a lot for a given characteristic that could be considered satisfactory as a process average, and beyond which it is desired to reject

the lot (Marguglio, 1977). This percentage is an indication to the producer that only 5% of the components in a lot may be rejected by the client, this is called the producer's risk (Kalpakjian & Schmid, 2006). Consumer's risk is that the client knows that 95% of the components are acceptable (Kalpakjian & Schmid, 2006).

There are two methods of sampling a lot, namely by:

- Attributes (ISO 2859-1, 1999), this is used when the inspected component either conforms or does not conform to the specification, by using go-nogo gauges.
- Variables (ISO 3951-1, 2013), this is used when a measurement conforms to a certain extent to the specification. There are two methods of evaluating a sample within the sampling by the variable plan (ISO 3951-2, 2006), it is either the "s" method or the "σ" method. "s" is defined as the standard deviation of the measured values of the quality characteristic, whereas "σ" is defined as the standard deviation of a process that is under statistical control. In short, the s-method uses the sample's standard deviation whereas the σ-method uses the presumed value of the process standard deviation (ISO 3951-1, 2013). The σ-method is more economical in terms of the sample size, however, before one could use this method, the value of σ must first be established (ISO 3951-1, 2013). Based on this statement, it was decided to use the s-method as there are various unknowns in this project.

Table 2-7 is the general rule of sample size selection for all acceptance sampling plans.

Table 2-7 – Sample Size Code Letters for ISO 2859-1 & ISO 3951-1 (ISO 3951-2, 2006)

Lot or batch size	Special inspection levels				General inspection levels		
	S-1	S-2	S-3	S-4	I	II	III
2 to 8	B	B	B	B	B	B	B
9 to 15	B	B	B	B	B	B	C
16 to 25	B	B	B	B	B	C	D
26 to 50	B	B	B	C	C	D	E
51 to 90	B	B	C	C	C	E	F
91 to 150	B	B	C	D	D	F	G
151 to 280	B	C	D	E	E	G	H
281 to 500	B	C	D	E	F	H	J
501 to 1 200	C	C	E	F	G	J	K
1 201 to 3 200	C	D	E	G	H	K	L
3 201 to 10 000	C	D	F	G	J	L	M
10 001 to 35 000	C	D	F	H	K	M	N
35 001 to 150 000	D	E	G	J	L	N	P
150 001 to 500 000	D	E	G	J	M	P	Q
500 000 and over	D	E	H	K	N	Q	R

NOTE The sample size code letters and inspection levels in this part of ISO 3951 correspond to those given in ISO 2859-1 and ISO 3951-1.

The sample size is determined by the lot size as well as by an inspection level. Two types of inspection levels could be used for the sample size selection:

- Special inspection level (SIL): In the case of SIL, only a few parts could be checked as the inspection process is, for example, either destructive or it takes a significant amount of time (hours or days) to get the results (Ernest Orlando Lawrence Berkeley National Laboratory, 2017).

- General inspection level (GIL): GIL is generally used for QC on consumer goods, whereas SIL is generally applied on parts where it is critical to meet a particular acceptance criterion (Ernest Orlando Lawrence Berkeley National Laboratory, 2017). The GIL is divided into the following 3 categories (Ernest Orlando Lawrence Berkeley National Laboratory, 2017):
    - **GIL-I (Reduced Inspection):** This is used when the company supplying the parts have rarely supplied their customer with nonconforming parts and the number of new parts from the suppliers does not warrant 100% inspection.
    - **GIL-II (Normal Inspection):** GIL-II is generally the default inspection level. GIL-II is used for suppliers who have supplied their client with parts that had varied performance through inspection and nonconformities have been identified but they do not indicate historical problems with quality.
    - **GIL-III (Tightened Inspection):** GIL-III is used when high-value parts are produced or when the supplier of the parts has had recent and/or historical quality issues and requires a higher level of inspection. Quality problems include multiple nonconformities during the inspection - when the number of nonconformities identified is above the required AQL etc.

The GIL is not a fixed parameter for the AQL system, there is a clause in the ISO 3951-2: 2006 for switching rules for normal, tightened, and reduced levels of inspection, as illustrated in Figure 2-33. The switching of rules discourages manufacturers to produce parts at quality levels worse than the AQL requirement (ISO 3951-2, 2006). This creates the option to tighten a suppliers GIL when the components delivered exceeds the required AQL (ISO 3951-2, 2006). It also gives the option to discontinue sample inspection altogether if the producer fails to comply with the required tightened inspection level and thus forces the supplier to rapidly improve his production line (ISO 3951-2, 2006). Furthermore, this also creates an opportunity to reduce the inspection level for suppliers who supply parts with a stable and reliable quality level, and at levels better than the required AQL (ISO 3951-2, 2006). However, this option is at the discretion of the responsible authority.

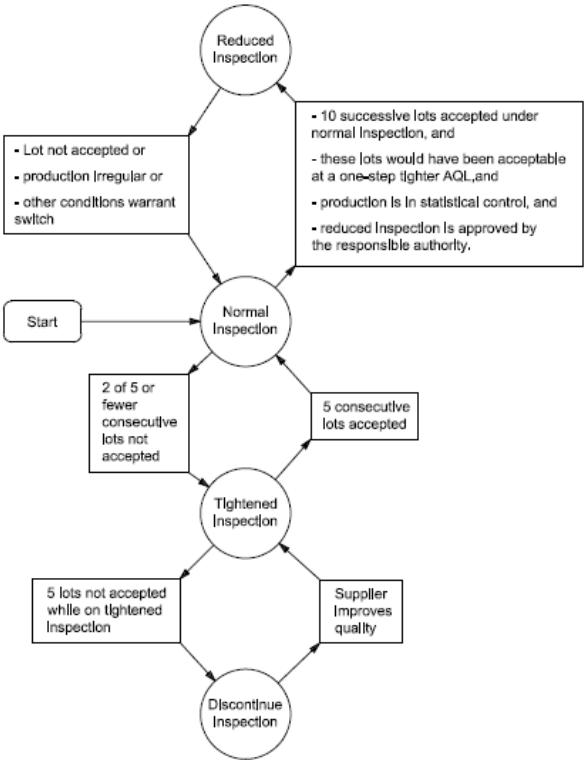

Figure 2-33 – ISO 2859-1 & ISO 3951-2 – Outline for switching rules (ISO 3951-2, 2006)

AQL is defined as the quality level that is the worst tolerable process fraction of non-conforming parts when a continuing series of lots is submitted for acceptance sampling (ISO 3951-1, 2013). Three types of defects are commonly used for most consumer goods (QualityInspection.org, 2018):

- AQL – 0,01 - This is used for critical defects. These are unacceptable defects, and users might be harmed if the regulations are not respected,
- AQL – 2,5 - This is used for major defects. These are defects that would usually not be acceptable for the customer.
- AQL – 4,0 - This is used for minor defects. These are defects that would generally be acceptable for the customer.

An AQL of 1.0 means that 1.0% of the lot will be defective and is used for a 95% or greater probability that the lot will be accepted.

Now that the sample size and the AQL is defined, the lot could be evaluated. The evaluation process uses dimensional tolerances as these characteristics only have an upper limit. This is the most straightforward procedure to evaluate single specification limits or to use when separate control of double specification limits are required (ISO 3951-2, 2006). By using the quality statistic (Q_U or Q_L), one could evaluate the acceptance of the lot, using the following rules:

a) Upper-quality limit (Q_U)

$$Q_U = \frac{U - \bar{x}}{s}$$	**Equation 2-1**

Acceptable if $Q_U \geq k$	**Equation 2-2**
Unacceptable if $Q_U < k$	**Equation 2-3**

b) Lower quality limit (Q_L)

$Q_L = \frac{\bar{x} - L}{s}$	**Equation 2-4**
Acceptable if $Q_L \geq k$	**Equation 2-5**
Unacceptable if $Q_L < k$	**Equation 2-6**

c) Double specification under separate control

Acceptable if $Q_U \geq k$ and $Q_L \geq k$	**Equation 2-7**
Unacceptable if $Q_U < k$ and/or $Q_L < k$	**Equation 2-8**

The k-value is defined as the acceptance constant and is found in the ISO 3951-2:2006 in Tables B.1 to B.3 depending on the level of inspection used for the specific component. Table 2-8 is a copy of Table B.2 in ISO 3951-2:2006, illustrating the *k*-values for a tightened inspection plan.

Table 2-8 – ISO/SANS 3951-2 – Sampling plan for tightened inspection

Table B.2 — Form k single sampling plans for tightened inspection (master table): "s" method

Code letter	Sample size	Acceptance quality limit (in percent nonconforming)															
		0,01	0,015	0,025	0,04	0,065	0,10	0,15	0,25	0,40	0,65	1,0	1,5	2,5	4,0	6,5	10,0
		k	k	k	k	k	k	k	k	k	k	k	k	k	k	k	k
B	3	↓	↓	↓	↓	↓	↓	↓	↓	↓	↓	↓	↓	↓	↓	0,954	0,818
C	4	↓	↓	↓	↓	↓	↓	↓	↓	↓	↓	↓	↓	↓	1,163	1,046	0,853
D	6	↓	↓	↓	↓	↓	↓	↓	↓	↓	↓	↓	↓	1,395	1,275	1,108	0,902
E	9	↓	↓	↓	↓	↓	↓	↓	↓	↓	↓	↓	1,615	1,494	1,338	1,159	0,907
F	13	↓	↓	↓	↓	↓	↓	↓	↓	↓	↓	1,830	1,712	1,565	1,405	1,189	0,938
G	18	↓	↓	↓	↓	↓	↓	↓	↓	↓	2,025	1,910	1,770	1,622	1,429	1,212	0,944
H	25	↓	↓	↓	↓	↓	↓	↓	↓	2,215	2,102	1,969	1,829	1,652	1,457	1,225	0,995
J	35	↓	↓	↓	↓	↓	↓	↓	2,399	2,289	2,160	2,028	1,862	1,684	1,476	1,242	1,010
K	50	↓	↓	↓	↓	↓	↓	2,569	2,461	2,336	2,209	2,052	1,885	1,693	1,481	1,277	1,044
L	70	↓	↓	↓	↓	↓	2,736	2,631	2,510	2,389	2,239	2,082	1,904	1,710	1,526	1,322	↑
M	95	↓	↓	↓	↓	2,889	2,787	2,670	2,553	2,410	2,261	2,093	1,913	1,745	1,559	↑	↑
N	125	↓	↓	↓	3,037	2,937	2,824	2,711	2,574	2,432	2,274	2,105	1,949	1,779	↑	↑	↑
P	160	↓	↓	3,179	3,082	2,973	2,865	2,733	2,597	2,447	2,288	2,141	1,984	↑	↑	↑	↑
Q	200	↓	3,310	3,215	3,109	3,004	2,877	2,747	2,603	2,452	2,313	2,165	↑	↑	↑	↑	↑
R	250	3,442	3,350	3,247	3,146	3,023	2,898	2,760	2,616	2,485	2,345	↑	↑	↑	↑	↑	↑

NOTE 1 The sample size code letters in this part of ISO 3951 correspond to those given in ISO 2859-1 and ISO 3951-1.

NOTE 2 Symbols: ↓ There is no suitable plan in this area; use the first sampling plan below the arrow. If the sample size equals or exceeds the lot size, carry out 100 % inspection.

↑ There is no suitable plan in this area; use the first sampling plan above the arrow.

2.5. LITERATURE REVIEW CONCLUSIONS

This literature study aimed to:

- review general single-point machining principles and relevant machining parameters of a cutting process for machining Zry-4
- investigate the best possible solution to prevent Zry-4 to spontaneously ignite during the machining process.

After reviewing the principles of a single point cutting process, and investigating the best-suited machining parameters, it was found that the best insert to use is a sharp insert with a large positive rake angle, to ensure that the cut can break through the work-hardened section of the material. Furthermore, it was found that the best cutting parameters for zirconium are at high feeds and low speeds and the process needs to be flooded with water to prevent spontaneous ignition. According to Reid (2011), the best-suited insert material for the machining of Zry-4 will be carbide inserts, as they tend to give higher productivity and better surface finishes. The cutting parameters for the carbide insert are summarised in Table 2-4 and Table 2-5 and the cutting insert angles are presented in Table 2-3.

Zry-4 is largely used inside PWR nuclear fuel assemblies, due to its excellent corrosion resistance at elevated temperatures and it has extremely low thermal neutron cross-section. However, Zry-4 is also a very ductile material, making it difficult to machine using cold-work techniques, such as single-point cutting and milling. Zry-4 tends to gall leading to work-hardening and it could spontaneously ignite when it has a big surface area at elevated temperatures, such as shavings. According to the NRC (2001) report on the fire protection of Zry-4, it could ignite at a temperature of around 1600 °C and according to calculations done by Doyle *et al.* (1958), the flame temperature is around 4650 °C. According to Reid (2011), the solution to the ignition hazard is to flood the machining process with water-soluble oils. Even though this is a quick and easy solution, the question arises whether it is the most efficient way of cooling the machining process of Zry-4. As mentioned in Section 2.2, the reason for adding cutting fluid to the machining process is to reduce the cutting temperatures, which in effect increases the tool life, dimensional stability, and surface finish of a part. In a study conducted by Naves *et al.* (2013), they found that the most efficient way of flooding is to use HPC through the cutting tool, leading to a reduction of around 40% in the flank wear of the insert, meaning that the insert could be used for a longer time. In an additional study, da Silva *et al.* (2013) confirmed Naves *et al.'s* (2013) research findings and found that by using the HPC, the tool life is significantly increased. In another study conducted by Dhananchezian *et al.* (2018), they investigated the effectiveness of cryogenic cooling of a ductile metal and found that the overall improvement of the quality of the machined component improved by a maximum of 23%.

Applying the results of these research findings on the machining of Zry-4 the assumption could be made that the HPC cooling would improve the machining of Zry-4 significantly, as the high pressure of the coolant would break and remove the chips from the cutting zone. This would reduce the amount of chip build-up on the edge of the cutting insert and the cutting temperature would be reduced, improving the overall quality of the part. However, it would not change the ductility of the material and it would not have any effect on the ductile-brittle transition temperature of Zry-4. The ductile-brittle transition temperature is defined as the minimum temperature at which material could absorb a specific amount of energy without breaking. Looking at the cryogenic cooling, this would have a direct effect on the ease of the machining process, as it would reduce the brittle-transition-temperature of Zry-4, meaning the material would break without any plastic deformation. This is expected to improve the dimensional consistency of the part drastically. The only challenge with cryogenic cooling is that it cannot be applied to a standard lathe, as they are not designed and built for these low temperatures and the challenge for the HPC is that a secondary system would be required to increase the pressure to 20 MPa, and additional equipment would be needed to ensure that the coolant remains cold and clean. Due to budget constraints, it was decided to use conventional flooding for this project, even though it is not the most efficient method of cooling, proven by the literature, it would still be efficient to reduce the risk of spontaneous ignition.

This leads to the specific purpose of this study, which is:

- finding the best combination of cutting tools to cut the required shape of the nuclear fuel endcaps,
- finding the best possible cutting parameters to machine Zry-4 nuclear fuel rod endcaps in high volume production to circumvent galling, and
- to measure the resulting dimensions and calculate the ensuing tolerances by using standard and numerical methods to verify the machining process.

3. NUCLEAR FUEL ENDCAP MACHINING SETUP

3.1. INTRODUCTION

The purpose of this chapter of the dissertation is:

- finding the best combination of cutting tools to cut the required shape of the nuclear fuel endcaps,
- finding the best possible cutting parameters to machine Zry-4 nuclear fuel rod endcaps in high volume production to circumvent galling and,
- to measure the resulting dimensions and calculate the ensuing tolerances by using standard and numerical methods to verify the machining process

3.2. CUTTING TOOL SELECTION

The machining was done on a DMG CTX 310 Ecoline CNC Lathe with a 12-piece turret that could rotate at a maximum speed of 5000 rpm and a maximum power of 16 kW. The machine was fitted with a collet chuck and bar-feeder capable of feeding a 1,5 m rod.

This section aimed to evaluate which combination of cutting tools and inserts are best suited for machining the required dimensions for the endcaps, as well as the best insert material for machining Zry-4 as there are no standard inserts on the market meeting the design presented in Table 2-3, however, this could be ground when using high-speed cutting steel, or it could be moulded, at excessive cost, by insert manufacturers. For this study, it was decided to use standard carbide inserts available from ISCAR.

As mentioned in Chapter 2, Zry-4 is an expensive and highly flammable material that is subjected to galling and tends to work harden due to its ductility. For these reasons, it was decided to first test the machining of the shape of the endcaps using alternative ductile materials. From the literature it was found that some machinists felt that Zr metal has similar machining behaviour to aluminium, however, according to an experienced machinist at Necsa, Zry-4 has similar machining behaviours to stainless steel SS316 (personal communication, Charl Botha, Necsa). For this reason, it was decided that the insert material selections would be conducted on both the insert materials, using aluminium alloy Al-6005-T5 and SS316. There were close collaborations with ISCAR South Africa for the shape of tools that can be used to cut the workpiece material to the required dimensions, illustrated in Figure 3-1.

Due to sensitive information, the drawing (Figure 3-1) was amended just to show the tolerances at which the component needs to be machined, except for the angles, as this is critical to the insert design.

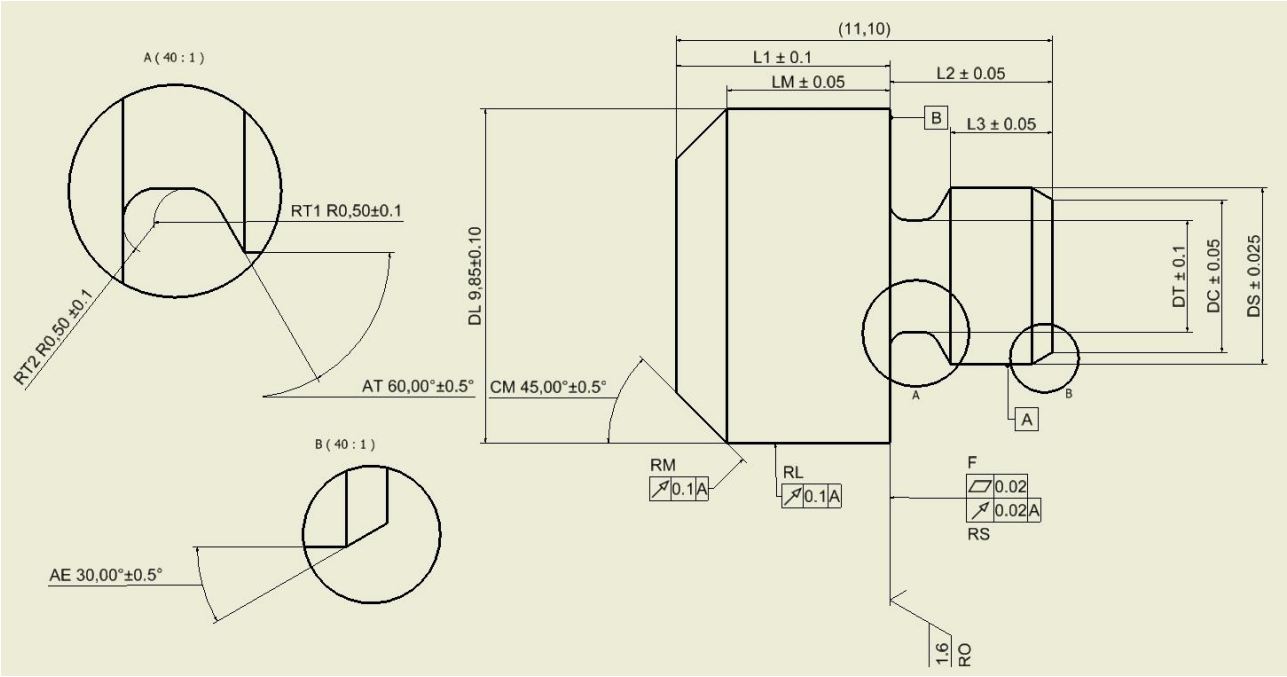

Figure 3-1 – Side-view illustration of the dimensional requirements of the Top-end fuel rod endcap[1]

3.2.1. Profiling

The profile cut of the endcaps is divided into two processes, the roughing cut, and the finishing cut. The roughing cut aims to remove as much as possible material in the shortest achievable time, and the purpose of the finishing cut is to smoothen out the part and remove the material left over from the roughing cut process.

Roughing cut

ISCAR suggested the SVJCL 2020K-11 (Figure 3-2) cutting tool which has a back-clearance angle of a maximum of 50° to be used for the roughing cuts of both the Al-6005-T5 and SS316 trails. The only difference between the Al-6005-T5 and the SS316 was their cutting inserts selection.

[1] Full size drawing is available in Appendix A

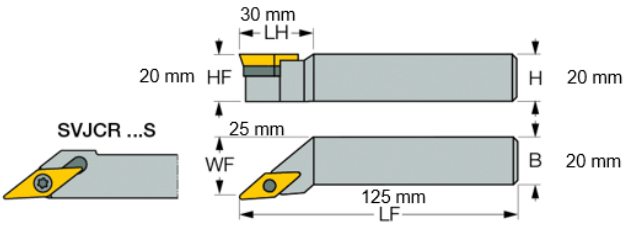

Figure 3-2 – 2D Representation of ISCAR's SVJCL 2020K-11 Tool Holder used for the roughing cut of the nuclear fuel endcaps (iscar.com, 2020a)

The cutting insert used for cutting the Al-6005-T5 was the VCGT-110304-AS IC20 insert (Figure 3-3). The IC20 material used for this insert is of an uncoated carbide that is ideally suited for aluminium and copper alloys (iscar.com, 2020b). This insert has a positive flank angle of 7° with a large positive rake angle and a sharp cutting edge.

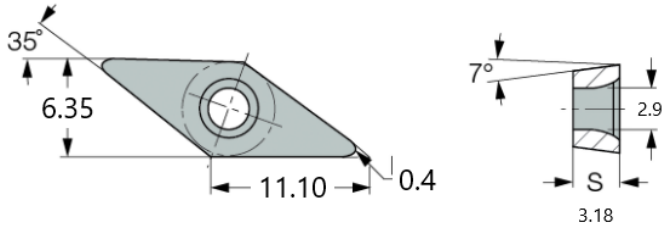

Figure 3-3 – Dimensional Sizes of ISCAR's VCGT-110304-AS IC20 Cutting Insert, used for Aluminium Cutting Roughing Cut (modified after iscar.com, 2018)

The VCMT 110302-F3M insert constructed from ISCAR's IC6025 material (Figure 3-4) was recommended for the machining of SS316. The IC6025 material is constructed of a tough substrate with a medium temperature chemical vapour deposition (MTCVD) of Al_2O_3 and TiCN coatings and ideal for stainless steels and cast steel (iscar.com, 2020c).

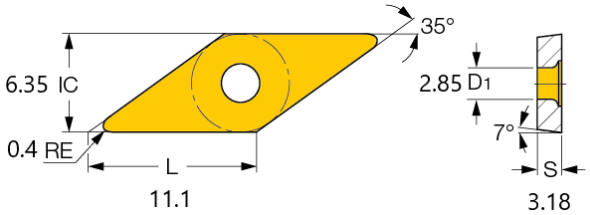

Figure 3-4 – Illustration of the dimensional sizes of ISCAR's VCMT 110302-F3M IC6025 cutting tool insert, used for the profiling cuts of SS316 (modified after iscar.com, 2020d)

Finishing cut

ISCAR suggested the PENTA cutter for the finishing cut of the aluminium and stainless-steel machining trails as part of the investigation on the best insert combination for the machining process. It consists of the PCHR 20-24 grooving tool (Figure 3-5-a) combined with the PENTA 24N100J050 insert (Figure 3-5-b). The PENTA-insert is constructed of an IC908 material which is a hard substrate with excellent chipping resistance coated with a TiAlN PVD coating. This insert could be used to

machine various types of materials, such as martensitic stainless steels, austenitic stainless steels, cast irons, high-temperature alloys, titanium, and hardened cast iron. The recommended grooving rate is between 0,03-0,07 mm/rev.

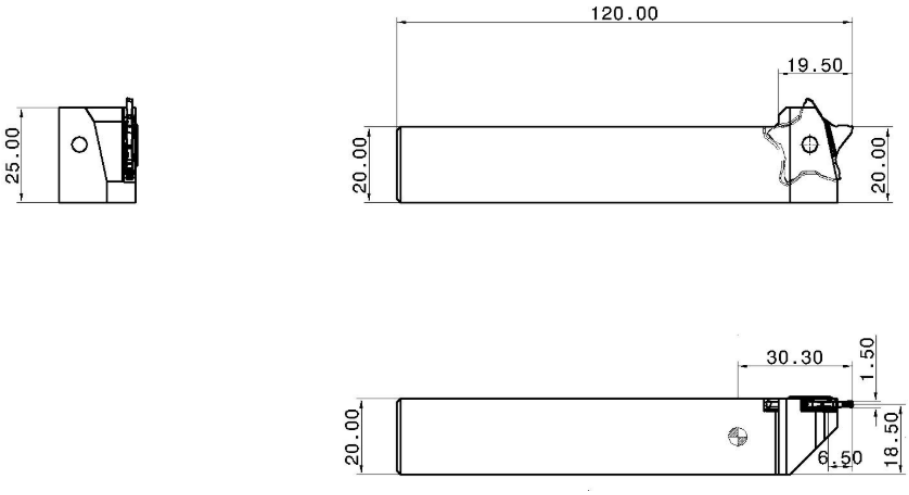

(a)

(b)

Figure 3-5 – a) Dimensional illustration of the PCHR 20-24 grooving tool used for the finishing cut of the endcap (iscar.com, 2020e). b) Dimensional illustration of the PENTA 24N100J050 IC908 insert for the finishing cut of the endcap (iscar.com, 2020e)

During the machining process using the PENTA cutter as the finishing tool, it was found that there was an excessive amount of chattering during the finishing cut. The chattering could have been caused by various aspects of the machining process, but the main explanation for the chattering could have been the cutting depth, as the chattering was mainly found when cutting the diameters DL and DS, in Figure 3-1, where it only needed to remove 0,05 mm of material.

After consultations with an experienced machinist from Necsa (Mr Charl Botha) and the sales consultant from ISCAR (Mr Michael Barnard), it was decided to use the V-shaped insert for both the roughing and finishing cuts. The major concern with this was the back-clearance angle on the tool setup. The maximum achievable back angle using the SVJCL tool is 50° where the required angle is 60°. The Siemens Simulink program was used for the evaluation process of the best-suited insert angle that could be used to achieve the required 60° back angle (AT). In the first simulation, the insert angle was kept at 35°, and after the completion of the simulation, it was found that there was

still stock material on the angle AT, as illustrated in Figure 3-6-a. The insert angle was changed a few times on Simulink, and the best-simulated insert angle was found to be 27°, as it was the first angle where there was no additional material left on the angle AT, as illustrated in Figure 3-6-b. Due to the lack of inserts with an angle of 27°, ISCAR offered to precision grind the conventional V-shaped inserts to meet the requirement for the profile, as shown in Figure 3-6(b).

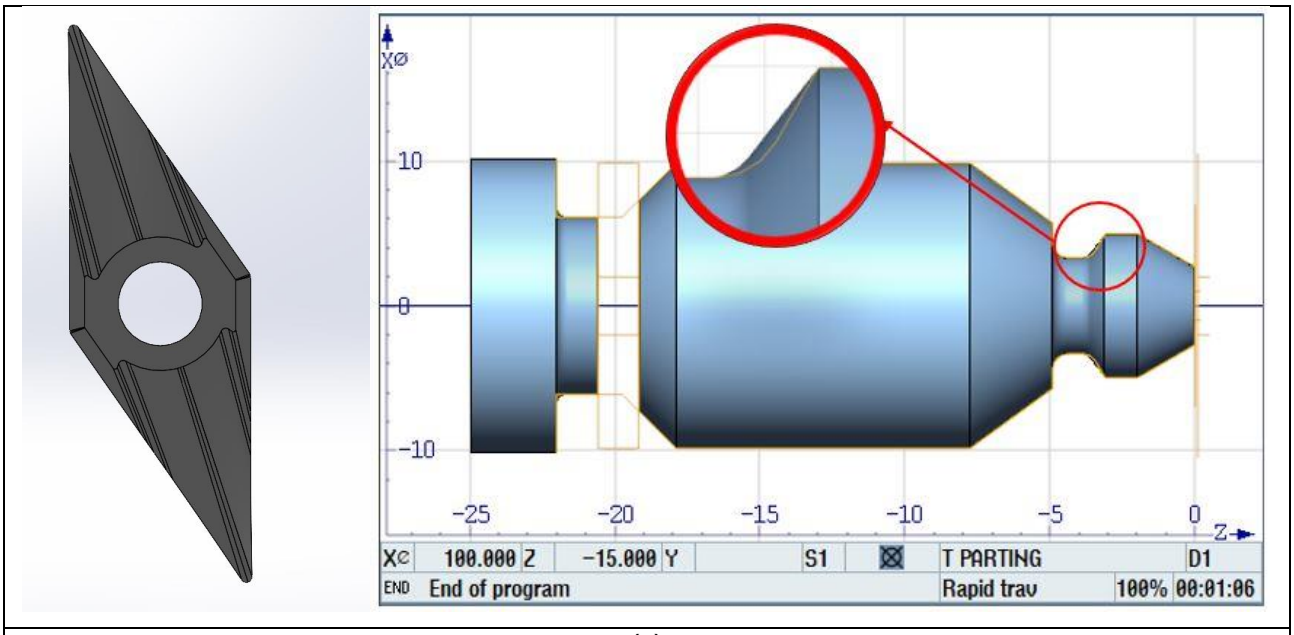

(a)

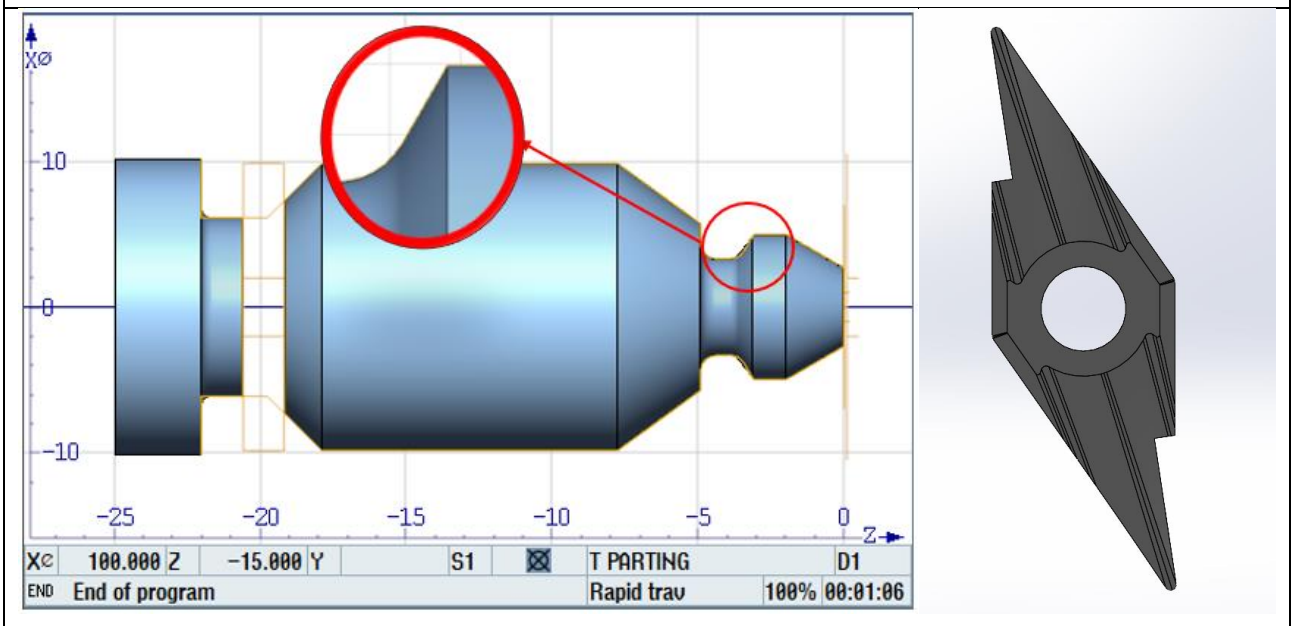

(b)

Figure 3-6 – a) Illustration of the leftover material on the right-hand side of the yellow line, representing the 60°-back angle when using a standard 35° V-shaped insert. b) Illustration of a clear-cut of the 60°-back angle when using a modified V-shaped insert ground to 27°

Table 3-1 - Tool setting on the Siemens Simulink program used to program for the machining of the endcaps.

Loc.	Type	Tool name	ST	D	Length X	Length Z	Radius				Pl. leng
1		UC–Roughing	1	1	0.000	0.000	0.400	←	91.0	35	11.0
2		PENTA – Finishing	1	1	0.000	0.000	0.500		1.000		3.5
3		PARTING	1	1	0.000	0.000	0.160		1.400		15.0
4		UC–Finishing	1	1	0.000	0.000	0.400	←	91.0	27	11.0

After completing the insert evaluations for the required profiles, using SS316 and Al-6005-T5 as workpiece material, the next step was to evaluate the chip formation of Zry-4, using the same shape inserts. The reasons for this evaluation were as follow:

- There was no clear indication of how the chips would form when cutting the Zry-4 with the VCMT & VCGT inserts.
- To evaluate the statements that Zry-4 has similar machining behaviours to SS316 and Al-6005-T5.

Table 3-2 summarises the cutting parameters used to test the chip formation of Zry-4 when using the VCMT or the VCGT inserts. The black values were the last cutting parameters used for the VCMT and the VCGT on the SS316 and the Al-6005-T5, respectively.

Table 3-2 – Machining parameters used to machine Zry-4 with the VCGT and the VCMT inserts to evaluate the chip formation during the machining process (values in black are the initial cutting parameters and values in green are the adjusted cutting parameters)

		VCGT		VCMT	
		Roughing	Finishing	Roughing	Finishing
Cutting Speed	rpm	5000	5000	5000	5000
		1000	2500	1000	2500
Feed Rate	mm/min	0,2	0,05	0,12	0,1
		0,25	0,09	0,15	0,12
Cutting Depth	mm	0,5	0,1	0,8	0,1
		0,8	0,07	2,0	0,1

Figure 3-7(a) and Figure 3-7(b) are photos of the chip formations found after machining two BECs using the black machining parameters presented in Table 3-2. Figure 3-7(a) is a photo of the chip formation result of the VCMT insert, generally used for machining SS316, and Figure 3-7(b) is a photo of the chip formation result after using the VCGT insert, generally used for aluminium, on the Zry-4. From both these photos, it is visible that there is no big difference in the chip formation at this current stage. Both chip formations are coarse, and the parts were entangled inside the chips.

After consulting Mr Botha regarding the issue at hand, the cutting speeds were reduced, and the feed rates were increased, as suggested by the literature found. The cutting parameters were as presented by the green values in Table 3-2. From Figure 3-7(c) and Figure 3-7(d), there is a clear

visible difference between the chip formation results of the cutting process using the VCGT insert - Figure 3-7(d) - and when using the VCMT insert - Figure 3-7(c). The chips formed when using the VCGT insert are long, fine strings of chips that flow easily away from the cutting zone, whereas the chip formation using the VCMT insert are still coarse chips that entangle the part as it is parted from the stock material.

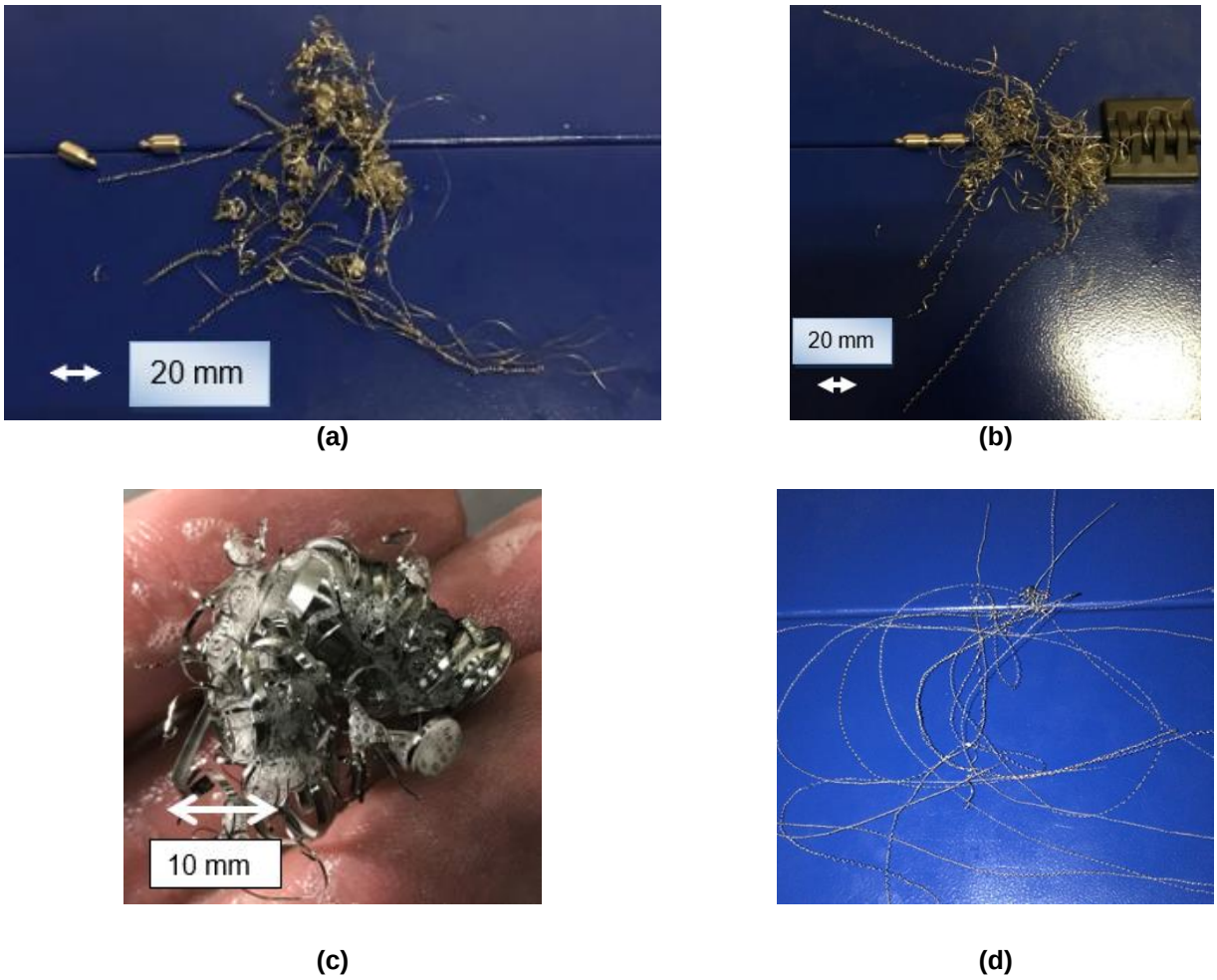

(a) **(b)**

(c) **(d)**

Figure 3-7 – a) Image of the coarse shavings formed during the machining of the Zry-4 at 5000 rpm with the VCMT insert. b) Image of the shavings formed during the machining of the Zry-4 at 5000 rpm using the VCGT insert (there was no difference between the shape and the hardness of the shavings between image a and b). c) Image of the coarse shavings formed during the machining of the Zry-4 at 2500 rpm when using the VCMT insert. d) Image of the fine ringlets formed during the machining of Zry-4 at 2500 rpm when using the VCGT insert

For this reason, the VCGT insert was chosen as the cutting insert for the machining of Zry-4 endcaps. The reasons why the VCGT insert had such a positive result, was due to the large positive flank angle and the sharpness of the cutting edge. Thus, it was decided to use the VCGT-inserts for all

the Zry-4 manufacturing, as the chips move away from the cutting zone as it removes the material from stock material, and it is envisaged that it would also aid in greater cooling.

3.2.2. Parting procedure

The TANG-GRIP IQ tool (Figure 3-8) in combination with the TAG R1.4J-8D insert (Figure 3-9) was recommended by ISCAR for the parting process. The insert is made from ISCAR's IC808 material, which is a hard, submicron substrate with excellent chipping resistance coated with a "SUMO TEC" TiAlN PVD coating. The insert could be used for parting a vast variety of workpiece materials, such as martensitic stainless steels, austenitic stainless steels, cast irons, high-temperature alloys, titanium, and hardened cast iron.

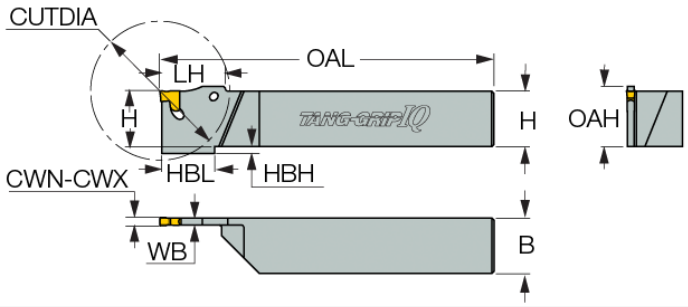

CWN	CWX	H	B	WB	OAL	OAH	LH	HBL	HBH	CUTDIA
1.40	1.45	20.0	20.0	1.05	140.00	20.0	-	16.00	-	30.0

Figure 3-8 – Dimensional illustration of ISCAR's TANG-GRIP IQ tool holder used for the parting process (iscar.com, 2020f)

Figure 3-9 – Dimensional illustration of ISCAR's TAG R1.4J-8D IC808 insert used for the cut-off cut of the nuclear fuel endcaps (iscar.com, 2020g)

The TANG-GRIP IQ parting tool was later replaced with ISCAR's DGTL 20B-1.4D30 parting tool, (Figure 3-10). The advantage of this new tool holder is that the insert is held in place using a screw mechanism, instead of the operator pressing the insert into place. This creates less opportunity for misaligning the tooltip.

The DGTL parting tool uses the DGL 1400JS-15D IC328 as a cutting insert (Figure 3-11) which is made of a tough substrate with a thin PVD coated layer of TiCN, considered to be suitable for low to

medium cutting speeds. It is recommended by ISCAR for unstable machining conditions and this insert is also used for machining ductile titanium alloys.

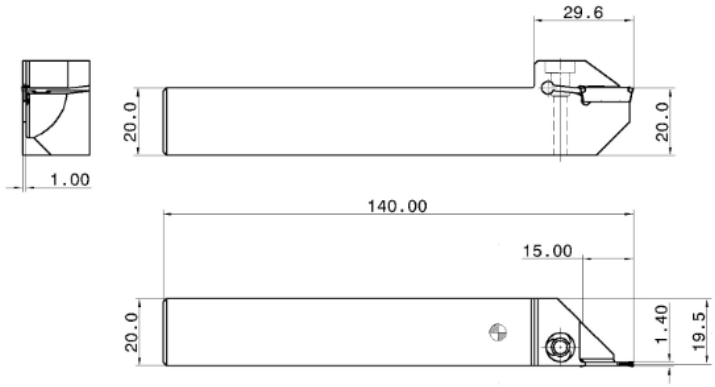

Figure 3-10 – Dimensional illustration of ISCAR's DGTL 20B-1.4D30 parting tool used for the parting operation of Zry-4 (iscar.com, 2020h)

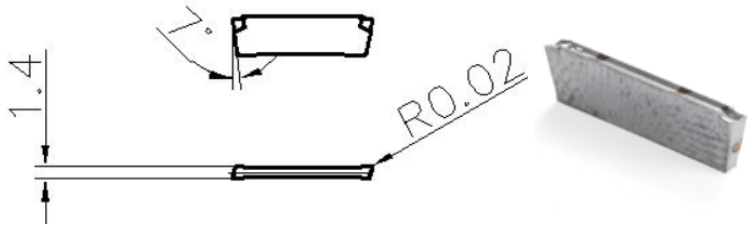

Figure 3-11 – The model on the left illustrates the basic dimensions of ISCAR's DGL 1400JS-15D insert IC328 (a TiCN coated ceramic) used for the parting operation of Zry-4. The model on the right-hand side is a photograph of the insert (iscar.com, 2020i)

3.2.3. Precision grinding

After parting was completed, an EWAG precision grinder was used to remove the stock material left after the component was parted from the bar material (Figure 3-12). The EWAG precision grinder (Figure 3-13) could remove 0,1 mm of material in the longitudinal direction.

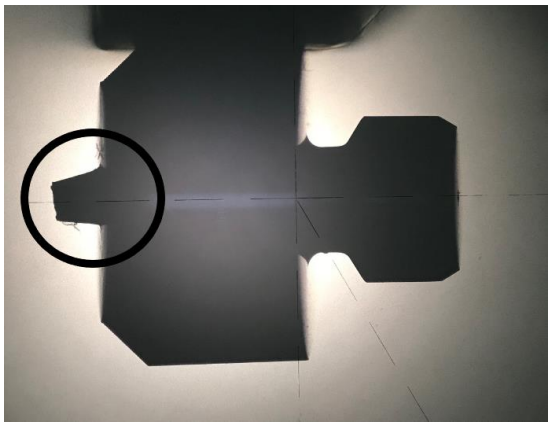

Figure 3-12 – Image of a BEC on the profile projector encircling the leftover material at the back of the endcap.

Figure 3-13 – Image of a Necsa artisan using the EWAG precision grinder to cut the endcaps to size.

3.3. ZRY-4 CUTTING PARAMETER SELECTION

The preliminary Zry-4 machining trails of the nuclear fuel endcaps had two goals, namely:

- to find the best combination of cutting tools for the required profile, and
- to find the best cutting parameters for the components.

In Section 3.2, the discussions were mainly based on the cutting tool selection, and the machining process used to machine the endcaps to their optimal form. In this section, the focus would be on the final parameters used for the machining process of the endcaps.

3.3.1. Cutting fluid

As mentioned in Section 2.5, there are two types of coolant applications that seem to be ideal for the machining of Zry-4, the high-pressure tool cooling and cryogenic cooling. However, both applications required additional modifications to the lathe and due to budget constraints, it was not possible to make these changes, and conventional flood cooling was performed. The coolant used for the machining process was the Flexilube BIOKOOL CU-2, which is a biostatic coolant mixed with a 20:1 ratio to water.

There was a loss of coolant incident during the initial tooling setup, where the machine lost coolant while cutting a bit of Zry-4 and the shaving caught fire immediately, due to spontaneous ignition. The shavings were burning with a bright white light, but they were extinguished very quickly when the coolant was reapplied. As highlighted in the literature study, the one biggest concern with the machining of Zry-4 is the risk of spontaneous ignition if the cutting environment is not properly controlled. As it happened in this case, the shavings were ignited by the heat generated at the cutting zone and due to the oxidised surfaces of the shavings at the edge of the cutting zone, the shavings caught fire. If this incident were not controlled properly the fire caused by the spontaneous ignition of the Zry-4 could have gotten out of hand and it could have led to a catastrophic failure, due to the extreme exothermic reaction Zr has with oxygen - as explained in the Literature Study. To prevent this from happening again, it was mandatory to have the coolant always running during the setup and machining procedures.

3.3.2. Cutting parameters

After machining 64 Zry-4 Bottom-Endcaps (further abbreviated as BECs) and 66 Zry-4 Top-Endcap (TECs), the cutting parameters were verified by machining two batches of 50 endcaps each (50 TECs and 50 BECs). The machining parameters used for the final verifications were as presented in Table 3-3. The cycle time for these machining parameters was 1’7” for the TEC and 1’20” for the BEC, these times do not include the time spent on the EWAG to grind the endcaps to size.

Table 3-3 – Summary of the final cutting parameters used for the machining of Zry-4 endcaps.

Description	Insert Used ISCAR Part Nr	Cutting Speed	Feed Rate	Depth of Cut
		rpm	mm/min	mm
Roughing Cut	VCGT	1000	0,25	0,80
Finishing Cut	VCGT	2500	0,09	0,03
Parting	DGL	2500	0,03 – 0,07	

3.4. DIMENSIONAL INSPECTION OF ENDCAPS

After completing the batch of 50 endcaps, the endcaps were measured endcap by endcap to capture all the dimensional sizes of the batch for process analysis. The dimension inspection of these endcaps is a critical part of the project as this was the only way that could be used to verify that the cutting parameters are adequately set for the requirements. Two types of measurement techniques were used for the measuring of the endcaps, namely:

- conventional measurement techniques, and
- coordinate measurement techniques

3.4.1. Conventional measurements

The purpose of the conventional measurement techniques was to evaluate whether the endcaps met the specification requirements as per drawings presented in Figure 3-1.

The measurements were done with the aid of conventional methods, such as the Microtechnica Titanus 6 profile projector [PP] (Figure 3-14) and the Mitutoyo Quickmike digital micrometre (Figure 3-15). All the equipment used in this section was supplied by Necsa and the measurements were done in their inspection facility. Table 3-4 tabulates the equipment used to measure the dimensional sizes of the components as well as the dimensions measured.

Figure 3-14 – Photograph of the Microtecnica Titanus 6 at Necsa used for the measurement of the longitudinal dimensions and diameters of the fuel rod endcaps

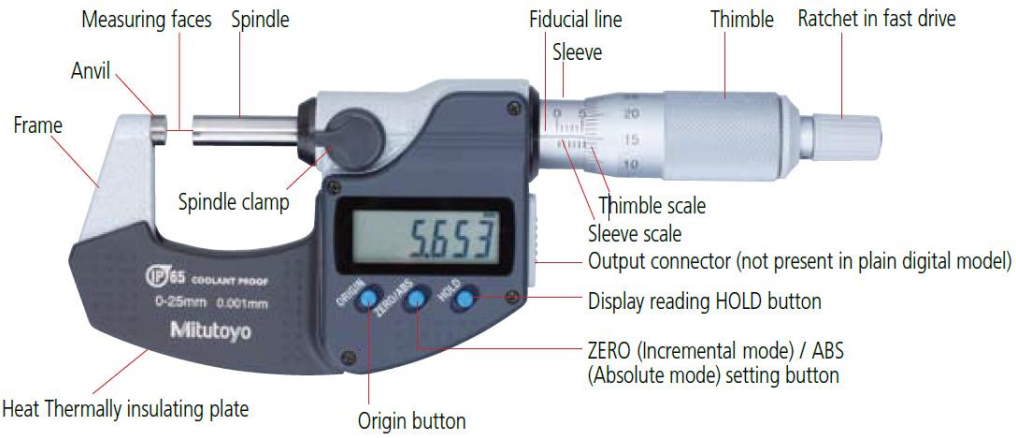

Figure 3-15 – Illustration of the Mitutoyo QuickMike used to measure small diameters of the fuel rod endcaps (Mitutoyo, S.S.)

Table 3-4 – Table of all the conventional equipment used to measure the nuclear fuel TEC

Type	Make	Model	Size	Resolution
Digital Micrometre	Mitutoyo	QuickMike	0 – 25 [mm]	0.001 mm
Profile Projector (PP)	Microtechnica	Titanus	Dimensional measurement	0.001 mm
			Angle measurement	0° 01’
Radius Overlay Chart (using the PP)			0.4 – 0.5 [mm]	0.02 mm

3.4.2. Coordinate measurement technique

The purpose of the coordinate measurement techniques was to verify the measurement results obtained from the conventional measuring equipment. The DEA Global coordinate-measurement

machine (CMM) (owned by the AIT at TUT) was used for this purpose. The DEA Global CMM is a bridge-type CMM (Figure 3-16 a) with a touch-trigger probe (Figure 3-16 b), with a probe diameter of 0,5 mm.

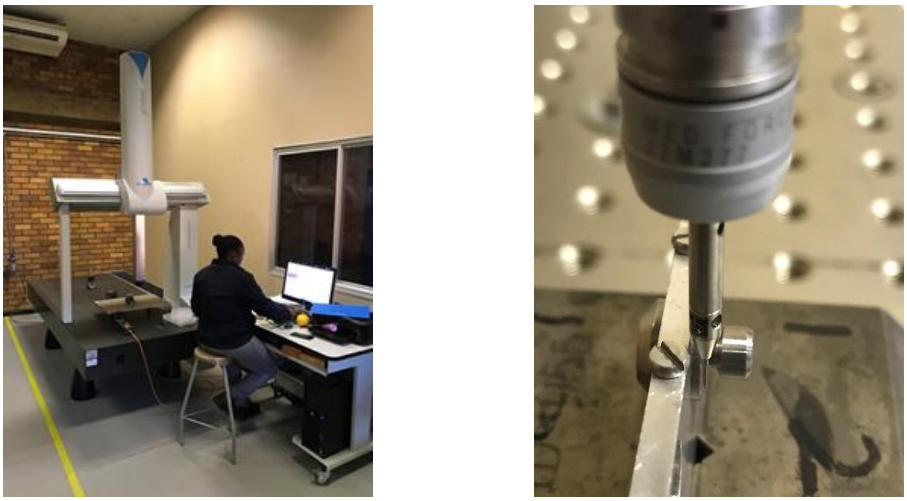

(a) **(b)**

Figure 3-16 – (a) Photograph of the DEA Global bridge-type CMM. (b) Image of the Renishaw touch-trigger probe system showing the relation of the probe to that of the endcap.

3.4.3. Measurement evaluation criteria

A three-rule evaluation system was introduced to evaluate the series of results obtained for each dimensional specification of the endcaps, using the different measurement techniques. The *three-rule* system used to evaluate the measurements were as follow:

- The average of the dimensional measurement must be within specification as per the drawings supplied at the beginning of this Chapter (Figure 3-1).
- The sampling by the variable system is used for the lot evaluation. For the sampling by variable, it was decided to use an AQL of 1,0 with a tightened inspection plan. Furthermore, it was also decided to slip the upper limit and lower limit as mentioned in Section 2.4, meaning that the data needs to comply with the following:
    - $Q_u \geq k \; and \; Q_L \geq k$ – Equation 2-6
    - $k = 2.052$ – Table 2-8

  The dimensions with single-sided tolerances, such as the geometric tolerances, need to comply with the following rule:
    - $Q_U \geq k$
    - $k = 2.052$ – Table 2-8
- The Cp_k the value must be higher than 1,33 to meet the nuclear standard for the confidence interval of 95.

Table 3-5 – Summary of the acceptance criteria for the measurement of the endcaps

Criteria	Rule
Sample average	$L \geq \bar{x} \leq U$
Double-sided tolerance	$Q_U \geq k$, and $Q_L \geq k$
Single-sided tolerance	$Q_U \geq k$
Cp_k	$Cp_k > 1{,}33$

3.4.4. Measurement evaluation

Before starting with the measurements of the machined components, a question regarding the repeatability of the measurement methods needed to be answered. It was decided to take one random component and measure it with the different techniques, to be able to justify whether a measurement error was due to the measurement method or due to something happening at the machining side. Three additional methods were added for this study to compare the repeatability of the current techniques used for this study with more advanced methods. The additional equipment added for this study were:

- Carl Zeiss O-Select - an optical non-touch probe that measures the components automatically.
- Carl Zeiss Duramax - a column type CMM that uses a 0,3 mm line scan touch probe to measure the dimension.
- Carl Zeiss O-Inspect - a bridge-type multi-sensor CMM that uses line scan touch probes in combination with an optical scanner to measure the tiny dimensions of the part.

4. DIMENSIONS AND ANALYSIS OF THE MACHINED TOP-ENDCAPS

The batch of 50 Zry-4-TECs was machined using the machining parameters as presented in Table 3-3. The ensuing dimensions of machined samples were measured making use of the conventional techniques, the Coordinate-Measurement Machine (CMM) and the procedures described in the previous Chapter. The data of these measurements are presented in Table XL and Table XLI in 7.APPENDIX D.

Before the measurement of the 50 TECs was completed a repeatability test on the two methods (as discussed in Section 3.4) was conducted. The results (Table XLVII in 7.APPENDIX C) of these measurements were used to calculate the measurement capability of the technique to measure the dimension, using the AQL approach explained in Section 2.4.

After measuring and analysing the measurement results of the 50-TEC batch, the data obtained from the profile projector and the CMM were compared to evaluate and verify the success of the machining process of the endcaps, using the acceptance criteria summarized in Table 3-5.

The following calculations were conducted for the analysis of the data to get a better understanding of the consistency of the machining process:

- The average difference of the measurement against the machined size

$$\Delta X = \frac{\sum \Delta x}{N} \qquad \textbf{Equation 4-1}$$

  Where:
  - ΔX is the average difference of the data.
  - $\sum \Delta x$ is the sum of all the differences in the machined size.
  - N is the number of samples.
- IN/OUT criteria are evaluating whether the average difference is within the tolerance of the specific dimension

$$LL \geq \Delta X \leq UL \qquad \textbf{Equation 4-2}$$

  Where:
  - LL is the lower tolerance limit of the dimension, shown in Figure 3-1
  - UL is the upper tolerance level of the dimension, shown in Figure 3-1
- The range is the difference between the highest value of the band and the lowest value of the data band, i.e., if the highest value is 0,075 mm for L1 and the lowest value is 0,052 mm for L1, then it means that the total data range for L1 is 0,023 mm.
- Standard deviation is a measure of the amount of dispersion within a set of values.

$$\sigma = \sqrt{\frac{\sum(x_i - \mu)^2}{N}}$$ **Equation 4-3**

Where:

- σ – population standard deviation
- N – number of samples
- x_i – each value of the population
- $\mu = \Delta X$ – the population means

- AQL, as explained in Section 2.4, is a measure of the maximum allowed percentage of defective components within the lot. This is calculated by using Equation 2-1 and Equation 2-4 and is evaluated using Equation 2-7 and Equation 2-8.
- CP_k is a measure calculating the number of standard deviations. The specification limits are from the centre of the process (Nielsen, 2018), and is calculated as follow:

$CP_k = \min(CP_L, CP_U) \geq 1.33$	**Equation 4-4**
$CP_L = \frac{\Delta X - LL}{3 * \sigma}$	**Equation 4-5**
$CP_U = \frac{UL - \Delta X}{3 * \sigma}$	**Equation 4-6**

Even though the repeatability results will show the results of other measuring methods, the focus for this study was only on the results of the PP and the point-scan CMM, as these were the methods used to evaluate the batch machining process.

Furthermore, all limits set in this chapter were set according to the specification in Figure 3-1.

4.1. LENGTH MEASUREMENT RESULT ANALYSIS

4.1.1. Length L1

L1 is the distance between the middle face of the endcap and the end of the endcap (Figure 3-1). During manufacturing, the endcap was parted from the stock material, using the parting tool with an additional 0,1 mm that still needed to be removed using the EWAG precision grinder as presented in Section 3.3.2.

Table 4-1 – Table showing the results of the data analysis of the 9 measurements taken of L1 during the repeatability test using the Point-scan CMM, Line-scan CMM, Multi-sensor CMM, optic measuring machine and the Profile Projector.

Position Name	Equipment Used	Tolerance	Unit	Average Difference	IN/OUT	Range	Standard Deviation	AQL	CPk	Acceptable/ Unacceptable
L1	Point Scan CMM	0.100	mm	0.056	IN	0.023	0.007	6.38	2.13	Acceptable
	Line Scan CMM			0.047	IN	0.001	0.000	154.53	51.51	Acceptable
	Multi-Sensor CMM			0.053	IN	0.000	0.000	580.47	193.49	Acceptable
	Optic Measuring Machine	-0.100		0.064	IN	0.013	0.004	9.09	3.03	Acceptable
	Profile Projector			0.046	IN	0.025	0.008	7.18	2.39	Acceptable

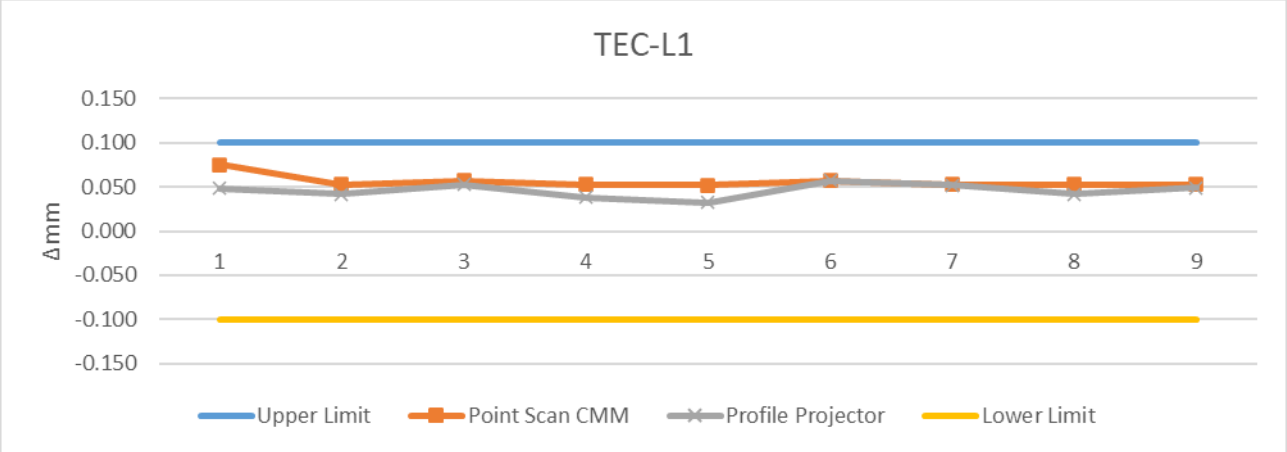

Figure 4-1 – Plot of the difference in measurement of the machined size in mm obtained in the repeatability test of the TEC length L1, using the PP and the CMM with an upper and lower tolerance, indicated with the blue and yellow lines, respectively.

As mentioned in Section 3.4.4, a repeatability test of the measurement methods was added to evaluate the repeatability of the measurement method. From Figure 4-1 and Table 4-1, it is evident, that the repeatability of the Point-scan CMM is better than that of the PP as the Point-scan CMM has a standard deviation of 7µm in comparison with the 8µm of the PP. However, the CP_k of the PP is again better than that of the Point-scan CMM, with a 2,39 in comparison to the 2,13 for the Point-scan CMM. This could be because the mean of the Point-scan data is higher than that of the PP, with a 10µm difference between the sample means of the CMM and the PP.

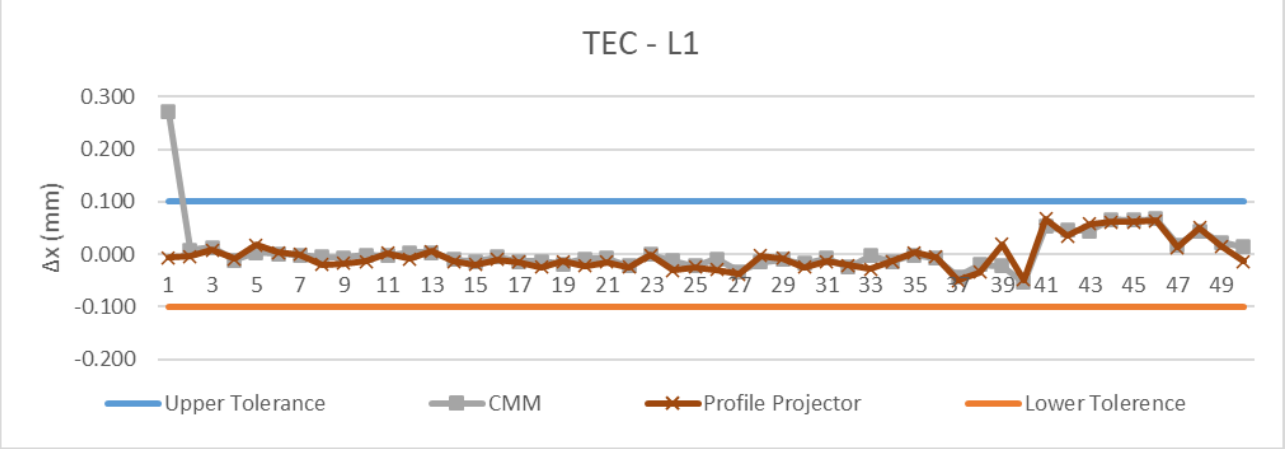

Figure 4-2 – Plot of the length L1 of 50 machined TEC, showing that the sample TEC-01 was measured outside of specification and that samples TEC-41 to TEC-46 were closer to the upper limit with an upper and lower tolerance, indicated with the blue and orange lines, respectively, showing TEC-01 measured outside of the tolerance band, using the CMM.

Table 4-2 – Table showing the analysis results of the average measurement difference, measurement range, process standard deviation, the AQL-value and the CP_k-value obtained from the production run (50-TEC) for the length L1 with a tolerance of ± 0,10 mm

Dimension	Equipment Used	Machined Tolerance	Unit	Average Difference	IN/OUT	Range	Standard Deviation	AQL	CPk	Acceptable/ Unacceptable
L1	CMM	0.100	mm	0.006	IN	0.324	0.046	2.028	0.676	Unacceptable
	Profile Projector	-0.100		-0.003	IN	0.117	0.029	3.375	1.125	Unacceptable

Figure 4-2 is a graphical illustration of the measurement results obtained for the length L1 of the top-endcap. From Figure 4-2 it is noticed how closely the CMM measurement and the conventional measurements compare to each other. Furthermore, there are two noticeable events in Figure 4-2:

- The first measurement of the batch components seems to be an outlier, as the component measures above the upper tolerance specified for the dimension.
- As for the last few components, the machining tends to have a downward trend between TEC-1 and TEC-39 and then there is a sudden spike between TEC-40 and TEC-41

After the analysis of the measurement data captured of TEC-L1, presented in Table 4-2, it was evident that TEC-L1 failed to comply with the AQL test and the CP_k for the measurements obtained by the CMM and it failed to comply with the CP_k criteria for the measurements done using the PP. After an analysis of Figure 4-2, it became evident that something happened in the machining process while cutting TEC-41 using the EWAG precision grinder.

With an understanding of the machining process using the EWAG to machine the backside of the component and looking at the measurement capability of both methods (Figure 4-1 and Table 4-1), it was evident that there was some sort of human error involved while the operator was cutting the length L1 using the EWAG from component 40 onward, and this could have been the reason for the failure of the CP_k value of the parts. The reason for the CMM failing the AQL test of L1 is due to the first component which was measured outside the tolerance band.

4.1.2. Length L2

Table 4-3, tabulates the result of the data analysis of the repeatability test measuring one random TEC's length, L2. Figure 4-3 is a visual representation of the data captured during the repeatability test of the length L2, using both the PP and the CMM. From these results, it was evident that the

repeatability of the CMM was far greater than that of the PP, with a CP_k of 3,87 for the CMM vs. a 0,90 for the PP.

Table 4-3 – Table showing the results of the data analysis of the 9 measurements taken of L2 during repeatability test using the Point-scan CMM, Line-scan CMM, Multi-sensor CMM, optic measuring machine and the Profile Projector.

Position Name	Equipment Used	Tolerance	Unit	Average Difference	IN/OUT	Range	Standard Deviation	AQL	CPk	Acceptable/ Unacceptable
L2	Point Scan CMM	0.050	mm	-0.017	IN	0.010	0.003	11.62	3.87	Acceptable
	Line Scan CMM			-0.022	IN	0.001	0.000	165.33	55.11	Acceptable
	Multi-Sensor CMM			-0.021	IN	0.000	0.000	270.43	90.14	Acceptable
	Optic Measuring Machine	-0.050		-0.029	IN	0.010	0.003	6.38	2.13	Acceptable
	Profile Projector			-0.021	IN	0.030	0.011	2.71	0.90	Unacceptable

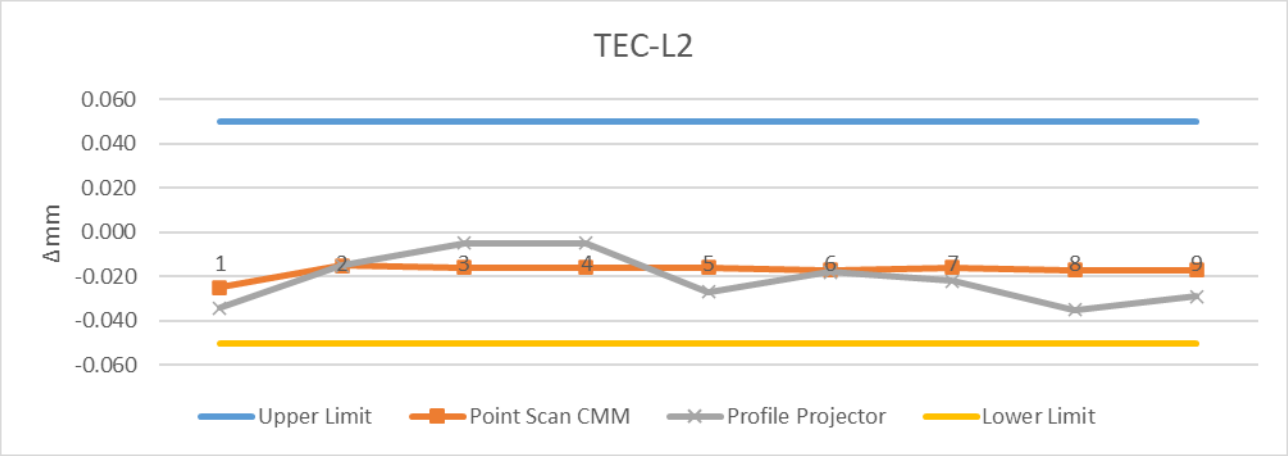

Figure 4-3 – Plot of the measurement results obtained in the repeatability test of the TEC length L2, using the PP and the CMM with an upper and lower tolerance, indicated with the blue and yellow lines, respectively.

Table 4-4 tabulates the data analysis results of length L2, measured from the production run. From these results, it became evident that both the measurements with the CMM and the PP satisfied the acceptance criteria set in Section 3.4.3. However, the data received from the CMM was more consistent in comparison to the data captured using the PP, with a CP_k of 1,701 and a standard deviation of 6µm for the CMM in comparison to a CP_k of 1,413 and a standard deviation of 10µm for the PP. This is also visible in Figure 4-4, illustrating the measurements obtained for the dimensional inspection of L2.

Table 4-4 – Table showing the analysis results of the average measurement difference, measurement range, process standard deviation, the AQL-value and the CP_k-value obtained from the production run (50-TEC) for the length L2 with a tolerance of ± 0,050 mm.

Dimension	Equipment Used	Machined Tolerance	Unit	Average Difference	IN/OUT	Range	Standard Deviation	AQL	CPk	Acceptable/ Unacceptable
L2	CMM	0.050	mm	0.019	IN	0.025	0.006	5.104	1.701	Acceptable
	Profile Projector	-0.050		0.006	IN	0.043	0.010	4.239	1.413	Acceptable

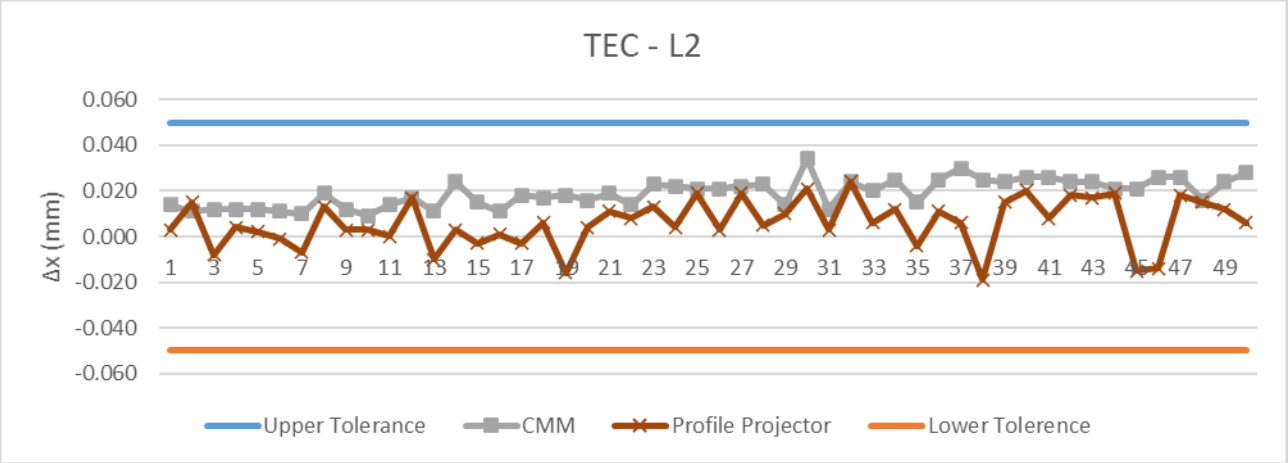

Figure 4-4 – Plot of the measurement results comparison between the PP and CMM measuring methods of the length TEC-L2 with an upper and lower tolerance, indicated with the blue and orange lines, respectively.

Furthermore, there is a slight upward trend observed in data of the CMM in Figure 4-4 as TEC-1 and TEC-50 differs by 14µm. This could be an indication of slight tool wear throughout the machining procedure.

4.1.3. Length L3

Length L3 of the TEC is the distance between the face of the endcap and the point where the diameter DS and angle AT intersect, as illustrated in Figure 3-1.

Table 4-5 – Table showing the results of the data analysis of the 9 measurements taken of L3 during the repeatability test using the Point-scan CMM, Line-scan CMM, Multi-sensor CMM, optic measuring machine and the Profile Projector.

Position Name	Equipment Used	Tolerance	Unit	Average Difference	IN/OUT	Range	Standard Deviation	AQL	CPk	Acceptable/ Unacceptable
L3	Point Scan CMM	0.050	mm	-0.004	IN	0.009	0.003	15.95	5.32	Acceptable
	Line Scan CMM			0.012	IN	0.001	0.000	107.89	35.96	Acceptable
	Multi-Sensor CMM			0.023	IN	0.001	0.000	101.56	33.85	Acceptable
	Optic Measuring Machine	-0.050		0.027	IN	0.006	0.002	13.08	4.36	Acceptable
	Profile Projector			0.012	IN	0.016	0.005	7.54	2.51	Acceptable

From Table 4-5, it is evident that both the CMM and the PP is capable of measuring the length L3, however, the CMM has greater constancy during the measurement, as the CP_k of the CMM is 5,32 whereas the CP_k of the PP is 2,51. This is also visible in Figure 4-5. Furthermore, it is also evident from this figure that there is a rather noticeable difference in the average measurement of the component as the measurement average of the CMM is less than that of the PP.

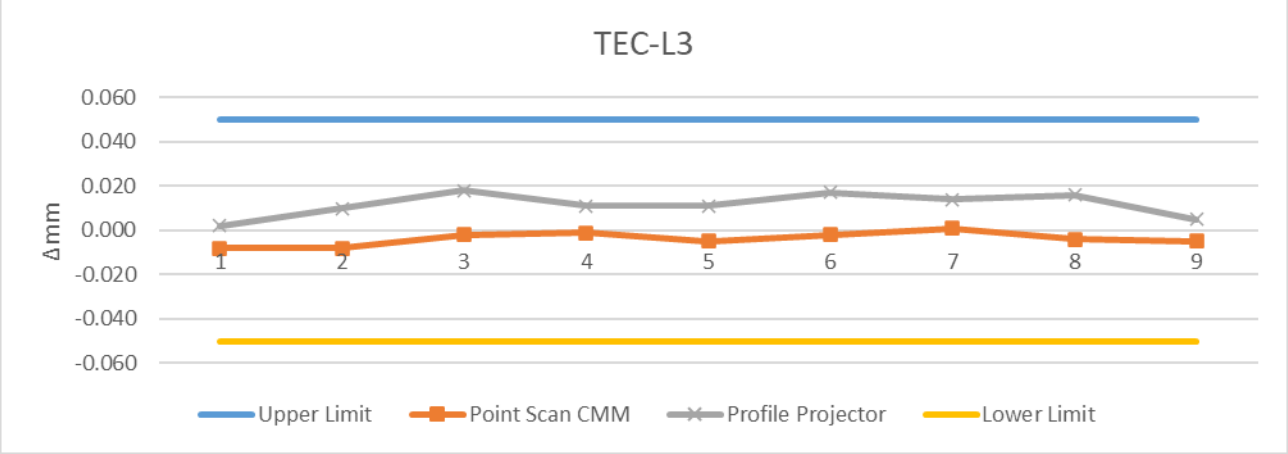

Figure 4-5 – Plot of the measurement results obtained in the repeatability test of the TEC length L3, using the PP and the CMM with an upper and lower tolerance, indicated with the blue and yellow lines, respectively.

The first clear observation that could be made from Figure 4-6, is the fact that both the measurement results obtained using the CMM and the PP, are above the upper tolerance line (blue line on Figure 4-6), suggesting that the dimension was manufactured outside the limits. The second observation is that the measurement result of the PP is a lot more constant than that of the CMM and it has a slight upward trend over the 50 parts.

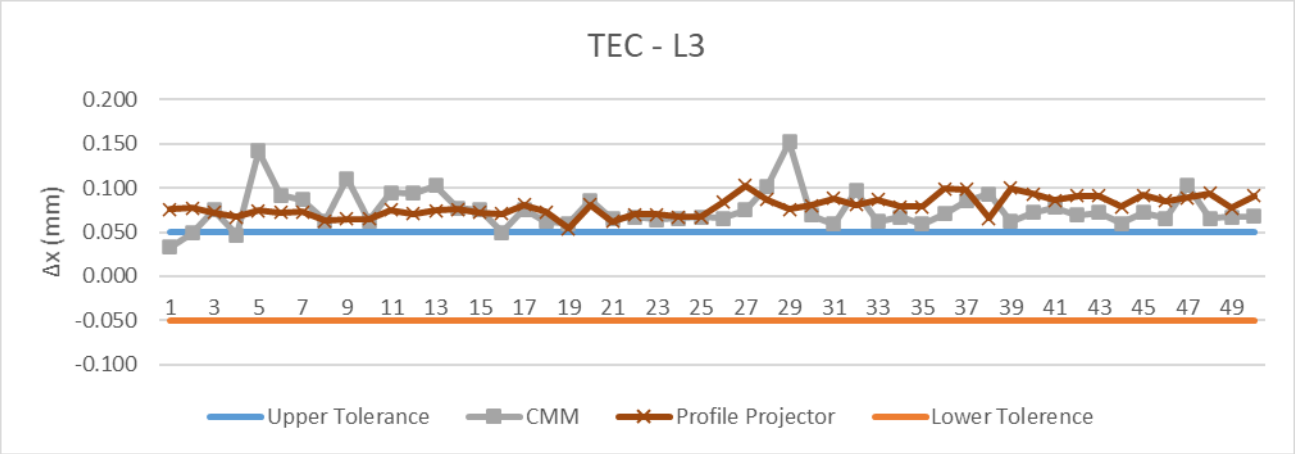

Figure 4-6 – Plot of the measurement results comparison between the PP and CMM measuring methods of the length TEC-L3 with an upper and lower tolerance, indicated with the blue and orange lines, respectively.

From Table 4-6 and Figure 4-6, it is evident that there is a problem with the dimension, as it is machined bigger than the allowable tolerance for this dimension. On average, the dimension was about 80 µm bigger than the machined value.

Table 4-6 – Table showing the results of the average measurement difference, measurement range, process standard deviation, the minimum value of the sampling procedure and the CP_k-value obtained from the production run (50-TEC) for the length L3 with a tolerance of ±0,05 mm

Dimension	Equipment Used	Machined Tolerance	Unit	Average Difference	IN/OUT	Range	Standard Deviation	AQL	CPk	Acceptable/ Unacceptable
L3	CMM	0.050	mm	0.076	OUT	0.119	0.022	-1.188	-0.396	Unacceptable
	Profile Projector	-0.050		0.079	OUT	0.049	0.011	-2.607	-0.869	Unacceptable

When looking at the machining procedure of L3, it is evident that there are some alterations needed to ensure that something like this would not happen again. One of these alterations would be to change the dimension on the cutting program, to make it 0,08 mm smaller (2,92 mm instead of 3,00 mm).

Focussing on the measurement method and looking at the measurement errors reflected in Table 4-6 of the CMM measurements could be directly linked to the measuring procedure used. For the PP, the operator is measuring a physical point on the PP display, whereas for the CMM, the machine is generating an extrapolated point between the values received from the diameter DS and the angle AT. If one of those measurements have any inconsistency in the measurements obtained, the probability of having inconsistency in the results of L3 is high.

4.1.4. Length LM

Length LM is the length from the flat surface and the intersection point of diameter DL and chamfer CM. Table 4-7 tabulates the measurement analysis results of the repeatability test of TEC-LM, using various measurement techniques, and Figure 4-7 is the graphical illustration of the repeatability results measuring the length LM.

Table 4-7 – Table showing the results of the data analysis of the 9 measurements taken of LM during repeatability test using the Point-scan CMM, Line-scan CMM, Multi-sensor CMM, optic measuring machine and the Profile Projector.

Position Name	Equipment Used	Tolerance	Unit	Average Difference	IN/OUT	Range	Standard Deviation	AQL	CPk	Acceptable/ Unacceptable
LM	Point Scan CMM	0.050	mm	0.025	IN	0.027	0.008	3.09	1.03	Unacceptable
	Line Scan CMM			0.011	IN	0.002	0.000	79.11	26.37	Acceptable
	Multi-Sensor CMM			0.006	IN	0.001	0.000	219.77	73.26	Acceptable
	Optic Measuring Machine	-0.050		0.020	IN	0.011	0.003	9.08	3.03	Acceptable
	Profile Projector			0.006	IN	0.049	0.014	3.22	1.07	Unacceptable

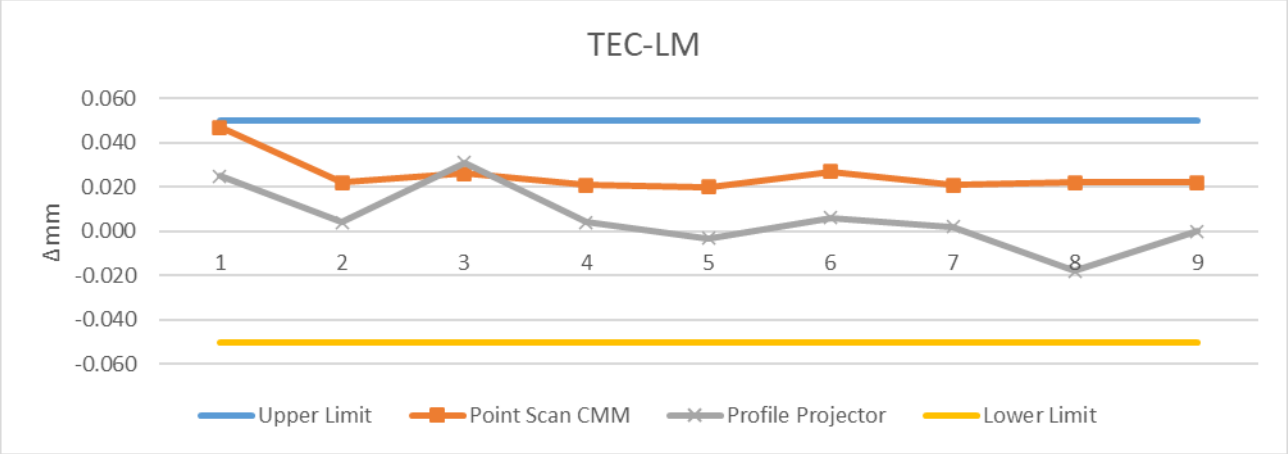

Figure 4-7 – Plot of the measurement results obtained in the repeatability test of the TEC length LM, using the PP and the CMM with an upper and lower tolerance, indicated with the blue and yellow lines, respectively.

From the results presented in Table 4-7 and Figure 4-7, both the CMM and PP fails consistency when used for the measurement of length LM. Furthermore, the PP measured the sample smaller than the CMM, on average, with a 0,019 mm difference between the two techniques.

When analysing Figure 4-8 and comparing the trend to the trend found in Figure 4-7, it is visible that the PP's results are again less than that of the CMM. The CMM results hover around -0,02 mm whereas 15 of the samples measured using the PP results are measured below the lower tolerance (orange line on Figure 4-8).

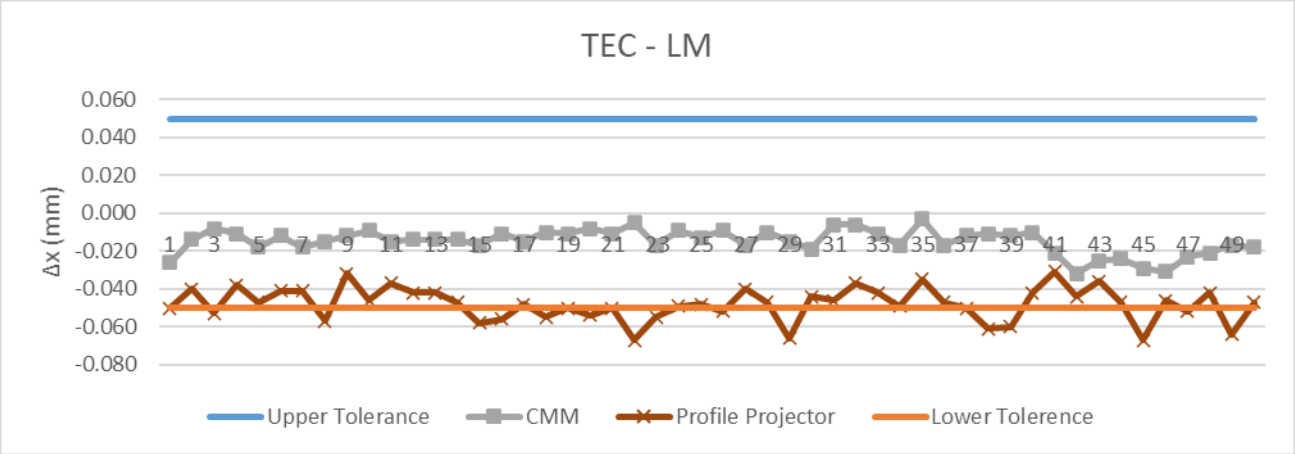

Figure 4-8 – Graphic illustration of the measurement results comparison between the PP and CMM measuring methods of the length LM of the TEC with an upper and lower tolerance, indicated with the blue and orange lines, respectively.

Table 4-8 – Table showing the results of the average measurement difference, measurement range, process standard deviation, the AQL-value and the CP_k-value obtained from the production run (50-TEC) for the length LM with a tolerance of ± 0,05 mm

Dimension	Equipment Used	Machined Tolerance	Unit	Average Difference	IN/OUT	Range	Standard Deviation	AQL	CPk	Acceptable/ Unacceptable
LM	CMM	0.050	mm	-0.015	IN	0.029	0.007	5.404	1.801	Acceptable
	Profile Projector	-0.050		-0.048	IN	0.036	0.009	0.236	0.079	Unacceptable

From the measurement data captured using the PP, it was calculated that the PP is failing to achieve a CP_k of 1,33 and higher (Table 4-8), and it is also failing the AQL requirement due to the excessive number of components that measured outside the tolerance band.

After reviewing the measurement procedure using the PP, it is expected that the reason for the excessive number of non-conformances might be due to the human interaction of the measurement procedure. The operator needs to place the vertical axis of the reticle of the PP on the flat surface of the shadow of the part (the vertical green line on Figure 4-9) and then move the part using the verniers on the table to align the reticle with the point LM (Figure 4-9), following the horizontal green line. If the part were placed skew or the focus of the shadow on the display of the PP is a bit out, it could lead to inconsistent measurements of the length LM.

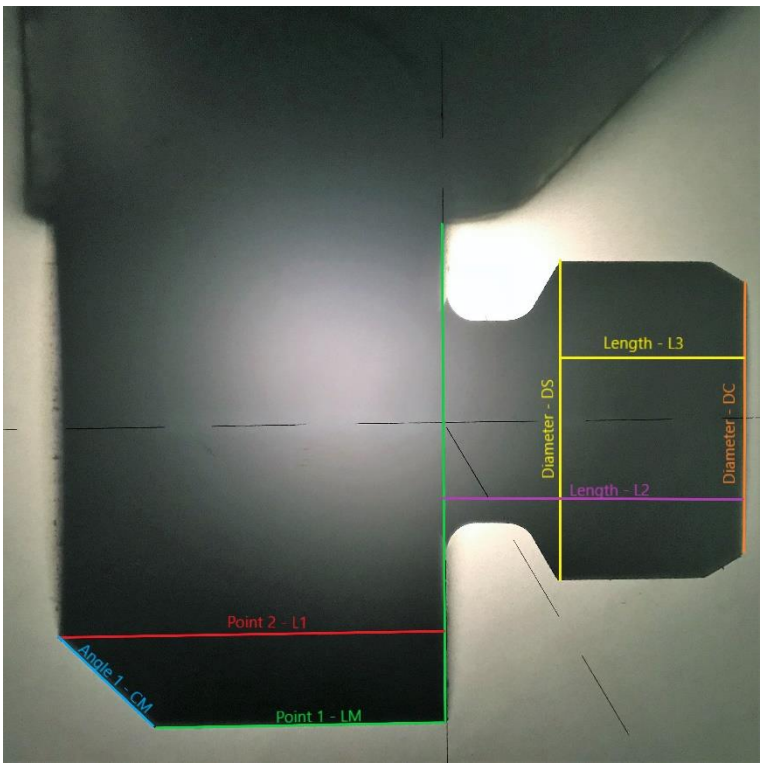

Figure 4-9 – A superimposed image of the dimensions on the TEC measured, using the 25-magnification lens on the Titanus PP. The black area represents the shadow of the TEC.

4.2. DIAMETER MEASUREMENT RESULT ANALYSIS

4.2.1. Diameter DC

Figure 4-10 is a graphical illustration of the repeatability tests of the diameter DC on the TEC, from this figure it is visible that the average measurement (-0,146mm) using the PP is a lot smaller than the average measurement (-0,022mm) of the CMM, and it is also failing the lower limit tolerance as per client specification. Furthermore, when comparing the consistency of the CMM results to that of the PP results, it is evident that the CMM has greater consistency (CP_k=2,34) of the measurement than that of the PP (CP_k=-2-79). The CMM measured the diameter DC with a standard deviation of 4µm in comparison to the 11µm for the PP.

Table 4-9 – Table showing the results of the data analysis of the 9 measurements taken of diameter DC during the repeatability test using the Point-scan CMM, Line-scan CMM, Multi-sensor CMM, optic measuring machine and the Profile Projector.

Position Name	Equipment Used	Tolerance	Unit	Average Difference	IN/OUT	Range	Standard Deviation	AQL	CPk	Acceptable/ Unacceptable
DC	Point Scan CMM	0.050	mm	-0.022	IN	0.015	0.004	7.03	2.34	Acceptable
	Line Scan CMM			-0.011	IN	0.002	0.001	73.07	24.36	Acceptable
	Multi-Sensor CMM			-0.028	IN	0.001	0.000	83.32	27.77	Acceptable
	Optic Measuring Machine	-0.050		-0.028	IN	0.001	0.000	83.32	27.77	Acceptable
	Profile Projector			-0.146	OUT	0.037	0.011	-8.38	-2.79	Unacceptable

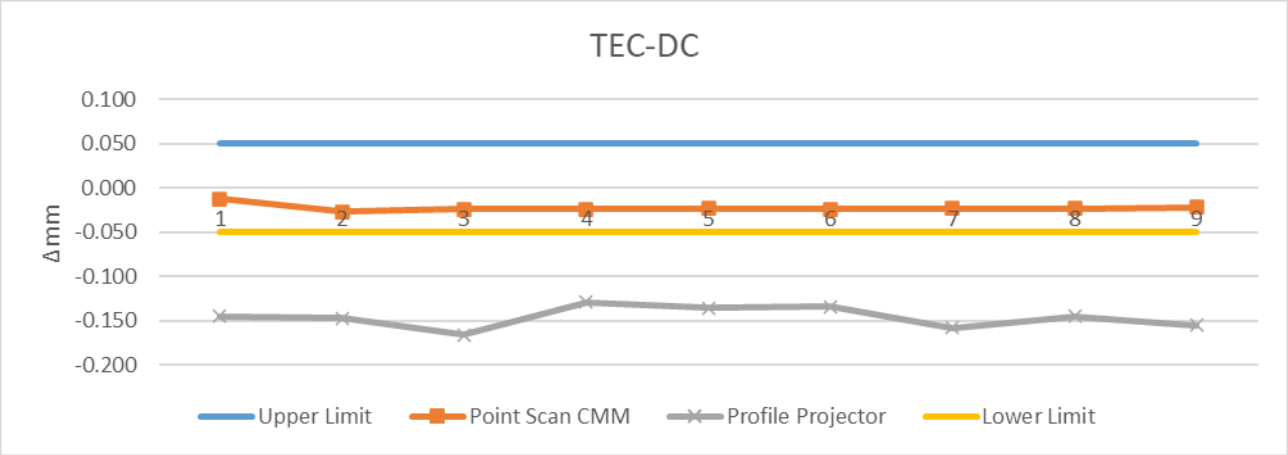

Figure 4-10 – Plot of the measurement results obtained in the repeatability test of the TEC diameter DC, using the PP and the CMM with an upper and lower tolerance, indicated with the blue and yellow lines, respectively.

From Figure 4-10, the expectation is to see another big difference between the PP and the CMM in Figure 4-11. However, this is not the case as the results are close to each other. From Figure 4-11 it is also noticeable that the measurement using the CMM is more consistent than that of the PP.

Furthermore, it is noticed in Figure 4-11, that there is a downward trend in the dimensional results obtained using the CMM for the diameter DC. This could be an indication of undercutting at the start of the component.

Diameter DC is the front face diameter of the top endcap, illustrated in Figure 3-1, and it is failing both the AQL test and the CP_k values for both the CMM and PP. The reason why both methods are failing the AQL test is because of the number of endcaps failing to adhere to the lower limit of the specification. There were 6 endcaps from the CMM results failing the lower limit, compared to the 22 endcaps failing the lower limit using the PP. It should also be noted from Figure 4-11 that there is a downward trend of diameter DC.

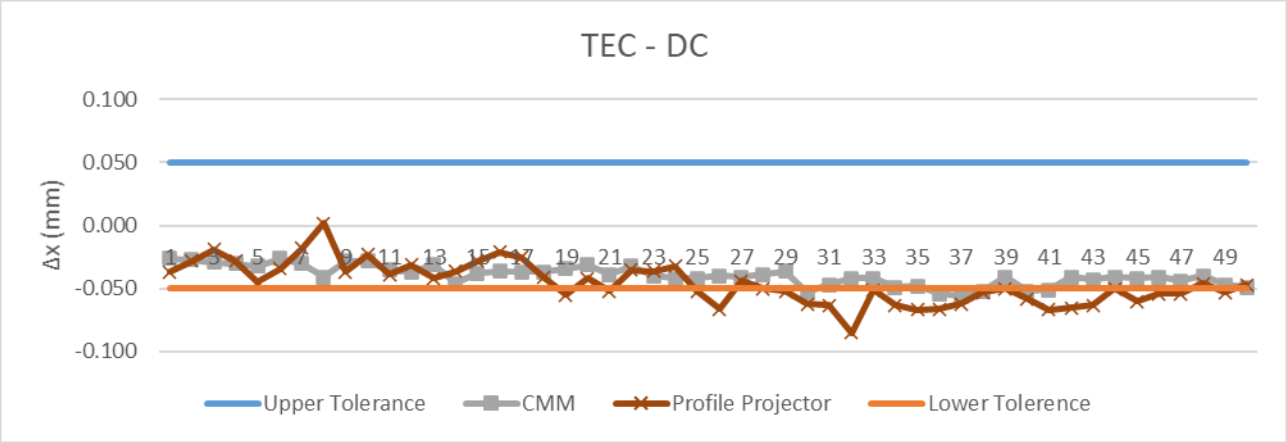

Figure 4-11 – Plot of the measurement results comparison between the PP and CMM measuring methods of the diameter DC of the TEC with an upper and lower tolerance, indicated with the blue and orange lines, respectively.

Table 4-10 – Table showing the results of the average measurement difference, measurement range, process standard deviation, the AQL-value and the CP_k-value obtained from the production run (50-TEC) for the diameter DC with a tolerance of ± 0,05 mm. Showing that the batch failed the CP_k and AQL values for both methods.

Dimension	Equipment Used	Machined Tolerance	Unit	Average Difference	IN/OUT	Range	Standard Deviation	AQL	CPk	Acceptable/ Unacceptable
DC	CMM	0.050	mm	-0.040	IN	0.030	0.008	1.311	0.437	Unacceptable
	Profile Projector	-0.050		-0.046	IN	0.087	0.016	0.261	0.087	Unacceptable

The reason for this could be due to an increase in material, shear strength and process temperature. As the parting insert starts getting blunt, the shear strength of the material increases, as the power required to part the endcap from the stock material increases. The CNC does not feel the effect of this increased shear strength and the power required to part the component is converted into thermal energy, making the part stronger and stronger after each parting process. The cutting sequence restarts with a facing cut to remove the material left over from the parting sequence at the front face of the part, before starting to cut the profile adding heat to the part and the insert, increasing the shear strength of the material even more. This could lead to thermal expansion on both the insert and the stock material side when the next insert is used to do the finishing cut, as the material strength at the front of the endcap is assumed to be significantly higher than its original strength, which could lead to the incremental decline in the part size at DC.

This steady decline in the part diameter could be offset by using a few different possibilities:

- A through tool cooled parting tool could be used to increase the life span of the parting insert, as the insert is kept well cooled and lubricated when parting the endcap.
- A cutting sequence change could be implemented since it might help with temperature control during machining.
- Reduction in feeds and speed for the parting process

- Shifting the starting diameter of the face upwards. The starting size for diameter DC was set as 4,450 mm, this could be moved upwards, for example, to 4,495 mm as it is evident from Figure 4-11 that there is a declining trend in the size of the dimension.

Getting back to the measurement errors summarised in Table 4-10, it is evident that the conventional method is failing CP_k value. The PP is highly dependent on the visual clarity of the corners of the diameter DC, as mentioned for LM. Figure 4-9 is an illustration of the typical view the operator has while measuring DC (vertical orange line). Note that the operator must place the reticle exactly on either the bottom or top point to measure the characteristic. The placement can be very tricky, depending on the quality of the part as well as the operator's fatigue level, the wearier the operator is, the less accurate the placement and thus the measurement will be. Furthermore, the magnification used on the PP also has a big influence on the quality of the backlight of the PP. All these factors are noticeable in the measurement standard deviation of 0,011 mm, compared to the 0,004 mm standard deviation for the CMM of the repeatability test (Table 4-9).

Focussing on the CMM, diameter DC is an interpolated point between the face plane of the endcap and the angle AE. If there are inconsistencies with the measurement of angle AE, it would have a direct effect on the diameter DC. The challenges of the measurement procedure using the CMM to measure angle AE will be discussed in Section 4.4.2.

4.2.2. Diameter DS

Table 4-11 and Figure 4-12 are the data analysis results of the repeatability study for the measurement of diameter DS. From the analysis, it is found that the PP, even though it measures all the cycles within spec, failed the CP_k value for the repeatability test. This could be due to a human error during the measurement procedure. The CMM had a CP_k -value of 23,45, whereas the PP had a value of 0,87. This indicates that the CMM has far better consistency in the measurement of diameter DS than the PP.

Table 4-11 – Table showing the results of the data analysis of the 9 measurements taken of diameter DS during the repeatability test using the Point-scan CMM, Line-scan CMM, Multi-sensor CMM, optic measuring machine and the Profile Projector. Showing the PP failed the repeatability test on the CP_k value.

Position Name	Equipment Used	Tolerance	Unit	Average Difference	IN/OUT	Range	Standard Deviation	AQL	CPk	Acceptable/ Unacceptable
DS	Point Scan CMM	0.025	mm	-0.003	IN	0.001	0.000	70.36	23.45	Acceptable
	Line Scan CMM			-0.001	IN	0.000	0.000	237.36	79.12	Acceptable
	Multi-Sensor CMM			0.000	IN	0.000	0.000	828.67	276.22	Acceptable
	Optic Measuring Machine	-0.025		-0.002	IN	0.002	0.001	41.21	13.74	Acceptable
	Profile Projector			0.004	IN	0.030	0.008	2.60	0.87	Unacceptable

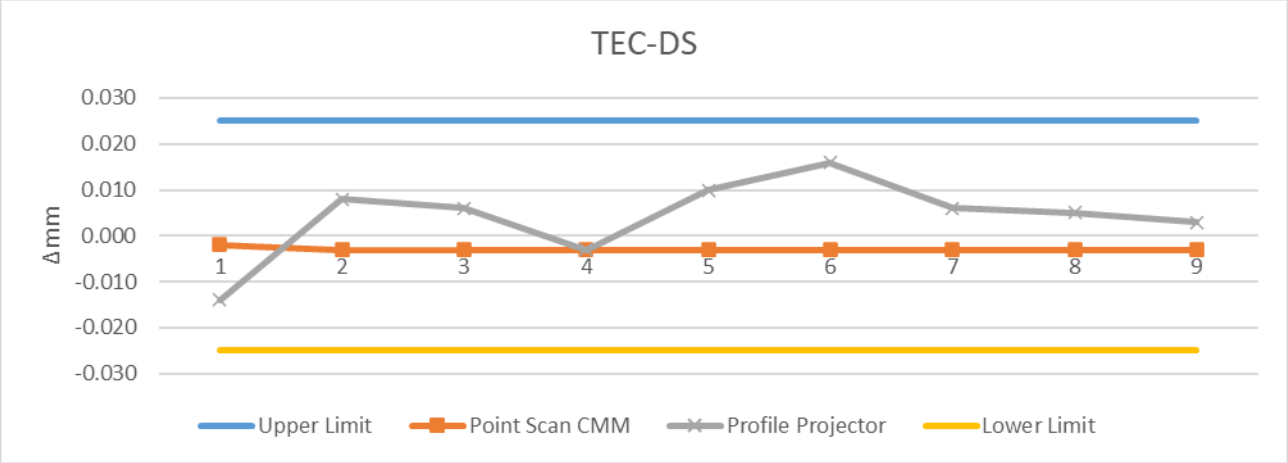

Figure 4-12 – Plot of the measurement results obtained in the repeatability test of the TEC diameter DS, using the PP and the CMM with an upper and lower tolerance, indicated with the blue and yellow lines, respectively.

It is clear from Figure 4-13, that there was some sort of abnormality in the measurement of the diameter DS using the CMM, as the value spiked from 0,02 mm to 0,021mm at sample TEC-39 and again at sample TEC-42, where after the measurement value stay constant until sample number TEC-50. This abnormality on the measurement leads to the CMM failing to comply with a CP_k of 1,33, Table 4-12.

Table 4-12 – Table showing the results of the average measurement difference, measurement range, process standard deviation, AQL-value and the CP_k value obtained from the production run (50-TEC) for the diameter DS with a tolerance of ± 0,025 mm, indicating that the 50-TEC measurement using the CMM failed the CP_k value.

Dimension	Equipment Used	Machined Tolerance	Unit	Average Difference	IN/OUT	Range	Standard Deviation	AQL	CPk	Acceptable/ Unacceptable
DS	CMM	0.025	mm	0.002	IN	0.034	0.010	2.242	0.747	Unacceptable
	Profile Projector	-0.025		-0.002	IN	0.020	0.005	4.792	1.597	Acceptable

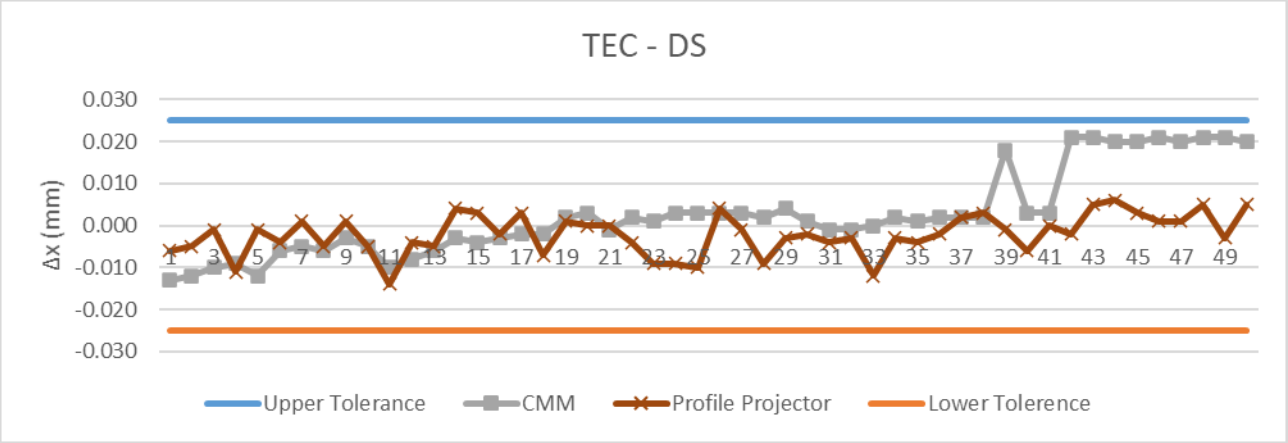

Figure 4-13 – Plot of the measurement results comparison between the PP and CMM measuring methods of the diameter DS of the top-endcap with an upper and lower tolerance, indicated with the blue and orange lines, respectively, showing an upward trend in measurement results with a sudden spike in value at sample TEC-39 and TEC-42

Before stating what could have caused this event, it is important to go and evaluate the measurement procedure. During the repeatability study, it was found that the CMM has a standard deviation of ±0,00 µm with a CP_k of 23,45 after 9 measurements measuring the same diameter DS (Table 4-11). This is a good indication that the confidence in the measurement is fairly high and it could be presumed that the abnormality is not with the measurement method, but rather with the machining process.

The change in diameter at TEC-39 could be a result of undercutting. This is something that could be connected to tool wear, as the part is cut bigger than it was programmed for. The best way to verify whether it was tool wear, is by comparing the trend of DS with the trends of DL (Figure 4-17), and DT (Figure 4-15), since the cutting processes are the same. When comparing these graphs, it becomes visible that all the graphs are showing the same trend at the same point of machining.

The reason for this rapid tool wear could also be the cause of various aspects of machining. The one possibility is due to thermal exposure in the process. As mentioned, Zry-4 tends to work harden over time and this could lead to high cutting temperatures. The higher the temperatures, the quicker the insert will start to wear.

4.2.3. Diameter DT

The sample mean of the repeatability study results for the measurement obtained using the CMM (ΔX=-0,006mm) and the PP (ΔX=-0,007mm) for diameter DT are very close to each other, as illustrated in Figure 4-14 and Table 4-20. However, the CMM had a greater consistency over its measurement results, with a range of 0,002 mm and a CP_k of 47,17, compared to the 0,004 mm range and 20,08 CP_k of the PP. Both these measurement procedures give a high level of confidence in the results obtained in the batch measurements.

Table 4-13 – Table showing the results of the data analysis of the 9 measurements taken of diameter DT during repeatability test using the Point-scan CMM, Line-scan CMM, Multi-sensor CMM, optic measuring machine and the Profile Projector.

Position Name	Equipment Used	Tolerance	Unit	Average Difference	IN/OUT	Range	Standard Deviation	AQL	CPk	Acceptable/ Unacceptable
DT	Point Scan CMM	0.100	mm	-0.006	IN	0.002	0.001	141.50	47.17	Acceptable
	Line Scan CMM			-0.012	IN	0.001	0.000	282.29	94.10	Acceptable
	Optic Measuring Machine	-0.100		-0.016	IN	0.004	0.001	68.67	22.89	Acceptable
	Profile Projector			-0.007	IN	0.004	0.002	60.24	20.08	Acceptable

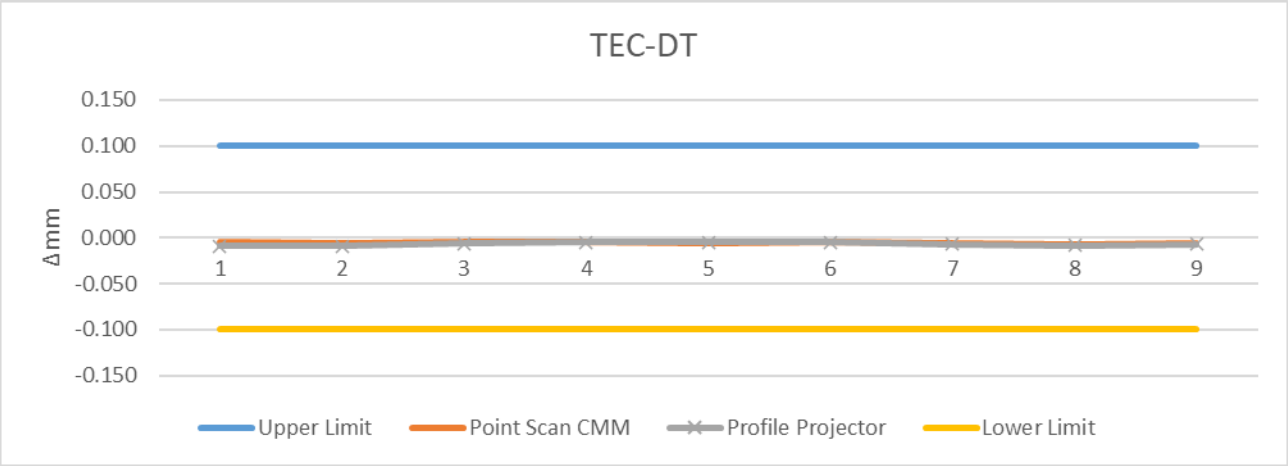

Figure 4-14 – Plot of the measurement results obtained in the repeatability test of the TEC diameter DT, using the PP and the CMM with an upper and lower tolerance, indicated with the blue and yellow lines, respectively

The orange line of Figure 4-12 shows a similar trend as Figure 4-13. The diameter is slowly but surely increasing, but there is a spike at TEC-39 and another one at TEC-42, because of what happened with diameter DS when focussing on the CMM data points. The only reason why the peak looks less aggressive with diameter DT than with diameter DS is that the tolerance band of diameter DT is four times bigger than the tolerance band of diameter DS.

Table 4-14 – Table showing the results of the average measurement difference, measurement range, process standard deviation, the AQL-value procedure and the CP_k-value obtained from the production run (50-TEC) for the diameter DT with a tolerance of ± 0,100 mm.

Dimension	Equipment Used	Machined Tolerance	Unit	Average Difference	IN/OUT	Range	Standard Deviation	AQL	CPk	Acceptable/ Unacceptable
DT	CMM	0.100	mm	0.005	IN	0.069	0.009	10.427	3.476	Acceptable
	Profile Projector	-0.100		-0.010	IN	0.027	0.005	16.385	5.462	Acceptable

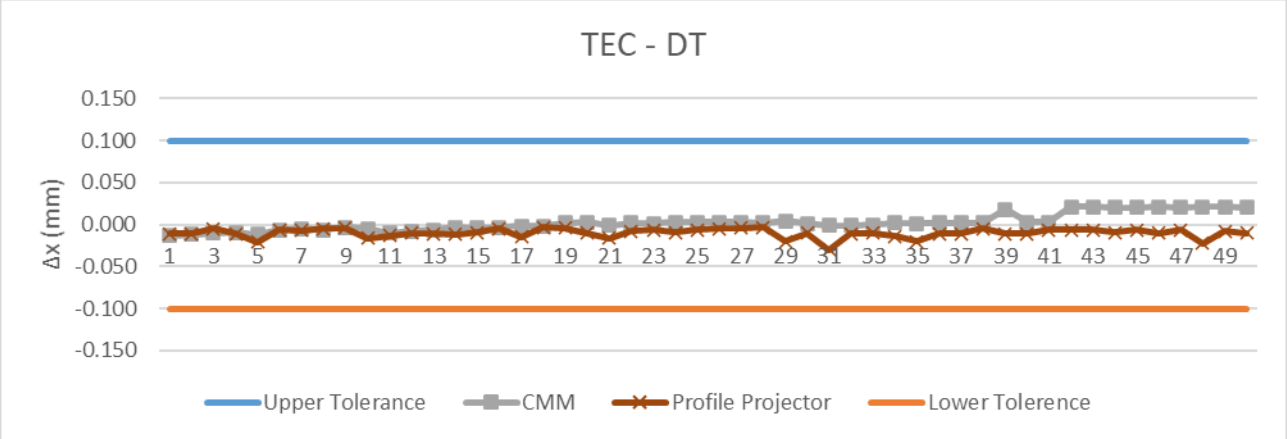

Figure 4-15 – Plot of the measurement results comparison between the PP and CMM measuring methods of the diameter DT of the top-endcap with an upper and lower tolerance, indicated with the blue and orange lines, respectively.

4.2.4. Diameter DL

When looking at the visualisation of the results in Figure 4-16, it is noticeable that the CMM measurement is a lot more constant during the repeatability test, with a CP_k of 35,67 (Figure 4-13). When looking at the results of the PP, it is noticeable that the results are not as linear (CPk=4,28) as that of the CMM and it is also noticeable that the results are a bit higher than that of the CMM (-0,011 mm).

Table 4-15 – Table showing the results of the data analysis of the 9 measurements taken of diameter DL during repeatability test using the Point-scan CMM, Line-scan CMM, Multi-sensor CMM, optic measuring machine and the Profile Projector.

Position Name	Equipment Used	Tolerance	Unit	Average Difference	IN/OUT	Range	Standard Deviation	AQL	CPk	Acceptable/ Unacceptable
DL	Point Scan CMM	0.100	mm	-0.029	IN	0.002	0.001	107.00	35.67	Acceptable
	Line Scan CMM			-0.021	IN	0.001	0.000	189.49	63.16	Acceptable
	Multi-Sensor CMM			-0.014	IN	0.000	0.000	1784.51	594.84	Acceptable
	Optic Measuring Machine	-0.100		-0.015	IN	0.001	0.000	236.82	78.94	Acceptable
	Profile Projector			-0.011	IN	0.025	0.007	12.85	4.28	Acceptable

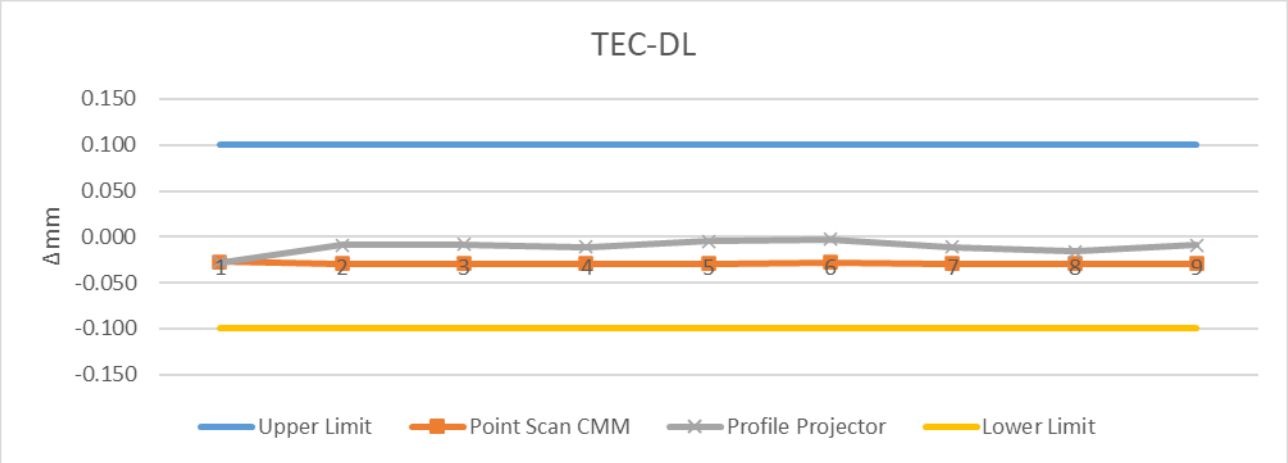

Figure 4-16 – Plot of the measurement results obtained in the repeatability test of the TEC diameter DL, using the PP and the CMM with an upper and lower tolerance, indicated with the blue and yellow lines, respectively. With the PP results slightly higher than the CMM results.

When examining the results of the PP of the batch (Figure 4-17) it is noticeable that it is also slightly higher than the CMM results, as expected with the repeatability study conducted. Another thing noticeable on the measurements is that the PP is not picking up the change in the dimension from sample TEC-41 and onwards, the line stays straight from around TEC-12.

Table 4-16 – Table showing the results of the average measurement difference, measurement range, process standard deviation, the AQL-value procedure and the CP_k-value obtained from the production run (50-TEC) for the diameter DL with a tolerance of ± 0,100 mm.

Dimension	Equipment Used	Machined Tolerance	Unit	Average Difference	IN/OUT	Range	Standard Deviation	AQL	CPk	Acceptable/ Unacceptable
DL	CMM	0.100	mm	-0.014	IN	0.047	0.010	8.314	2.771	Acceptable
	Profile Projector	-0.100		0.018	IN	0.020	0.004	18.696	6.232	Acceptable

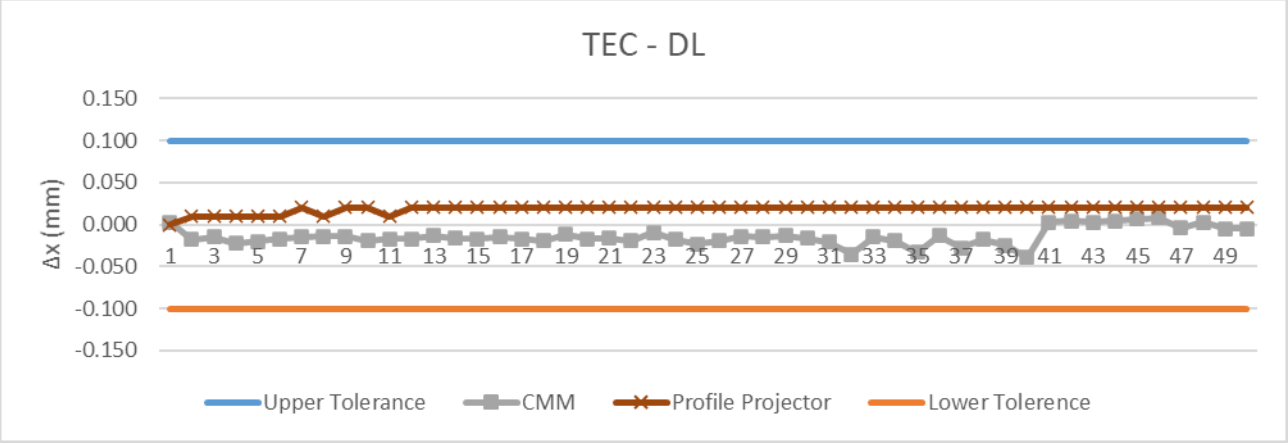

Figure 4-17 – Plot of the measurement results comparing the PP and CMM measuring methods of the diameter DL of the TEC with an upper and lower tolerance, indicated with the blue and orange lines, respectively.

The change in the diameter DL from sample TEC-41 onwards is also due to the same incident experienced at diameter DS, as all these diameters have flat areas and are subject to similar cutting conditions.

4.3. RADII MEASUREMENT RESULTS ANALYSIS

Both Figure 4-19 and Figure 4-20 are the repeatability study results of using the overlay chart on the PP to measure the radii, as illustrated in Figure 4-18. Even though both graphs showed a constant measurement graph when using the PP, both RT1 and RT2 failed CP_k as calculated in Table 4-17. This is a clear indication that many factors were influencing the measurement results when doing this dimension on the PP, i.e. the clarity of the radii on the PP.

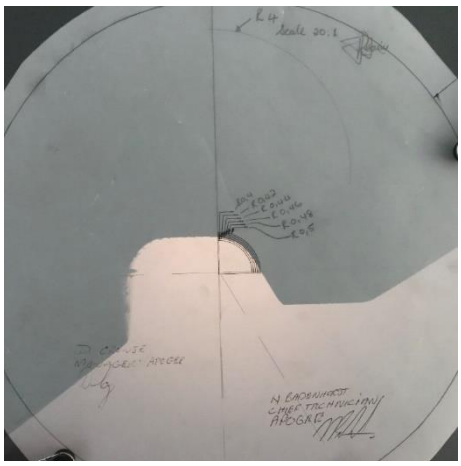

Figure 4-18 – Image of the side view of a BEC illustrating the measurement procedure, using a radius overlay chart on the PP to measure the Radii RT1 & RT2. The shadow is the projection of the endcap from the measurement table of the PP.

Table 4-17 – Table showing the results of the data analysis of the 9 measurements taken of the radii RT1 and RT2 during repeatability test using the Line-scan CMM, Multi-sensor CMM and the Profile Projector. Indicating that the only acceptable method for the measurement of RT is the Multi-sensor CMM.

Position Name	Equipment Used	Tolerance	Unit	Average Difference	IN/OUT	Range	Standard Deviation	AQL	CPk	Acceptable/ Unacceptable
RT1	Multi-Sensor CMM	0.100	mm	-0.088	IN	0.003	0.001	14.45	4.82	Acceptable
	Profile Projector	-0.100		-0.084	IN	0.020	0.008	1.87	0.62	Unacceptable
RT2	Line Scan CMM	0.100	mm	0.092	IN	0.026	0.009	0.89	0.30	Unacceptable
	Multi-Sensor CMM			-0.043	IN	0.027	0.008	7.48	2.49	Acceptable
	Profile Projector	-0.100		-0.091	IN	0.020	0.010	0.89	0.30	Unacceptable

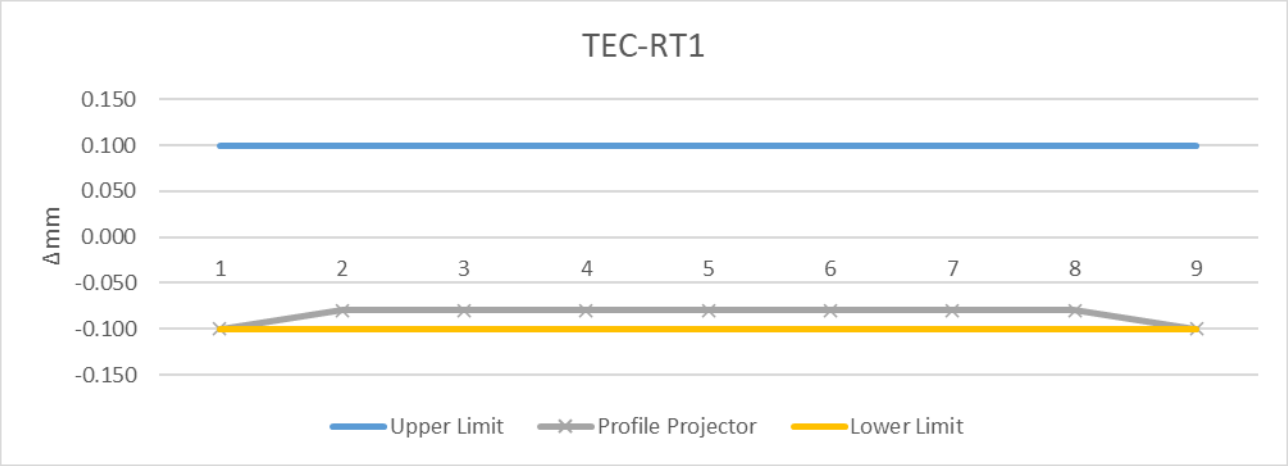

Figure 4-19 – Plot of the measurement results obtained in the repeatability test of the TEC radius RT1 using the PP with an upper and lower tolerance, indicated with the blue and yellow lines, respectively.

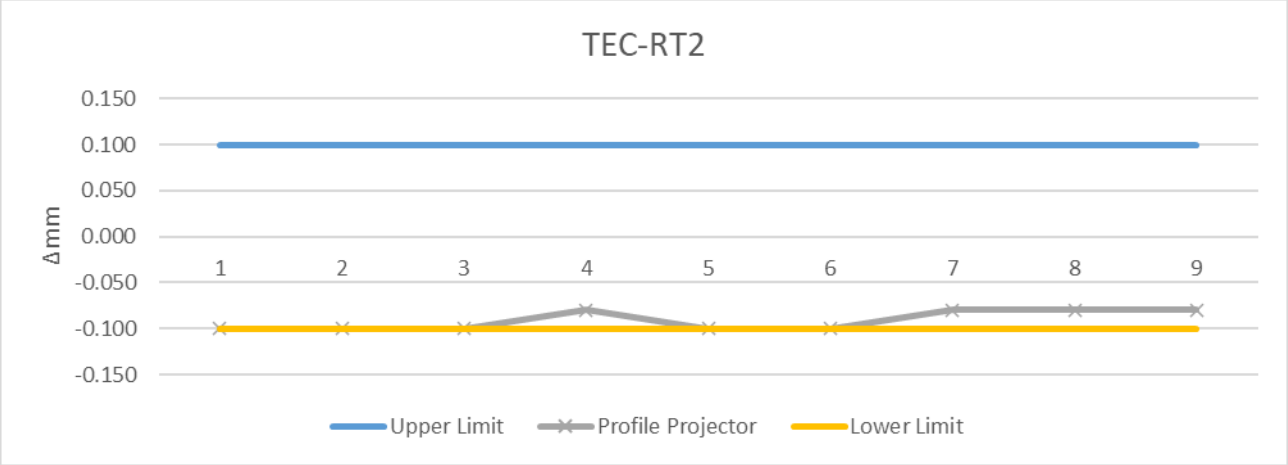

Figure 4-20 – Plot of the measurement results obtained in the repeatability test of the TEC radius RT2 using the PP with an upper and lower tolerance, indicated with the blue and yellow lines, respectively.

Table 4-18 – Table showing the results of the average measurement difference, measurement range, process standard deviation, the AQL value procedure and the CP_k value obtained from the production run (50-TEC) for the radii RT1 and RT2 with a tolerance of ± 0,100 mm.

Dimension	Equipment Used	Machined Tolerance	Unit	Average Difference	IN/OUT	Range	Standard Deviation	AQL	CPk	Acceptable/ Unacceptable
RT1	CMM	0.100	mm							
	Profile Projector	-0.100		0.000	IN	0.000	0.000			Acceptable
RT2	CMM	0.100	mm							
	Profile Projector	-0.100		-0.038	IN	0.040	0.012	9.137	1.682	Acceptable

Table 4-18 indicates that only the PP was used to measure the radii. The reason being the fact that the 0,5mm on the CMM was too big to give any valuable data for this dimension. Focussing on the measurement using the PP, Figure 4-21 is the illustration of the batch measurements of radius RT1. This figure shows that there were no recorded changes in the radius over the 50 endcaps machined.

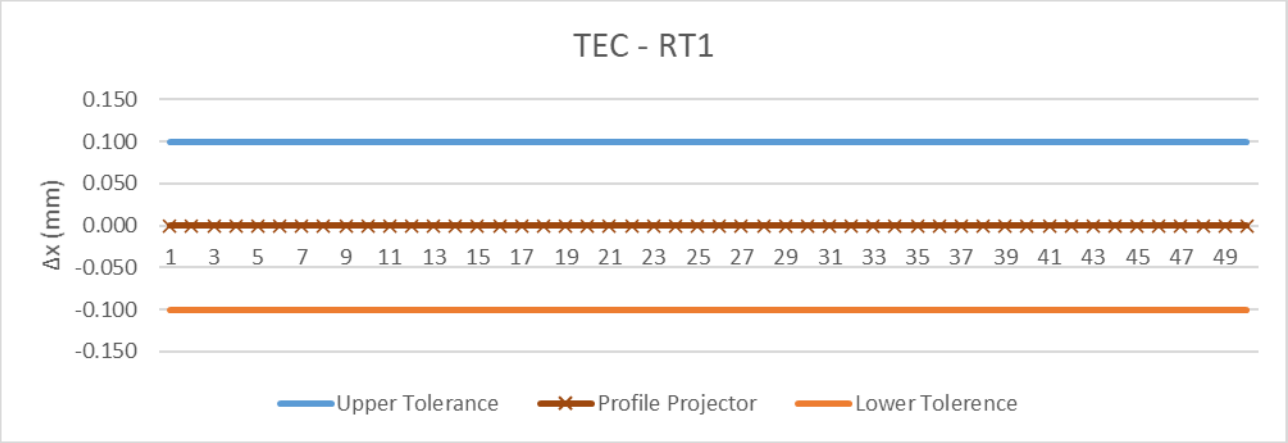

Figure 4-21 – Plot of the measurement results obtained from using the overlay chart on the PP, measuring the radius RT1 of the TEC with an upper and lower tolerance, indicated with the blue and orange lines, respectively.

Figure 2-20 illustrates the batch measurement results of the radius RT2. On this figure, it could be noticed that there were slight changes to the measurement result.

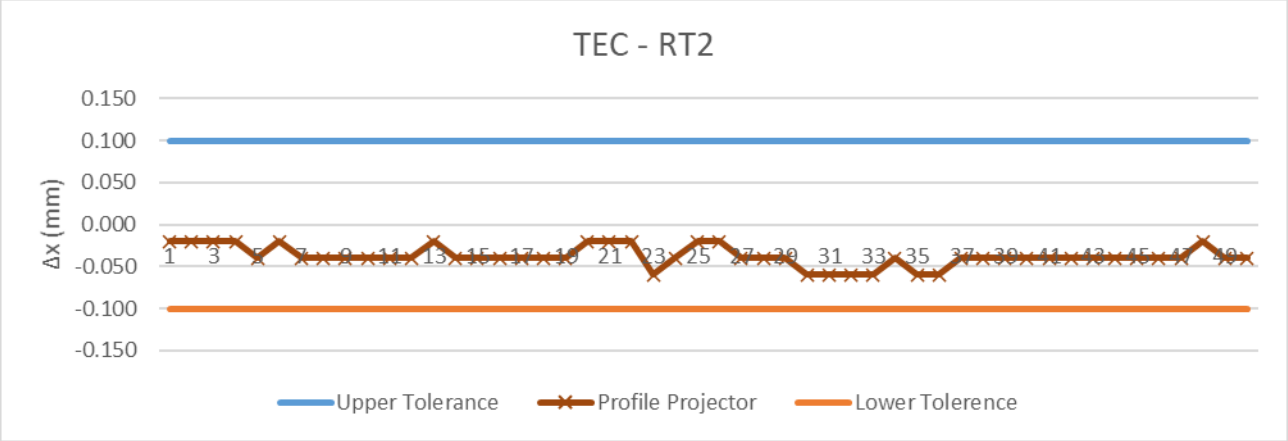

Figure 4-22 – Plot of the measurement results obtained from using the overlay chart on the PP, measuring the radius RT2 of the TEC with an upper and lower tolerance, indicated with the blue and orange lines, respectively.

The challenge with the results obtained from the PP is the fact that there was no second method that could have been used to verify the results. Looking at the repeatability test of RT, it becomes clear from the result that a second method is needed to verify the results since the PP failed CP_k and AQL on the RT measurements.

4.4. ANGLES MEASUREMENT RESULTS ANALYSIS

4.4.1. Angle AT

Angle AT, as illustrated in Figure 3-1, is the angle leading into the diameter DT. Figure 4-23 illustrates the results of the repeatability study of angle AT and Table 4-19 tabulates the analysis results of the repeatability test. Looking at Table 4-19, one could notice that neither the point-scan CMM nor the PP complied with the CP_k requirement of 1.33. This has a direct influence on the confidence level of the results obtained during the batch analysis.

Table 4-19 – Table showing the results of the data analysis of the 9 measurements taken of the angle AT during the repeatability test using the Point-scan CMM, Line-scan CMM, Multi-sensor CMM and the Profile Projector. Indicating that neither the point-scan CMM nor the PP met the CP_k requirement.

Position Name	Equipment Used	Tolerance	Unit	Average Difference	IN/OUT	Range	Standard Deviation	AQL	CPk	Acceptable/ Unacceptable
AT	Point Scan CMM	0.500	Degrees	0.216	IN	0.403	0.142	2.00	0.67	Unacceptable
	Line Scan CMM			0.257	IN	0.035	0.009	26.54	8.85	Acceptable
	Multi-Sensor CMM	-0.500		0.254	IN	0.033	0.011	23.30	7.77	Acceptable
	Profile Projector			0.191	IN	0.367	0.134	2.31	0.77	Unacceptable

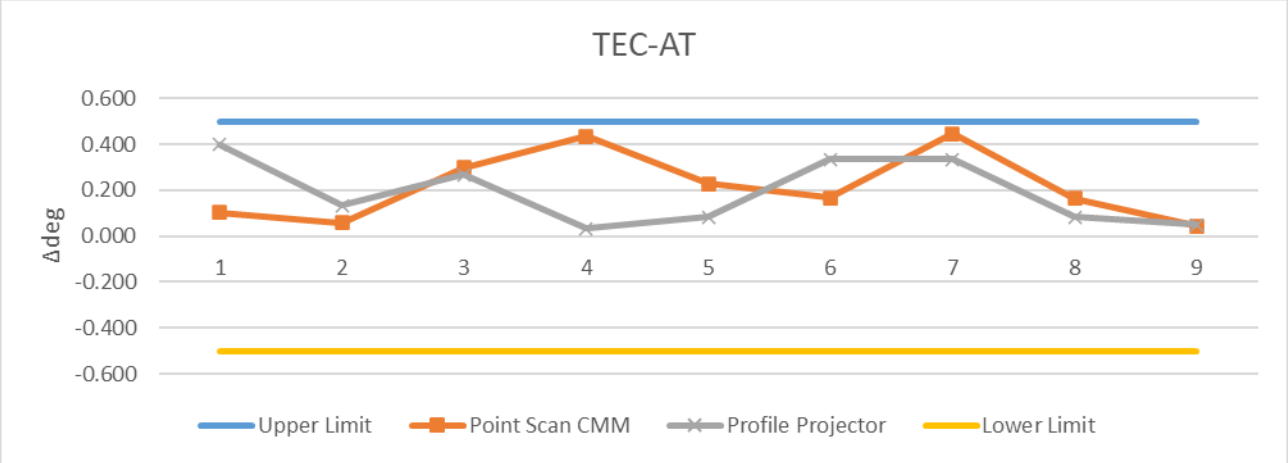

Figure 4-23 – Plot of the measurement results obtained in the repeatability test of the TEC angle AT using the PP and the CMM with an upper and lower tolerance, indicated with the blue and yellow lines, respectively.

Due to the failure to comply with the CP_k requirements during the repeatability test, the confidence in the measurement results obtained during the batch measurement is low, considering the lack of repeatability of the measurements. The same trend is seen in Figure 4-24, for both the CMM and the PP. The results are widely scattered (CMM CPk = 0,465 and PP CPk=1,023), making it difficult to conclude why this might have happened.

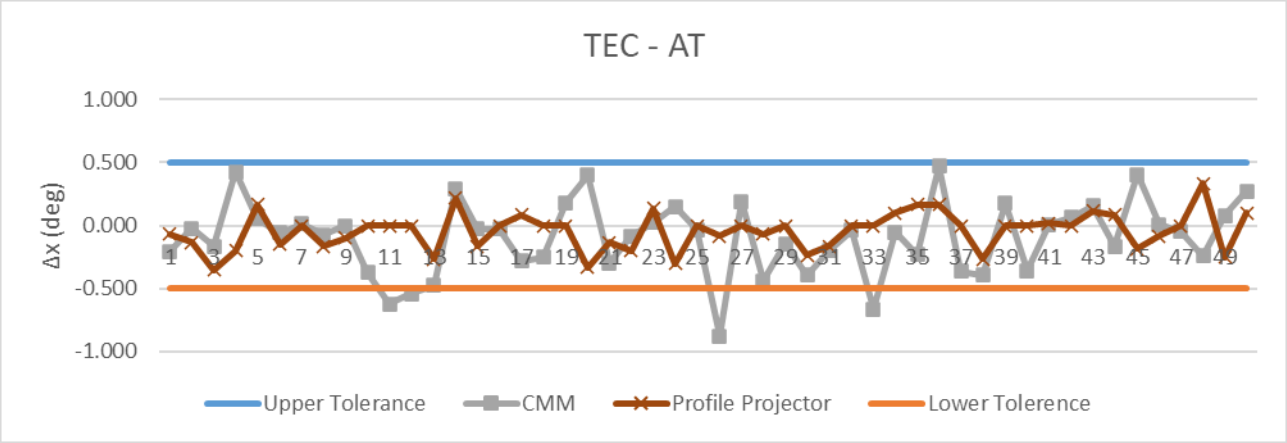

Figure 4-24 – Plot of the measurement results obtained from the batch measurements of angle AT, using the PP and the CMM with an upper and lower tolerance, indicated with the blue and orange lines, respectively, showing 4 endcaps not meeting the lower tolerance specification for the CMM.

As summarised in Table 4-20, angle AT fails the CP_k value for both the PP and the CMM. Also, the CMM failed the AQL test. The reason for the CMM's failure of the AQL test is the three endcaps that were measured out of specification, failing to meet the lower tolerance. Through the analysis of Figure 4-24, it becomes clear that the consistency of measurements across the board is incredibly low, with a measured range of 1,348° using the CMM, and a range of 0,683° using the PP. From this data, it becomes evident that the measurement range of the PP is roughly half of that of the CMM. To understand why there is such inconstancy when measuring AT, one needs to understand the method of measurement.

Table 4-20 – showing the results of the average measurement difference, measurement range, process standard deviation, the AQL-value and the CP_k-value obtained from the production run (50-TEC) for the angle AT with a tolerance of ± 0,5 degrees.

Dimension	Equipment Used	Machined Tolerance	Unit	Average Difference	IN/OUT	Range	Standard Deviation	AQL	CPk	Acceptable/ Unacceptable
AT	CMM	0.500	Degrees	-0.095	IN	1.348	0.290	1.395	0.465	Unacceptable
	Profile Projector	-0.500		-0.044	IN	0.683	0.148	3.070	1.023	Unacceptable

Focussing first on the capability of the measurement methods, one could notice that the consistency of the measurement was low in the repeatability study graph (Figure 4-23), and Table 4-19 confirms this, with CP_k values of 0,67 and 0,77 for the CMM and the PP measurements, respectively.

Analysing the measurement data retrieved from the measurements conducted using the CMM, it could be seen in Figure 4-23, the measurement is very inconsistent. This could mainly be due to how the measurement was conducted using the CMM. To get an accurate measurement of the CMM, the minimum recommended number of points needed for any dimension is three. The measurement area of the dimension is extremely small, as is illustrated in Figure 4-25(a), with a measurement line of 0,4 mm and a measurement probe with a diameter of 0,5 mm. This emphasises the fact that great consideration must be given to the placement of the probe, to get the angle

measurement as accurate as possible. Figure 4-25(b) illustrates the placement of the probe positions when taking the measurements, and it is visible that the working space is extremely small. During the repeatability study, it was found that the CMM had a standard deviation of ±0,142° and a CP_k of 0,66.

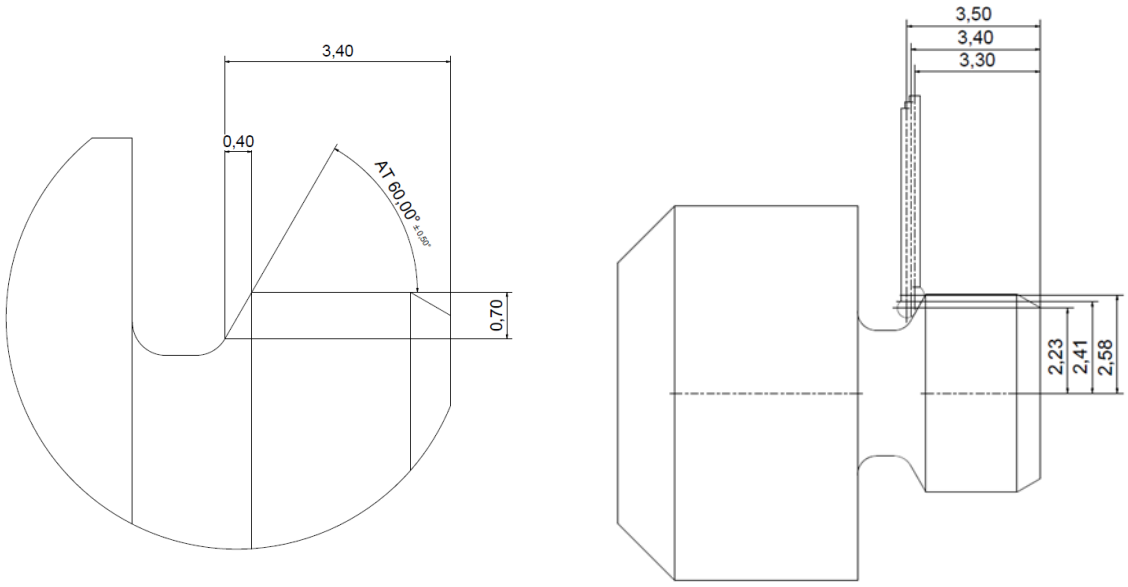

(a) (b)

Figure 4-25 – a) Super-exposed sectional view of the TEC, showing the position and values of angle AT. b) Side view drawing of the TEC showing X-axis positions of the CMM probe used to measure and calculate with the corresponding Y-axis positions, the angle AT.

The problem with angle AT is its location. A typical finishing or profiling tool has a maximum back clearance angle of 55°, where the endcap requires a back-clearance angle of more than 60°. Even though that insert is precision ground to 27°, it does not mean that there is no tool rubbing when cutting angle AT. Tool rubbing could explain the inconsistency of the angle. However, the fact is still that not one of the two methods used to measure angle AT is optimal, making it difficult to conclude what exactly is happening at angle AT during the machining process.

4.4.2. Angle AE

The data from the repeatability test (Figure 4-26) of the angle AE showed similar low levels of repeatability as previously seen with the repeatability test of the angle AT, the reason being that the measurement area of the angle AE – similar as with angle AT – is very small. The data is also scattered all over the measurement band when using the PP, however, when using the CMM tends the curve tends to be more linear with an average measurement closer to the upper limit.

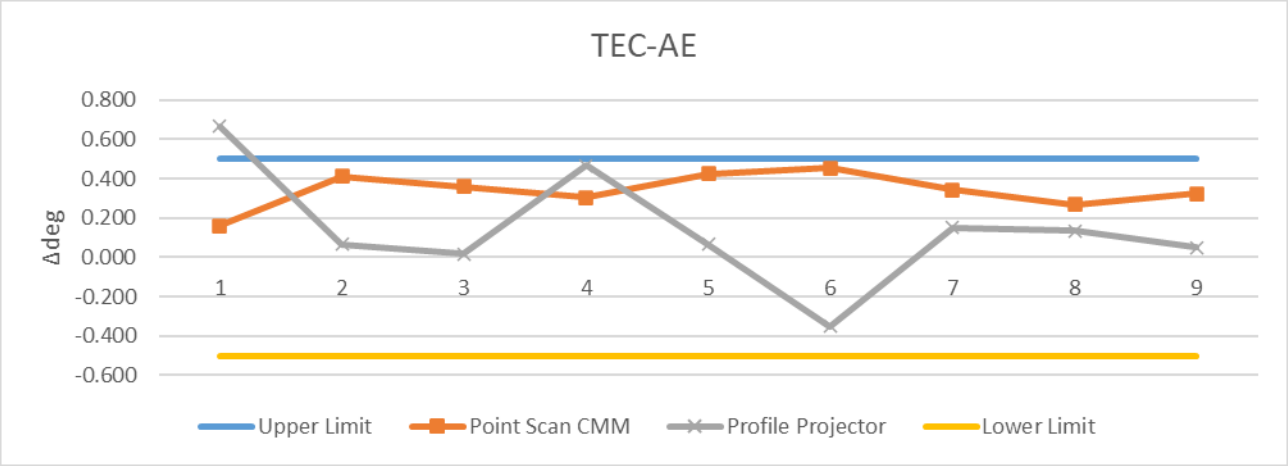

Figure 4-26 – Plot of the measurement results obtained in the repeatability test of the TEC angle AE using the PP and the CMM with an upper and lower tolerance, indicated with the blue and yellow lines, respectively. With the CMM showing greater consistency over the measurements than the PP.

Even though both the measurement methods failed the CP_k requirement, as indicated in Table 4-21, it is noticed that the CMM has a better measurement consistency over the 9 measurements and a lower value range than that of the PP, making it more valuable to consider as a benchmark.

Table 4-21 – Table showing the results of the data analysis of the 9 measurements taken of the angle AE during the repeatability test using the Point-scan CMM, Line-scan CMM, Multi-sensor CMM and the Profile Projector. Indicating that neither the point-scan CMM nor the PP met the CP_k requirements.

Position Name	Equipment Used	Tolerance	Unit	Average Difference	IN/OUT	Range	Standard Deviation	AQL	CPk	Acceptable/ Unacceptable
AE	Point Scan CMM	0.500	Degrees	0.338	IN	0.292	0.084	1.92	0.64	Unacceptable
	Line Scan CMM			-0.335	IN	0.042	0.015	10.83	3.61	Acceptable
	Multi-Sensor CMM	-0.500		-0.008	IN	0.024	0.008	62.82	20.94	Acceptable
	Profile Projector			0.141	IN	1.017	0.270	1.33	0.44	Unacceptable

When looking at the batch results (Figure 4-27), the results of the two methods are scattered all over the tolerance band, with a range of 1,010° for the CMM and 0,567° for the PP, as per Table 4-22. Once again with the batch measurements, the PP showed greater consistency over the 50 endcaps, with a range about half the size of that of the CMM and a CP_k greater than that of the CMM. The reason why the CMM is failing the AQL level is due to the one endcap (TEC-42) which was measured out of specification and another endcap that measured close to the bottom tolerance (TEC-32).

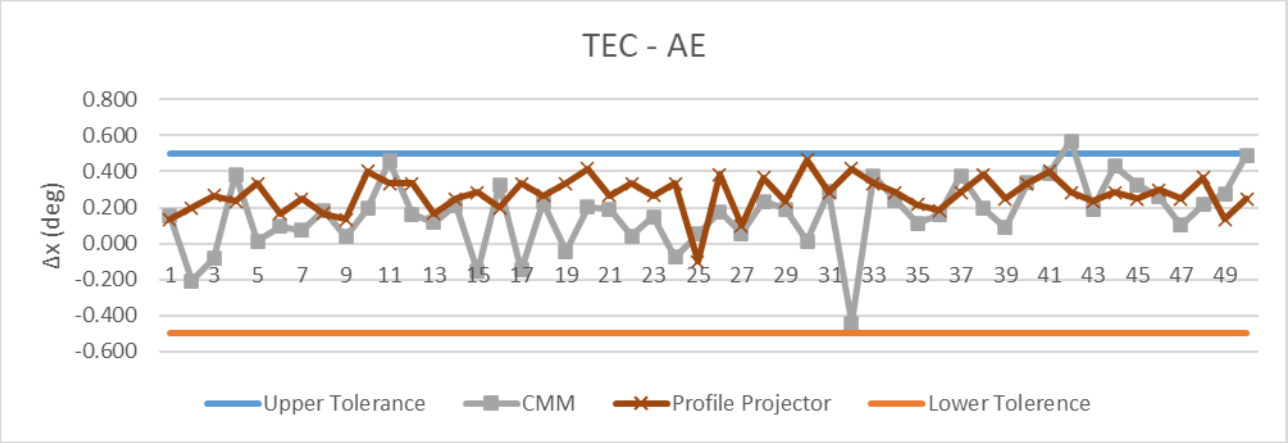

Figure 4-27 – Plot of the measurement results obtained from the batch measurements of angle AE using the PP and the CMM with an upper and lower tolerance, indicated with the blue and orange lines, respectively, showing one endcap not meeting the upper tolerance specification for the CMM.

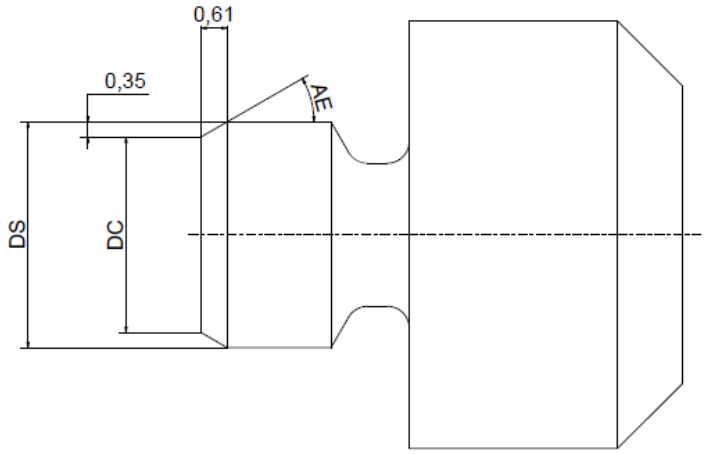

Figure 4-28 – TEC side view illustrating angle AE about diameter DC and DS

Table 4-22 – Table showing the results of the average measurement difference, measurement range, process standard deviation, the minimum value of the sampling procedure and the CP_k value obtained from the production run (50-TEC) for the angle AE with a tolerance of ±0,5 degrees.

Dimension	Equipment Used	Machined Tolerance	Unit	Average Difference	IN/OUT	Range	Standard Deviation	AQL	CPk	Acceptable/ Unacceptable
AE	CMM	0.500	Degrees	0.165	IN	1.010	0.189	1.771	0.590	Unacceptable
	Profile Projector	-0.500		0.271	IN	0.567	0.099	2.314	0.771	Unacceptable

Angle AE is the angle connecting the diameter DC and DS, as illustrated in Figure 4-28. Looking at Figure 4-27 it becomes evident that there is a similar issue regarding the consistency of measurement using the PP and the CMM on AE. This is confirmed with the calculation of the CP_k values, resulting in 0,590 and 0,771 for the CMM and the PP, respectively.

Angle AE had a similar low level of repeatability than previously noticed in the measurement of the angle AT when using the CMM for measurement. The usable area to take points on the angle is

extremely small and using a Ø 0,5 mm probe makes the measurement process even more difficult. The measurement using the PP with a 50X magnification makes the measurement easier, however, the human interference is still creating a large inconsistency in the measurement.

The measurement inconsistency of the angle AE using the CMM has a direct effect on the diameter DC, as the diameter is a calculation between the angle measurements and the position of the front face of the part by extrapolating the points. If the AE's measurement result is stable, it is presumed that DC's measurements would also be stable, and it will therefore be easier to conclude whether the downward trend of DC is due to the material expansion and whether the machining process of DC is adequate.

The best solution would be to use an optical method to measure this dimension and, in case that is not possible, to trail a Ø 0,2 mm probe to get more points to measure the angle.

4.4.3. Chamfer CM

Figure 4-29 illustrates the repeatability study of chamfer CM, using the PP and the CMM to measure a single component nine times, and Table 4-23 is the data analysis results of the repeatability test comparing the results of the PP and the point-scan CMM to various other methods. Looking at Figure 4-29, it seems like the CMM measurements (orange line) should be more consistent than that of the PP (grey line), however, when comparing the standard deviation and the CP_k values of these measurements, it is clear that both the CMM and PP have similar capabilities with regards to the measurement of chamfer CM.

Table 4-23 – Table showing the results of the data analysis of the 9 measurements taken of the chamfer CM during the repeatability test using the Point-scan CMM, Line-scan CMM, Multi-sensor CMM and the Profile Projector.

Position Name	Equipment Used	Tolerance	Unit	Average Difference	IN/OUT	Range	Standard Deviation	AQL	CPk	Acceptable/ Unacceptable
CM	Point Scan CMM	0.500	Degrees	0.002	IN	0.391	0.114	4.37	1.46	Acceptable
	Line Scan CMM			-0.043	IN	0.012	0.004	116.08	38.69	Acceptable
	Multi-Sensor CMM			-0.016	IN	0.017	0.005	91.86	30.62	Acceptable
	Optic Measuring Machine	-0.500		-0.026	IN	0.058	0.017	28.69	9.56	Acceptable
	Profile Projector			-0.031	IN	0.333	0.106	4.41	1.47	Acceptable

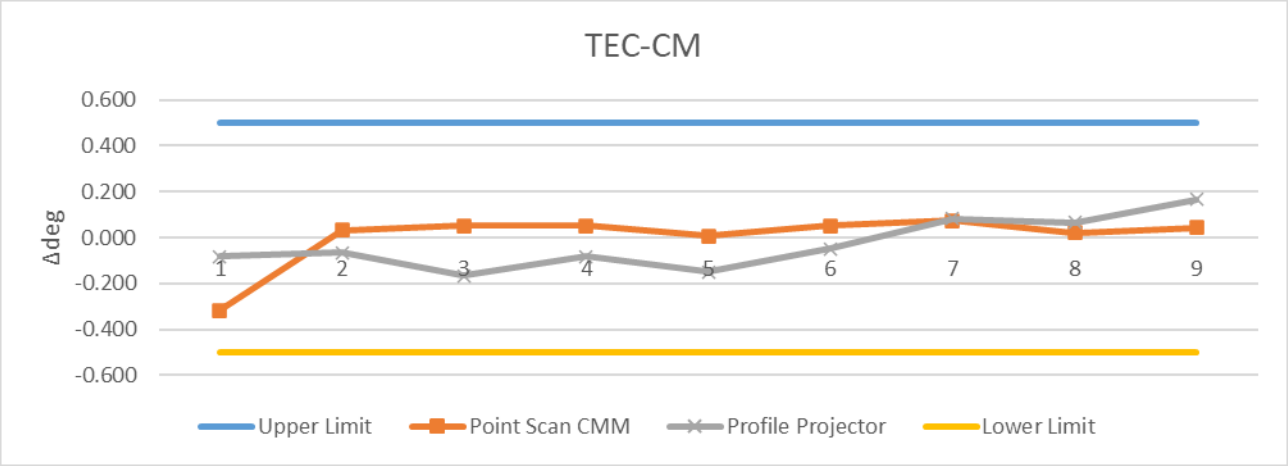

Figure 4-29 – Plot of the measurement results obtained in the repeatability test of the TEC chamfer CM using the PP and the CMM with an upper and lower tolerance, indicated with the blue and yellow lines, respectively.

Figure 4-30 illustrates the results obtained from the batch. It shows that both methods gave scattered results across the 50 components, with both having a similar range of results.

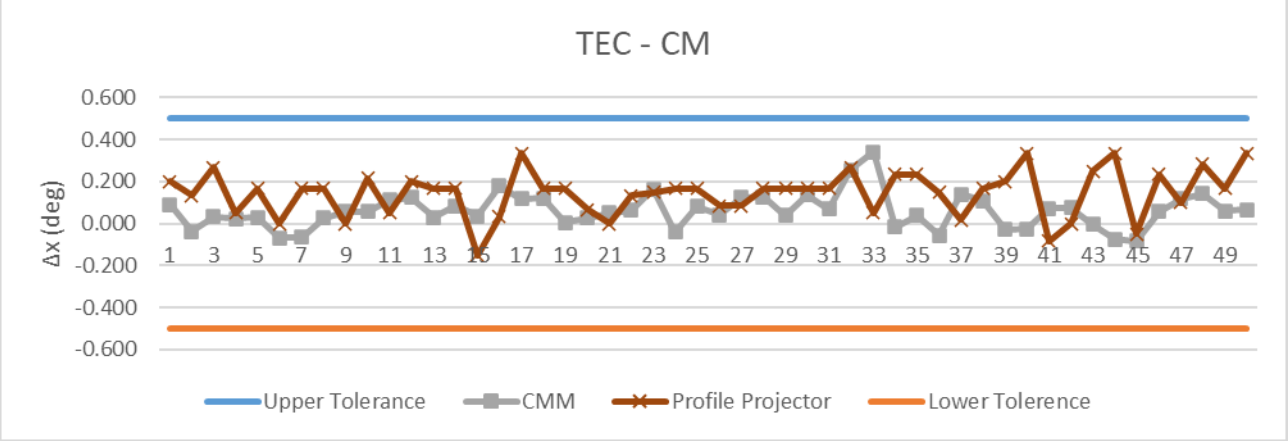

Figure 4-30 – Plot of the measurement results obtained from the batch measurements of chamfer CM using the PP and the CMM with an upper and lower tolerance, indicated with the blue and orange lines, respectively.

The chamfer CM is the angle at the end of the endcap, as illustrated in Figure 3-1, and Table 4-24 shows that the PP fails the CP_k value with a value of 1,089. This could be due to a variety of reasons, with the most obvious one probably being chip built-up. There is always some level of built-up even though that the chips were long and fine ringlets since the cooling was not optimal. The amount of built-up increase as the part is machined, due to the lack of sufficient cooling, the built-up is the most at the end of the part, thus affecting the quality of the chamfer, due to a large amount of interference at the cutting zone. However, this could only be confirmed with surface roughness testing.

The solution to eliminating this issue is to see how cooling could be improved, even when using conventional flood cooling.

Table 4-24 – Table showing the results of the average measurement difference, measurement range, process standard deviation, the minimum value of the sampling procedure and the CP_k-value obtained from the production run (50-TEC) for the chamfer CM with a tolerance of ± 0,5 degrees.

Dimension	Equipment Used	Machined Tolerance	Unit	Average Difference	IN/OUT	Range	Standard Deviation	AQL	CPk	Acceptable/ Unacceptable
CM	CMM	0.500	Degrees	0.060	IN	0.424	0.082	5.347	1.782	Acceptable
	Profile Projector	-0.500		0.145	IN	0.483	0.109	3.267	1.089	Unacceptable

Another reason for the inconsistency of measurement could have been due to human interference with the measurement using the PP. From Table 4-24 it is noted that the measurement range of the two methods is fairly similar, however, the average of the measurements for the PP is much larger than the average for the CMM, and the standard deviation of the CMM measurements are much smaller than that of the PP.

4.5. GEOMETRIC TOLERANCES MEASUREMENT RESULTS ANALYSIS

Geometric tolerance is a symbolic language used to specify size, shape, form orientation and location features on a component, to help with the proper assembling of the mating part and to improve quality, resulting in reduced component cost (Cogorno, 2006).

4.5.1. Flatness F

The Flatness F is on the face of the step of the TEC, as illustrated in Figure 3-1. Table 4-25 and Figure 4-31 illustrates the data analysis from the repeatability study results of the Flatness F of TEC, measured using the CMM. From this data, it is evident that the CMM could measure the flatness of TEC with great confidence.

Table 4-26 shows that the average measurement for the flatness F is 0,001 mm, with a measurement range of 3µm. The flatness F has an upper tolerance of 0,200 mm. This is a good indication that the material is clamped properly inside the chuck when machining the endcaps.

Table 4-25 – Table showing the results of the data analysis of the 9 measurements taken of the flatness (F) during the repeatability test using the Point-scan CMM, Line-scan CMM and the Multi-sensor CMM.

Position Name	Equipment Used	Tolerance	Unit	Average Difference	IN/OUT	Range	Standard Deviation	AQL	CPk	Acceptable/ Unacceptable
F	Point Scan CMM	0.200	mm	0.002	IN	0.005	0.002	130.22	43.57	Acceptable
	Line Scan CMM			0.000	IN	0.000	0.000	1730.99	541.27	Acceptable
	Multi-Sensor CMM			0.000	IN	0.000	0.000	2605.06	831.98	Acceptable

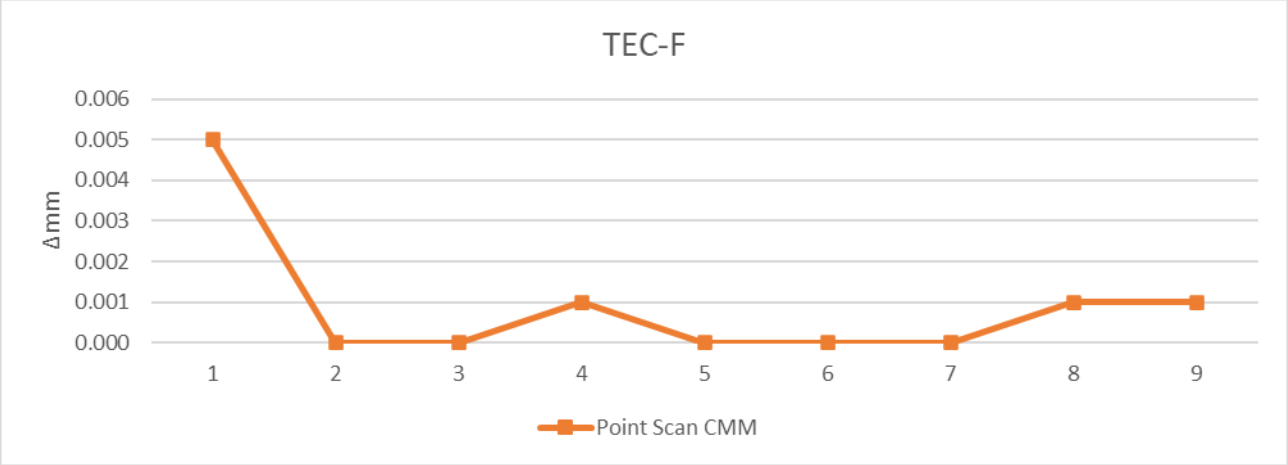

Figure 4-31 – Graphic illustration of the measurement results obtained in the repeatability test of Flatness F of the TEC, using the point scan CMM.

Table 4-26 – Table showing the results of the data analysis of the 50 TEC batch measurements taken of the flatness F using the Point-scan CMM

Dimension	Equipment Used	Machined Tolerance	Unit	Average Measurement	Average Difference	IN/OUT	Range	Standard Deviation	AQL	CPk	Acceptable/ Unacceptable
F	CMM	0.200	mm	0.001	0.199	IN	0.003	0.001	295.504	98.501	Acceptable

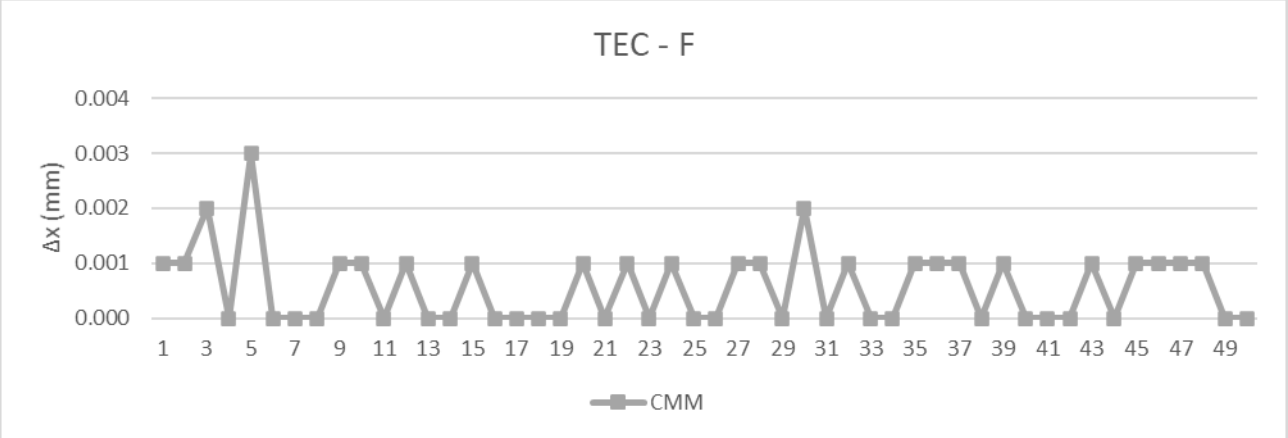

Figure 4-32 – Graphic illustration of the geometric tolerance Flatness F measurement results obtained using the CMM measuring method of the top endcap.

4.5.2. Runout RM

The runout tolerance, per definition, “is used to control the location of a circular part feature relative to its axis” (eMachineShop, 2018). In simpler words, runout is how much the specified feature vary in respect to a datum axis when it is rotated 360° around the defined datum axis (“Runout”, 2014).

The runout RM is measured on the surface of the chamfer CM with its datum given as the diameter DS, as indicated in Figure 3-1. Table 4-27 and Figure 4-33 are the analysis results of the repeatability study results of runout RM. From this data, it is evident that the point-scan CMM could measure the runout with confidence, with a standard deviation of 0,005 mm and a CP_k of 6,04.

Table 4-27 – Table showing the results of the data analysis of the 9 measurements taken of the runout RM during repeatability test using the Point-scan CMM, Line-scan CMM and the Multi-sensor CMM.

Position Name	Equipment Used	Tolerance	Unit	Average Measrement	Average Difference	IN/OUT	Range	Standard Deviation	AQL	CPk	Acceptable/ Unacceptable
RM	Point Scan CMM	0.100	mm	0.010	0.005	IN	0.018	0.005	18.97	6.04	Acceptable
	Line Scan CMM			0.014	0.000	IN	0.001	0.000	230.70	66.65	Acceptable
	Multi-Sensor CMM			0.007	0.000	IN	0.000	0.000	599.12	186.80	Acceptable

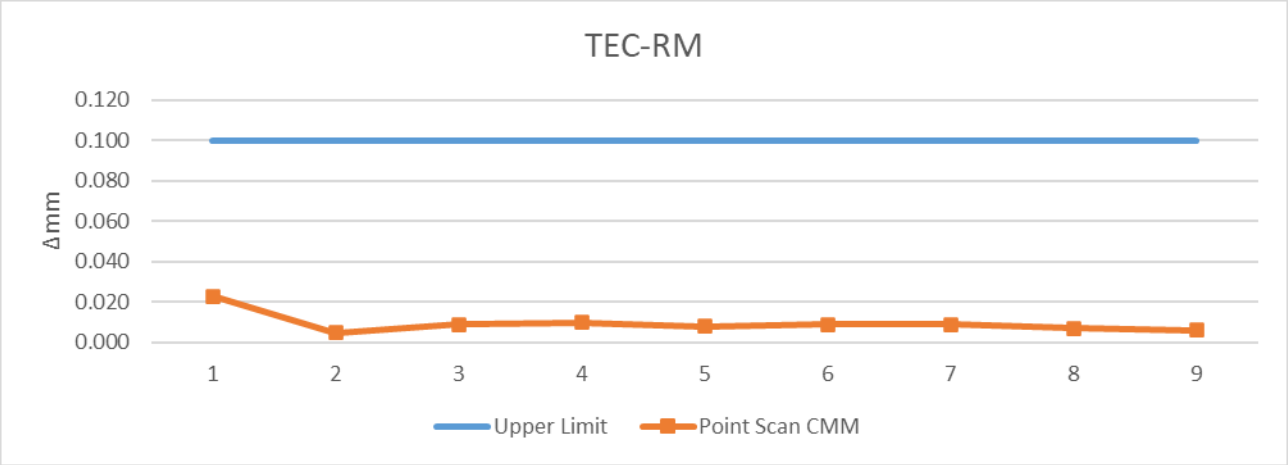

Figure 4-33 – Plot of the measurement results obtained in the repeatability test of Runout RM of the TEC using the point scan CMM, with the blue line as the dimensional tolerance for the runout.

From Table 4-28 and Figure 4-34, one could notice how data is scattered over a range of 0,033 mm across the 50 TEC measured using the CMM. This could be an indication of light vibrations throughout the machining process when cutting the chamfer CM.

Table 4-28 – Table showing the results of the data analysis of the 50 TEC batch measurements taken of the runout RM using the Point-scan CMM.

Dimension	Equipment Used	Machined Tolerance	Unit	Average Measurement	Average Difference	IN/OUT	Range	Standard Deviation	AQL	CPk	Acceptable/ Unacceptable
RM	CMM	0.100	mm	0.014	0.086	IN	0.033	0.006	15.088	5.029	Acceptable

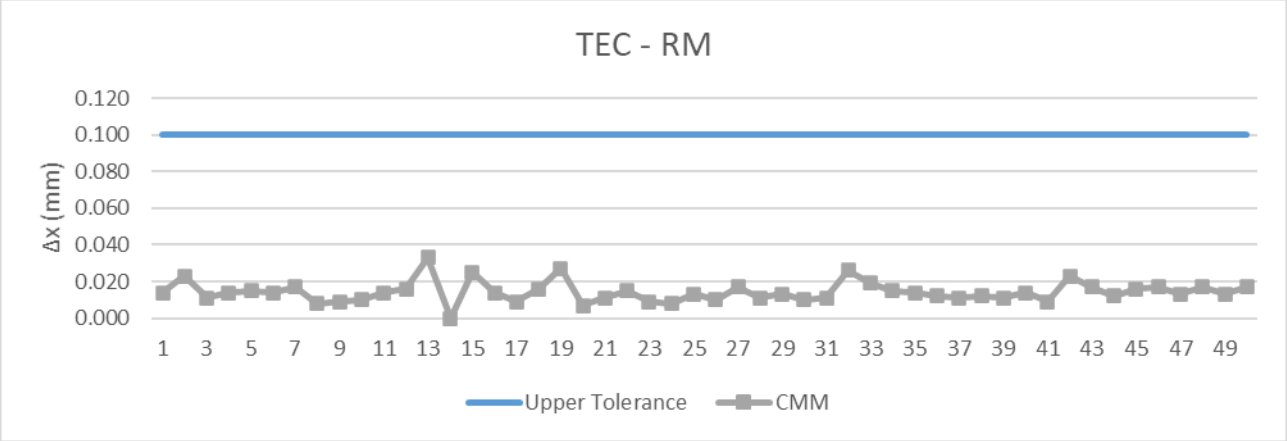

Figure 4-34 – Plot of the geometric tolerance RM (runout on the surface CM with DS as datum) measurement results obtained using the CMM during the TEC-50 batch run, with the blue line as the dimensional tolerance of the runout.

4.5.3. Runout RS

Runout RS is on the face of the flat surface used to measure the flatness of the endcap using diameter DS as the datum, as illustrated in Figure 3-1. For the repeatability study, it is noticeable that there is some movement of the runout RS (Figure 4-35). Furthermore, it is also noticeable that the first measurement of RS is outside the tolerance band, which could be an internal calibration issue on the first measurement. Furthermore, the measurement RS is also not meeting the CP_k specification set at 1,33. This raises a fair number of questions about the capability of the CMM to measure this specific runout.

Table 4-29 – Table showing the results of the data analysis of the 9 measurements taken of the runout RS during the repeatability test using the Point-scan CMM, Line-scan CMM and the Multi-sensor CMM.

Position Name	Equipment Used	Tolerance	Unit	Average Measrement	Average Difference	IN/OUT	Range	Standard Deviation	AQL	CPk	Acceptable/ Unacceptable
RS	Point Scan CMM	0.020	mm	0.008	0.005	IN	0.018	0.005	2.91	0.77	Unacceptable
	Line Scan CMM			0.026	0.000	IN	0.001	0.000	42.02	-4.55	Unacceptable
	Multi-Sensor CMM			0.012	0.000	IN	0.001	0.000	43.38	6.14	Acceptable

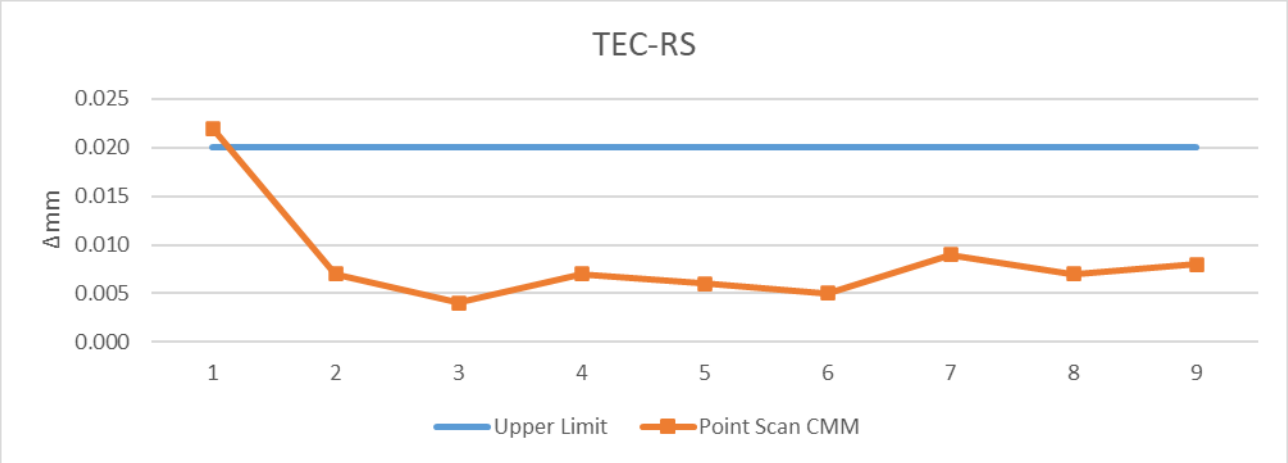

Figure 4-35 – Plot of the measurement results obtained in the repeatability test of Runout RS of the TEC using the point scan CMM, with the blue line as the dimensional tolerance for the runout, showing one measurement not meeting specification.

Figure 4-36 is a plot of the measurement results obtained from measuring runout RS of the 50-TEC batch using the CMM. Looking at this figure, one could see that the data is fairly scattered across the entire tolerance band, and Table 4-30 confirms this with a range of 0,023 mm, indicating that there could have been some vibrations when machining the face of the step. Furthermore, the TEC-50 batch is also failing the CP_k value with a value of 0,721, confirming the inconsistency in the measurement seen in Figure 4-36. However, there was already some questions regarding the point-scan CMM's capability in measuring the runout RS due to the inconsistency recorded in the repeatability study.

Table 4-30 – Table showing the results of the data analysis of the 50 TEC batch measurements taken of the runout RM using the Point-scan CMM.

Dimension	Equipment Used	Machined Tolerance	Unit	Average Measurement	Average Difference	IN/OUT	Range	Standard Deviation	AQL	CPk	Acceptable/ Unacceptable
RS	CMM	0.020	mm	0.009	0.011	IN	0.023	0.005	2.162	0.721	Unacceptable

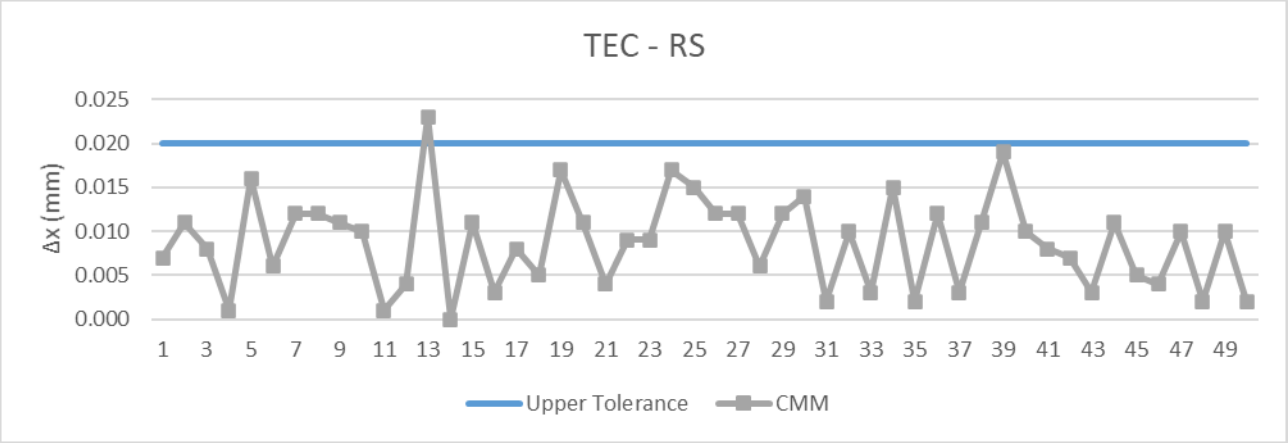

Figure 4-36 – Plot of the geometric tolerance RM (runout on the surface CM with DS as datum) measurement results obtained using the CMM during the TEC-50 batch run, with the blue line as the dimensional tolerance of the runout, with one endcap (TEC-13) not meeting specification.

4.5.4. Runout RL

Runout RL is the runout on the diameter DL with DS as its datum, as shown in Figure 3-1. From the repeatability study analysis presented in Figure 4-37 and Table 4-31, it is fair to say that the CMM could measure the runout RL with a fair amount of confidence, with a standard deviation of 17µm and a CP_k of 5,23.

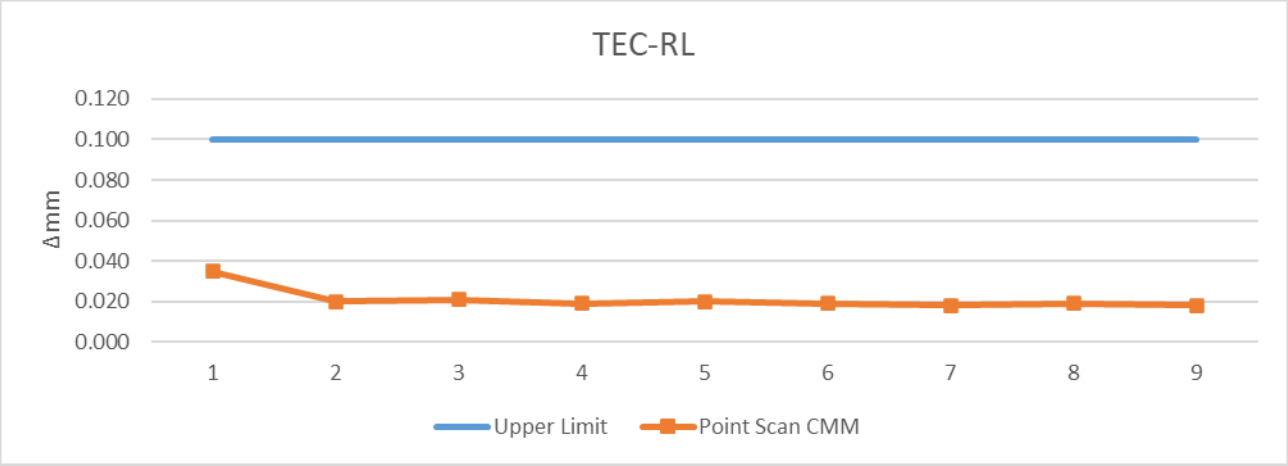

Figure 4-37 – Plot of the measurement results obtained in the repeatability test of Runout RL of the TEC using the point scan CMM, with the blue line as the dimensional tolerance for the runout, showing one measurement not meeting specification.

Table 4-31 – Table showing the results of the data analysis of the 9 measurements taken of the runout RL during repeatability test using the Point-scan CMM, Line-scan CMM and the Multi-sensor CMM.

Position Name	Equipment Used	Tolerance	Unit	Average Measrement	Average Difference	IN/OUT	Range	Standard Deviation	AQL	CPk	Acceptable/ Unacceptable
RL	Point Scan CMM	0.100	mm	0.021	0.005	IN	0.017	0.005	18.81	5.23	Acceptable
	Line Scan CMM			0.017	0.001	IN	0.002	0.001	198.40	55.08	Acceptable
	Multi-Sensor CMM			0.004	0.001	IN	0.002	0.001	180.99	58.45	Acceptable

When looking at the results obtained from the batch measurements (Figure 4-38 and Table 4-32) it is again noticeable how scattered the results are across the tolerance band, with three endcaps not meeting specification and a range almost double the tolerance band.

Table 4-32 – Table showing the results of the data analysis of the 50 TEC batch measurements taken of the runout RL using the Point-scan CMM, showing that the CMM does not comply with the acceptance criteria of AQL and CP_k.

Dimension	Equipment Used	Machined Tolerance	Unit	Average Measurement	Average Difference	IN/OUT	Range	Standard Deviation	AQL	CPk	Acceptable/ Unacceptable
RL	CMM	0.100	mm	0.054	0.046	IN	0.180	0.028	1.670	0.557	Unacceptable

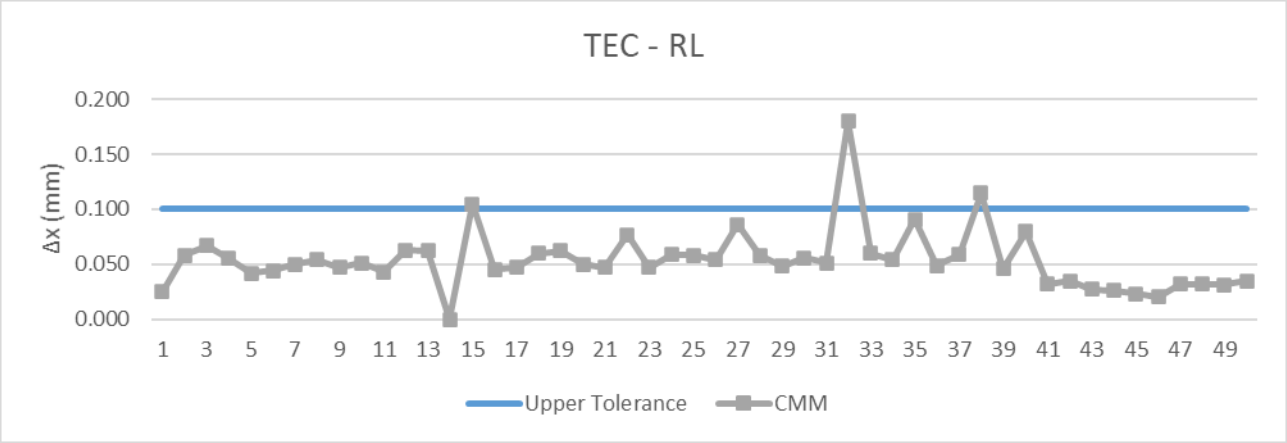

Figure 4-38 – Plot of the geometric tolerance RM (runout on the surface CM with DS as datum) measurement results obtained using the CMM during the TEC-50 batch run, with the blue line as the dimensional tolerance of the runout, with 3 endcaps (TEC-15, TEC-32 and TEC-37) not meeting specification.

From Figure 4-36 and Figure 4-38 it is clear that there a low level of repeatability in the runout measurements for RS and RL using the CMM. The reason for these inconsistent runouts might be due to several factors, but the most probable one is the clocking of the collet chuck. If the machine is not properly clocked before the machining starts, the part might start experiencing vibrations during the machining sequence. Furthermore, an additional reason for the inconsistency in the runouts could also be the amount of stock material inside the bar-feeder and how the material is controlled at the bar-feeder end during the machining operations. In the case of this machining, it could have

been both, as there were some problems with the collet chuck during the installation of the chuck, and because the material was not properly secured during the machining operations.

However, there the question remains on the validity of using a CMM to measure the runout of a component, as equipment such as the Zeiss Rondcom (Figure 4-39) is typically used to test the runout of components. The following is recommended when the machining is done again:

- Secure the stock material using a pipe/tube at the bar-feeder end of the machine, so that the stock material would not be able to generate an extensive amount of vibration on the endcap when it rotates.
- Use an additional machine to verify the runout measurements of the CMM.

Figure 4-39 – Illustration of the Zeiss Rondcom.

5. DISCUSSION

After completing the data analysis on the batch measurements of the TEC, using the three-rule criteria presented in Subsection 3.4.3, it was evident from Table 5-1, that 13 of the 30 dimensions measured (38%) complied with the acceptance criteria, 15 out of the 30 dimensions failed (44%) to comply with the criteria and 6 dimensions were not measured (18%).

Table 5-1 – Table showing the values of the average measurement difference of the dimensional size to the machined value of the endcap, measurement, measurement range, standard deviation, AQL test and the CP_k-values obtained from the production run of the 50-TEC, showing that 44% of the measurements did not comply with the acceptance criteria set, 38% complied with the acceptance criteria and 18% were not measured.

Top-Endcaps Measurement Results Summary											
Dimension	Equipment Used	Machined Tolerance	Unit	Average Measurement	Average Difference	IN/OUT	Range	Standard Deviation	AQL	CPk	Acceptable/ Unacceptable
L1	CMM	0.100	mm		0.006	IN	0.324	0.046	2.028	0.676	Unacceptable
	Profile Projector	-0.100			-0.003	IN	0.117	0.029	3.375	1.125	Unacceptable
L2	CMM	0.050	mm		0.019	IN	0.025	0.006	5.104	1.701	Acceptable
	Profile Projector	-0.050			0.006	IN	0.043	0.010	4.239	1.413	Acceptable
L3	CMM	0.050	mm		0.076	OUT	0.119	0.022	-1.188	-0.396	Unacceptable
	Profile Projector	-0.050			0.079	OUT	0.049	0.011	-2.607	-0.869	Unacceptable
LM	CMM	0.050	mm		-0.015	IN	0.029	0.007	5.404	1.801	Acceptable
	Profile Projector	-0.050			-0.048	IN	0.036	0.009	0.236	0.079	Unacceptable
DC	CMM	0.050	mm		-0.040	IN	0.030	0.008	1.311	0.437	Unacceptable
	Profile Projector	-0.050			-0.046	IN	0.087	0.016	0.261	0.087	Unacceptable
DS	CMM	0.025	mm		0.002	IN	0.034	0.010	2.242	0.747	Unacceptable
	Profile Projector	-0.025			-0.002	IN	0.020	0.005	4.792	1.597	Acceptable
DT	CMM	0.100	mm		0.005	IN	0.069	0.009	10.427	3.476	Acceptable
	Profile Projector	-0.100			-0.010	IN	0.027	0.005	16.385	5.462	Acceptable
DL	CMM	0.100	mm		-0.014	IN	0.047	0.010	8.314	2.771	Acceptable
	Profile Projector	-0.100			0.018	IN	0.020	0.004	18.696	6.232	Acceptable
RT1	CMM	0.100	mm								
	Profile Projector	-0.100		0.500	0.000	IN	0.000	0.000			Acceptable
RT2	CMM	0.100	mm								
	Profile Projector	-0.100		0.462	-0.038	IN	0.040	0.012	9.137	1.682	Acceptable
AT	CMM	0.500	Degrees	59.905	-0.095	IN	1.348	0.290	1.395	0.465	Unacceptable
	Profile Projector	-0.500		59.956	-0.044	IN	0.683	0.148	3.070	1.023	Unacceptable
AE	CMM	0.500	Degrees	30.165	0.165	IN	1.010	0.189	1.771	0.590	Unacceptable
	Profile Projector	-0.500		30.271	0.271	IN	0.567	0.099	2.314	0.771	Unacceptable
CM	CMM	0.500	Degrees	45.060	0.060	IN	0.424	0.082	5.347	1.782	Acceptable
	Profile Projector	-0.500		45.145	0.145	IN	0.483	0.109	3.267	1.089	Unacceptable
F	CMM	0.200	mm	0.001	0.199	IN	0.003	0.001	295.504	98.501	Acceptable
	Profile Projector										
RM	CMM	0.100	mm	0.014	0.086	IN	0.033	0.006	15.088	5.029	Acceptable
	Profile Projector										
RS	CMM	0.020	mm	0.009	0.011	IN	0.023	0.005	2.162	0.721	Unacceptable
	Profile Projector										
RL	CMM	0.100	mm	0.054	0.046	IN	0.180	0.028	1.670	0.557	Unacceptable
	Profile Projector										
					IN	26	76%	Acceptable		38%	13
					Out	2	6%	Unacceptable		44%	15
					Not Measured	6	18%	Not Measured		18%	6
					Total	34	100%	Total		100%	34

Keeping the aim of this study in mind, the question is whether the machining process was a success. The aim of the study was as follows:

- To find the best combination of cutting tools to cut the required shape of the endcaps.
- To find the best possible cutting parameters to machine the endcaps with to circumvent galling and

- To measure the resulting dimensions and to calculate the ensuing tolerances by using standard and numerical methods to verify the machining process.

When looking at this purpose, it is fair to say that there were major challenges in the process to fulfil these points completely.

- Focussing first on the six unmeasured dimensions.
    - There were some constraints in the measurement of these dimensions, as the conventional setup did not allow for a dial indicator setup which could have been used to measure the runout of the endcaps after fabrication. A question was also raised regarding the validity of a CMM measuring runout. The dial gauge setup rotates the component around the datum, whereas the CMM moves around the datum of the component while taking the measurements while the component is fixed.
    - For the two radii not measured, the probe selection on the CMM was too big to measure the radii, as the probe diameter was 0,5 mm, compared with the 0,5mm radius that needed to be measured. From the repeatability study results, it was clear that the best machine that could be used to measure these characteristics is a Multi-sensor CMM with a large zooming capability.
- Focussing on 44% of the components not complying with the acceptance criteria set in Chapter 3.
    - One of the dimensions (L3) was machined outside the tolerance band and both measurement techniques confirmed this error. As explained in the previous chapter, the reason for this error might have been due to the modified inserts, as the inserts were ground to satisfy the shape requirement. This could be controlled by the casting insert specially designed for this shape, or by doing a minor adjustment on the program, i.e., by changing the point location on the program with 0,08 mm.
    - For dimension L1 not complying, this could have been due to a human error during the second step of the machining process. As explained, the manufacturing process of the endcaps exists of three steps, namely CNC machining, EWAG precision grinding (a manual process), and the measurement of the endcaps. During this second step of the manufacturing process, the operator could have lost concentration and started grinding the endcaps inaccurately. However, following the trend lines of L1, DS, DL and DT, this could also have been due to tool wear presented in the diameter measurements. If the tool started to wear out the flat surface of the endcap could have been undercut, leading to the change in the length L1.
    - For the angles, the major challenge with the angles was the available measurable size, as shown in Figure 4-25 and Figure 4-28. The measurable length of the angles was around 0,4 mm and 0,6 mm in the x-directions. With the methods used to

measure the angles, the probe was not small enough for the CMM and the zoom setting on the profile projector was also very blurry, making it very difficult to conclude whether there were any abnormalities during the machining process.

In conclusion for this discussion, the one major lesson learnt during the machining process was that if there is little to no confidence in the measurement procedure, the results obtained after a production run do not add any value to the decision needed to be made to improve the machining process.

Furthermore, the cooling of the cutting was not as efficient as one would have hoped, there was still a lot of edge-build-up and excessive cutting temperatures experienced during the machining process. This led to various failures in the consistency of dimensions and surface quality.

Furthermore, in additional tests, the initial cutting speed used to machine the Zry-4 was set at 5000 rpm, but it resulted in coarse shavings being formed during this run and an excessive amount of edge-build-up that was found at the cutting zone. This resulted in surface damages on the endcaps. After reducing the cutting speed to 1000 rpm and 2500 rpm, for roughing and finishing, respectively, and increasing the feed rate from 0,10 mm/rev to 0,12 mm/rev, using the VCMT insert, it was found that the shavings generated were less coarse and that the amount of edge build-up was reduced significantly as the shavings moved away from the cutting zone, resulting in a smoother surface and suggesting that the parameters were optimal for the machining setup used for the project.

The importance of cutting fluid was illustrated in a separate, isolated, incident where there was a loss of coolant incident during the machine set-up. In this incident, the loss of coolant led to the spontaneous ignition of the Zry-4 shavings. The shavings ignited and a bright white flame was seen in the process. Once the coolant had been reactivated, the flame was extinguished and the machining could return to normal, as predicted in the literature study.

The ideal machining parameters were identified after doing various iterations and the parameters presented in Table 3-3. These parameters were then used to machine a batch sample of 50 of the top-endcaps. As mentioned in the literature review, a machining process could consist of only one process or a combination of processes. For this study, it was decided to use a combination of processes to meet the client specification, as there was leftover material at the back of the endcaps coming out of the CMM. In addition to the CNC lathe, it was decided to use the EWAG precision grinder to finish off the part where it was parted from the stock material.

The galling was minimized as well as possible; however, it could have been better if either the effect of HPC or cryogenic cooling could have been tested in the process. As mentioned in the literature

study, these coolant application methods are great for keeping the cutting temperature as low as possible. The cryogenic cooling method has the added advantage of the change in the ductile-to-brittle transition temperature. It is expected that the Zry-4 would have reacted as a brittle material under these extremely low temperatures, eliminating galling completely.

After doing all the measurements of the nuclear fuel rod endcaps (50 TEC), using the conventional measurement equipment, it was found that some dimensions did not meet the acceptance criteria set in Chapter 3, as only 35% of the TEC's dimensions met the acceptance criteria using the PP. After verifying the measurement using the bridge-type CMM, it was found that only 41% of the dimensions of the TEC met the acceptance criteria.

After doing an investigation on the various characteristics not meeting specification, it was found that most of the characteristics failing consistency when using the conventional method could have been due to human error, as the profile projector available to be used for this study was an old Microtecnica machine (Figure 3-14) that was dependant on the experience of the operator, whereas newer machines tend to have mechanisms that assist the operator. After investigating the characteristics that failed to meet the measurement specifications when using the bridge-type CMM, it was found that there was some dimension where the measurement contact area was too small for the 0,5 mm probe and where more advanced optical measurements, such as a Multi-sensory CMM, could have been more advantageous.

After eliminating the measurement errors caused by the machines used, and after analysing the data obtained through the measurement process, the following conclusions were made based on the machining process:

- During the investigation on L3's unacceptable measurements, it was found that there was an error in the calculation of how the lathe was cutting the dimension, leading it to be out of tolerance for both measurements with the PP and CMM.
- When investigating the dimension DC, it is expected that there could have been a property change during the parting process, leading to thermal expansion when machining the dimension DC.
- During the investigation of the failures of dimension DS, the increase in the diameter was explained by tool wear. The reason being that when the focus was given to diameter DL, it was found that a similar occurrence happened at a similar point of the machining process for DL. The reason why it was not picked up during the measurements of DL, was its large tolerance band of ± 0,200 mm for DL in comparison to ± 0,05 mm for DS.
- During the investigation of the chamfer CM, it was found that one of the reasons why it failed consistency, could be due to chip build-up on the edge of the tip. This means that the probability of chips and the amount thereof is more likely at the end of the finishing cut of the

endcap. This could have been rectified by using HPC to remove all the chips from the cutting edge.

- The runout errors experienced on RL and RS could be explained by vibrations experienced during the cutting process. It is visible from the batch test that it is extremely important to keep the stock material as stable as possible, as it has a major effect on the part that is being machined. So, recommendations could be to place the stock material in a tube to ensure that it has a small movement as possible or to use shorter pieces. However, by using shorter pieces, the number of waste increases.

6. CONCLUSION

In conclusion, after doing a review on the single point cutting principles of ductile materials with special reference to Zry-4, it was found that the best way to machine Zry-4 is at low speed, high feed rates and flooded with coolant to prevent ignition. Furthermore, it was also found in the literature study that the best insert that could be used for the machining purposes of Zry-4, is a sharp carbide (TiC) insert with a large positive rake angle. After conducting various machining trails with Zry-4, it became evident that the ISCAR VCMT TiC insert is best suited to machine the endcaps, as it is a sharp carbide insert normally used for aluminium machining with a large positive rake angle.

In conclusion, it is possible to machine Zry-4 nuclear fuel rod endcaps by using conventional machining methods, however as seen in the batch run, there are a lot of constraints when it comes to mass production capability. To ensure that mass production is successful, the following recommendations could be made (it is a combination of research covered in this dissertation and research conducted outside the scope of the dissertation):

- The conventional lathe could be replaced with a Swiss-type machine, this would allow the part to be machined to greater accuracy and exposed to less vibration.
- More in-depth research on the usage of cryogenic cooling, to enable the machining process to operate in the brittle fracture zone of Zry-4. This is expected to increase the dimensional stability of the components and allow quicker machining cycles.
- The improvement of the cutting angle of the insert, or even the investigation of a forming tool (Figure 6-1) that could be used to cut the front dimensions of the parts to closer tolerances.

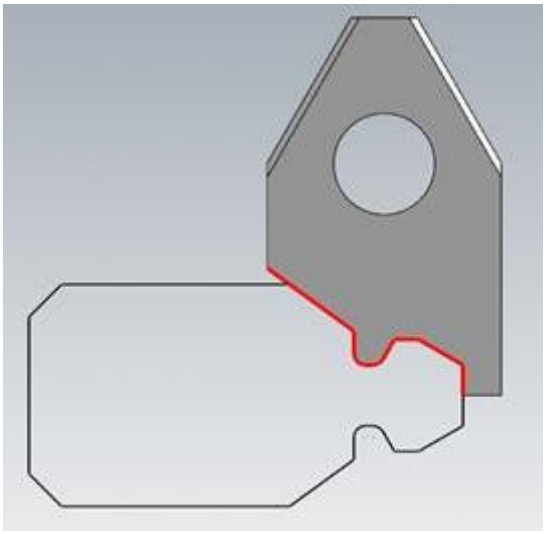

Figure 6-1 – ISCAR's forming tool concept for cutting the front-end dimensions of the bottom endcap of the nuclear fuel rod.

- The measurement capability needs to be improved. This could be done by using a multi-sensor CMM, such as the Zeiss O-Inspect (Figure 6-2). During the repeatability study, this

machine showed excellent levels of repeatability and was able to measure all the characteristics in about 5 minutes.

Figure 6-2 – Illustration of the Zeiss O-Inspect multi-sensor CMM.

- More research and practical work need to be done on roughness testing, as this is the only true measurement that would show if there is any deterioration happening on the cutting edge of the endcap, however, if a forming tool is used, then the focus would need to be on the dimensional tolerance.

7. REFERENCES

Aggarwal, A. & Singh, H. 2005. Optimization of machining techniques — A retrospective and literature review. *Sadhana*. 30(6):699–711.

ASM Aerospace Specification Metals Inc. 2020a. *AISI Type 316 Stainless Steel, annealed sheet*. http://asm.matweb.com/search/SpecificMaterial.asp?bassnum=MQ316A Date of access: 19 Apr. 2017.

ASM Aerospace Specification Metals Inc. 2020b. *Titanium Ti-6Al-4V (Grade 5), STA*. http://asm.matweb.com/search/SpecificMaterial.asp?bassnum=MTP642 Date of access: 02 Feb. 2020.

ASM Handbook Committee & ASM International eds. 1978. *ASM Handbook, Vol. 16, Machining*. 9th ed. Metals Park, Ohio: American Society for Metals.

Cogorno, G.R. 2006. *Geometric Dimensioning and Tolerancing for Mechanical Design*. McGraw-Hill.

Dhananchezian, M., priyan, M.R., Rajashekar, G. & Narayanan, S.S. 2018. Study The Effect Of Cryogenic Cooling On Machinability Characteristics During Turning Duplex Stainless Steel 2205. *Materials Today: Proceedings*. 5(5, Part 2):12062–12070.

Doyle, W.L., Conway, J.B. & Grosse, A.V. 1958. The combustion of zirconium in oxygen. *Journal of Inorganic and Nuclear Chemistry*. 6(2):138–144.

eMachineShop. 2018. GD&T Runout Definition | eMachineShop,com. *eMachineShop*. https://www.emachineshop.com/gdt-runout-definition/ Date of access: 23 Aug. 2018.

Ernest Orlando Lawrence Berkeley National Laboratory. 2017. https://commons.lbl.gov/download/attachments/115671581/Guidelines%20for%20Acceptance%20Sampling%20052217%20Rev.%200.pdf?version=1&modificationDate=1495563090785&api=v2.

Groover, M.P. 2010. *Fundamentals of Modern Manufacturing: Materials, Processes, and Systems*. 4th ed. John Wiley & Sons.

Habrat, W.F., Laskowski, P. & Markopoulos, A.P. 2016. 3. Machining with High-Pressure Cooling. In: J.P. Davim, ed. *Metal Cutting Technologies*. Berlin, Boston: De Gruyter.

Hasib, A., Al-Faruk, A. & Ahmed, N. 2010. Mist Application of Cutting Fluid. *International Journal of Mechanical & Mechatronics Engineering*. 10(04):7.

iscar.com. 2018. *ISCAR Cutting Tools - Metal Working Tools - VCGT-AS*. https://www.iscar.com/eCatalog/MoreInfo.aspx?mapp=IS&fnum=742&app=88 Date of access: 28 Sep. 2018.

iscar.com. 2020a. *ISCAR Cutting Tools - Metal Working Tools - ISO-Turning - Ext. 35° Diamond 93° Approach - SVJCR/L*. https://www.iscar.com/eCatalog/Family.aspx?fnum=423&mapp=IS&app=24&GFSTYP=M Date of access: 02 May 2020.

iscar.com. 2020b. *ISCAR Cutting Tools - Metal Working Tools - Grade : IC20*. https://www.iscar.com/eCatalog/Grade.aspx?grade=IC20&item=5540016&fnum=742&mapp=IS&app=0 Date of access: 22 Aug. 2020.

iscar.com. 2020c. *ISCAR Cutting Tools - Metal Working Tools - Grade : IC6025*. https://www.iscar.com/eCatalog/Grade.aspx?grade=IC6025&item=5568801&fnum=3753&mapp=IS&app=0 Date of access: 22 Aug. 2020.

iscar.com. 2020d. *ISCAR Cutting Tools - Metal Working Tools - VCMT-SM : 5566979 - VCMT 160402-SM*. https://www.iscar.com/eCatalog/Item.aspx?cat=5566979&fnum=869&mapp=IS&GFSTYP=M&srch=1 Date of access: 09 May 2020.

iscar.com. 2020e. *ISCAR Cutting Tools - Metal Working Tools - PENTA 24N-J (full radius) : 6004811 - PENTA 24N100J050*. https://www.iscar.com/eCatalog/Item.aspx?cat=6004811&fnum=2626&mapp=TG&GFSTYP=M&srch=1 Date of access: 02 May 2020.

iscar.com. 2020f. *ISCAR Cutting Tools - Metal Working Tools - TGTR/L-IQ : 2302353 - TGTR 2020-1.4-IQ*. https://www.iscar.com/eCatalog/Item.aspx?cat=2302353&fnum=2274&mapp=TG&GFSTYP=M&srch=1 Date of access: 06 May 2020.

iscar.com. 2020g. *ISCAR Cutting Tools - Metal Working Tools - TAG R/L-J/JS : 6004466 - TAG R1.4J-8D*. https://www.iscar.com/eCatalog/Item.aspx?cat=6004466&fnum=2394&mapp=TG&GFSTYP=M&srch=1 Date of access: 06 May 2020.

iscar.com. 2020h. *ISCAR Cutting Tools - Metal Working Tools - DGTR/L-B/BC-D : 2301385 - DGTL 20B-1.4D30*. https://www.iscar.com/eCatalog/Item.aspx?cat=2301385&fnum=557&mapp=TG&GFSTYP=M&srch=1 Date of access: 09 May 2020.

iscar.com. 2020i. *ISCAR Cutting Tools - Metal Working Tools - DGR/L-J/JS : 6002745 - DGL 1400JS-15D*. https://www.iscar.com/eCatalog/item.aspx?cat=6002745&fnum=2257&mapp=TG&app=0&GFSTYP=M Date of access: 09 May 2020.

ISO 2859-1. 1999. https://www.iso.org/standard/1141.html.

ISO 3951-1. 2013. https://www.iso.org/obp/ui/#iso:std:iso:3951:-1:ed-2:v2:en Date of access: 23 Nov. 2018.

ISO 3951-2. 2006. https://www.iso.org/cms/render/live/en/sites/isoorg/contents/data/standard/03/92/39293.html Date of access: 06 Apr. 2021.

Jadhav, Mr.S.R. 2019. Cryogenic Machining: A Sustainable Solution. *International Journal for Research in Applied Science and Engineering Technology*. 7(12):465–468.

Jayal, A.D. & Balaji, A.K. 2009. Effects of cutting fluid application on tool wear in machining: Interactions with tool-coatings and tool surface features. *Wear*. 267(9):1723–1730.

Kalpakjian, S. & Schmid, S. 2006. *Manufacturing, Engineering and Technology*. 6th Edition in SI Units ed. Pearson.

Marguglio, B.W. 1977. *Quality Systems in the Nuclear Industry (and in Other High Technology Industries)*. ASTM International.

matweb.com. 2017a. *Zircaloy-4 Zirconium Alloy*. http://www.matweb.com/search/DataSheet.aspx?MatGUID=e36a9590eb5945de94d89a35097b7faa Date of access: 19 Apr. 2017.

matweb.com. 2017b. *Aluminum 6005-T1*. http://www.matweb.com/search/DataSheet.aspx?MatGUID=5549c15257814a918aaa4fb2edfa70a7 Date of access: 23 Jun. 2017.

Mitutoyo Corp. 2018. *Quickmike Series 293-IP-54 ABSOLUTE Digimatic Micrometers*. https://ecatalog.mitutoyo.com/Quickmike-Series-293-IP-54-ABSOLUTE-Digimatic-Micrometers-C1088.aspx Date of access: 09 May 2018.

Muntean, A. & Inţă, M. 2013. Optimization of Cutting Parameters for Special Alloys -- Zircaloy 2. *Academic Journal of Manufacturing Engineering*. 11(2):93–98.

Naves, V.T.G., Da Silva, M.B. & Da Silva, F.J. 2013. Evaluation of the effect of application of cutting fluid at high pressure on tool wear during turning operation of AISI 316 austenitic stainless steel. *Wear*. 302(1):1201–1208.

Nielsen, M. 2018. *Cp, Cpk, Cm, Cmk, control limits*. *Statistical Process Control*. http://www.statisticalprocesscontrol.info/glossary.html#Cm Date of access: 28 Aug. 2018.

NRC. 2001. *ML011870499 - Fire Protection Evaluation of the Phenomena of a Zirconium Fire*. https://www.nrc.gov/docs/ML0118/ML011870499.pdf Date of access: 23 Jul. 2020.

Parisot, J.-F. & France eds. 2009. *Nuclear fuels*. (Den monographs). Paris: Éditions le Moniteur : CEA.

Podgornik, B. & Jerina, J. 2012. Surface topography effect on galling resistance of coated and uncoated tool steel. *Surface and Coatings Technology*. 206(11–12):2792–2800.

QualityInspection.org. 2018. *What is the AQL (Acceptance Quality Limit) in QC Inspections? QualityInspection.org*. https://qualityinspection.org/what-is-the-aql/ Date of access: 23 Mar. 2019.

Reid, J. 2011. *Zirconium Machining & Forming Operations*. https://www.atimetals.com/Products/Documents/datasheets/zirconium/alloy/zirconium-machining-forming-operations.pdf Date of access: 07 May 2018.

Reid, J. 2014. *Zirconium Alloys*. https://www.atimetals.com/Products/Documents/datasheets/zirconium/alloy/Zr_nuke_waste_disposal_v2.pdf.

“Runout”. 2014. *GD&T Basics*. https://www.gdandtbasics.com/runout/ Date of access: 23 Aug. 2018.

Schemel, J.H. 1977. *ASTM Manual on Zirconium and Hafnium*. ASTM International.

Shum, M.A. & MachiningCloud Inc. 2016a. *Introduction to Selecting Turning Tools*. *Download Courses*. https://www.machiningcloud.com/download-courses/.

Shum, M.A. & MachiningCloud Inc. 2016b. *Introduction to Turning Tools and Their Application*. *Download Courses*. https://www.machiningcloud.com/download-courses/.

da Silva, R.B., Machado, Á.R., Ezugwu, E.O., Bonney, J. & Sales, W.F. 2013. Tool life and wear mechanisms in high-speed machining of Ti–6Al–4V alloy with PCD tools under various coolant pressures. *Journal of Materials Processing Technology*. 213(8):1459–1464.

Stefánsson, T. 2014. Application of Cryogenic Coolants in Machining Processes. Stockholm: Royal Institute of Technology (KTH).

APPENDIX A. DIMENSIONAL DRAWING OF THE TOP-ENDCAP

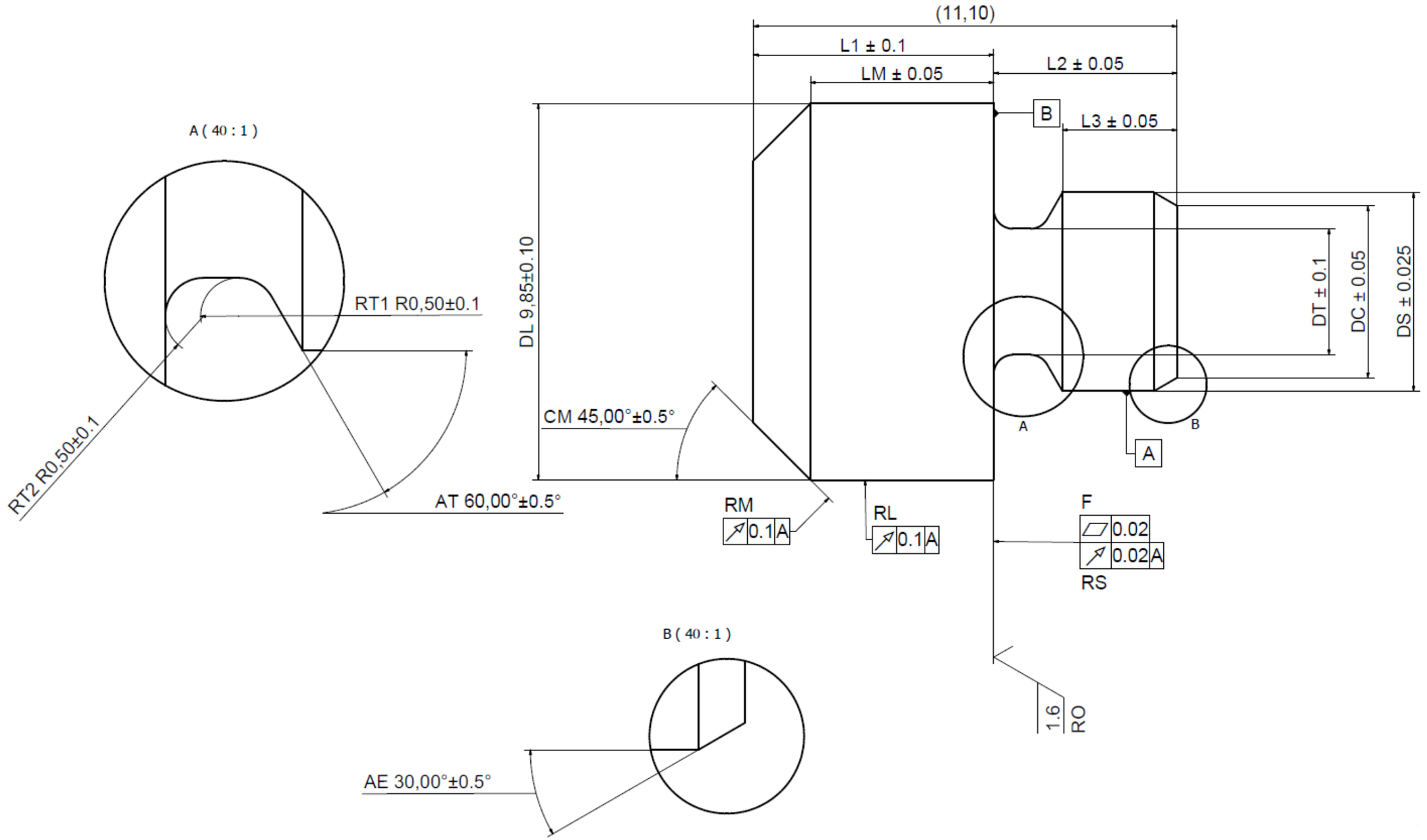

Figure 7-1 – Side view dimensional drawing of the TEC (Not to Scale)

APPENDIX B. MEASUREMENT PROCEDURE FOR THE MEASUREMENT OF TOP NUCLEAR FUEL ROD ENDCAPS USING A COMBINATION OF DIGITAL MICROMETRE AND PROFILE PROJECTOR

The following steps were followed to get the best possible results from measuring the top nuclear fuel rod endcaps using the profile projector:

1. Zero the digital micrometre.
2. Measure the large diameter (DL) with the digital micrometre and record it to the data capture program
3. Zero the digital micrometre.

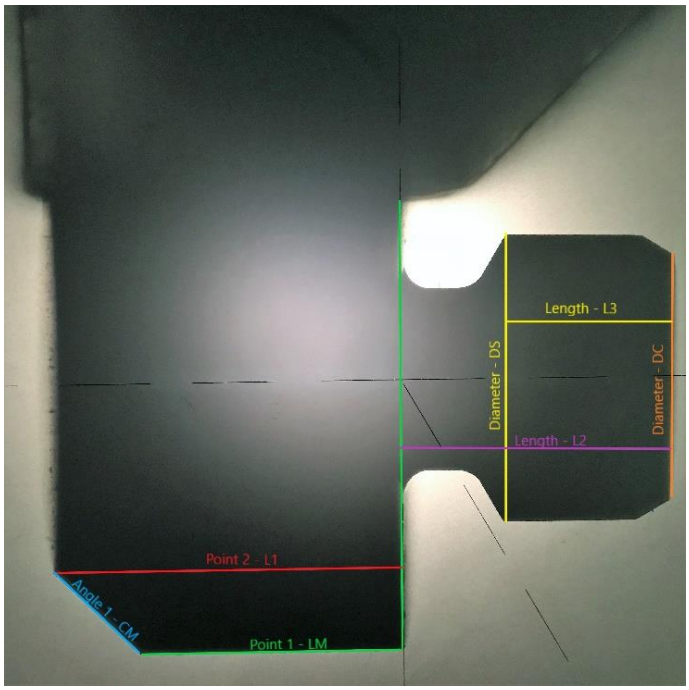

Figure 7-2 – A superimposed side view image of the dimensional layout of the TEC using the 25-magnification lens on the Titanus PP.

4. Ensure that the lens of the PP is on the 25-magnification lens.
5. Place the component on to the v-block on the bed of the PP table.
6. Ensure that the component is in focus, by moving the bed closer or further from the lens.
7. Ensure that the component is properly referenced and that the x, y and angle are on zero before starting to measure on the PP.
8. Measure the length of the chamfer's starting point (LM) by moving the

component to the right-hand side until the vertical line of the display and the point intersects. The movement is presented in Figure 7-2 as the red line. Do not clear the results yet.

9. From LM, move the part towards the end of the component until the horizontal line intercepts the end of the component, as shown by the red line in Figure 7-2. Record the x-value to the data capture program, and then clear the display of the PP.
10. From LM, move the component so that the origin point of the PP display is on the CM (blue line on Figure 7-2). Turn the knob in a clockwise direction until the vertical line and the chamfer line are “one”. Then use the angle Vernier scale on the side of the PP to get the result of the chamfer.
11. After the chamfer measurement, ensure that the angle gauge is zeroed before taking the next measurements.
12. From CM, move the component so that the horizontal line is at the bottom corner of DC (the bottom of the orange line - Figure 7-2), and the vertical line is on the right-hand side of the component. Ensure that the digital readout is also zeroed after the position set.
13. Measure DC (top of the orange line - Figure 7-2) and record the size in the data capture program.
14. From DC, move the component so that the horizontal line and the top point of the yellow vertical line are touching. Zero the digital readout and measure the diameter DS. Record the size of the data capturing program.
15. The next characteristic to be measured is the length L3. Bring the vertical line to the orange line until they are one, zero the digital readout of the PP. From there, move the component until the vertical line intersects the second angle point – the yellow line, Figure 7-2. Take the y-reading and record it to the data capture program.
16. From L3 move the purple line, Figure 7-2, towards the initial starting point of the component. Record the size as L2 and record it to the data capture program.
17. Press the Turret button on the right side of the lenses to select the 50-magnification lens.
18. Move the origin point of the PP display until it is on the yellow line (AE), Figure 7-3. Turn the angle gauge knob clockwise until the horizontal line and the yellow line (AE) are parallel to each other. Record the angle using the angle Vernier scale on the left-hand side of the PP display. Record it to the data

capturing program and zero the angle scale once finished.

19. From AE, move the component until the horizontal line and the bottom blue line, Figure 7-3, are one. Zero the digital readout and measure the diameter DT. Once finished with the measurement, record it to the data capturing program. Move the display origin to the green line (AE), and measure the angle of AE by Turing the angle gauge knob clockwise until the horizontal line and the green line is one. Record the measurement.

Figure 7-3-A superimposed image of the TEC indicating the dimensional positions of DT (blue line), AE (yellow line) and AT (green line), using the 50-magnification lens on the PP

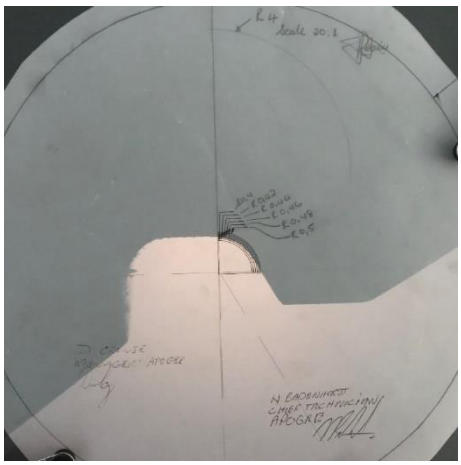

Figure 7-4 – Image of the radius measurement process, using a radius overlay chart on the PP at a magnification of 50

20. Place the overlay chart on the PP Display. Move the part in such a way that the starting point of the radius on the chart, is at the starting point of the radius of the part. Move the component up and down until one of the lines on the chart is on the radius of the part. As illustrated in Figure 7-4. Record the size of the radius. Do this for both RT1 and RT2.

APPENDIX C. TOP-ENDCAP REPEATABILITY STUDY

Table XLVII – Measurement results obtained from measuring one random TEC 9 times using various measurement equipment

Position Name	Method of Inspection	Limits Upper Limit	Limits Lower Limit	Unit	1	2	3	4	5	6	7	8	9	Average Difference	IN/OUT	Range	Measurement Standard Deviation	Q_min	CPk	Acceptable/ Unacceptable
L1	Point Scan CMM	0.100		mm	0.075	0.053	0.057	0.053	0.052	0.057	0.053	0.053	0.053	0.056	IN	0.023	0.007	6.381	2.127	Acceptable
	Line Scan CMM				0.047	0.047	0.047	0.047	0.047	0.048	0.047	0.047	0.047	0.047	IN	0.001	0.000	154.532	51.511	Acceptable
	Multi-Sensor CMM		-0.100		0.053	0.053	0.053	0.053	0.052	0.053	0.053	0.052	0.052	0.053	IN	0.000	0.000	580.474	193.491	Acceptable
	Optic Measuring Machine				0.060	0.065	0.057	0.062	0.070	0.068	0.065	0.066	0.062	0.064	IN	0.013	0.004	9.091	3.030	Acceptable
	Profile Projector				0.048	0.042	0.053	0.038	0.032	0.057	0.052	0.042	0.049	0.046	IN	0.025	0.008	7.182	2.394	Acceptable
L2	Point Scan CMM	0.050		mm	-0.025	-0.015	-0.016	-0.016	-0.016	-0.017	-0.016	-0.017	-0.017	-0.017	IN	0.010	0.003	11.625	3.875	Acceptable
	Line Scan CMM				-0.022	-0.022	-0.022	-0.022	-0.022	-0.022	-0.022	-0.022	-0.022	-0.022	IN	0.001	0.000	165.326	55.109	Acceptable
	Multi-Sensor CMM		-0.050		-0.021	-0.021	-0.021	-0.021	-0.021	-0.021	-0.021	-0.021	-0.021	-0.021	IN	0.000	0.000	270.432	90.144	Acceptable
	Optic Measuring Machine				-0.029	-0.031	-0.025	-0.031	-0.033	-0.032	-0.029	-0.031	-0.023	-0.029	IN	0.010	0.003	6.379	2.126	Acceptable
	Profile Projector				-0.034	-0.015	-0.005	-0.005	-0.027	-0.018	-0.022	-0.035	-0.029	-0.021	IN	0.030	0.011	2.710	0.903	Unacceptable
L3	Point Scan CMM	0.050		mm	-0.008	-0.008	-0.002	-0.001	-0.005	-0.002	0.001	-0.004	-0.005	-0.004	IN	0.009	0.003	15.953	5.318	Acceptable
	Line Scan CMM				0.012	0.012	0.012	0.012	0.012	0.012	0.013	0.013	0.013	0.012	IN	0.001	0.000	107.887	35.962	Acceptable
	Multi-Sensor CMM		-0.050		0.023	0.023	0.022	0.023	0.023	0.023	0.023	0.022	0.023	0.023	IN	0.001	0.000	101.565	33.855	Acceptable
	Optic Measuring Machine				0.025	0.026	0.027	0.026	0.024	0.029	0.030	0.028	0.024	0.027	IN	0.006	0.002	13.075	4.358	Acceptable
	Profile Projector				0.002	0.010	0.018	0.011	0.011	0.017	0.014	0.016	0.005	0.012	IN	0.016	0.005	7.536	2.512	Acceptable
F	Point Scan CMM	0.200		mm	0.005	0.000	0.000	0.001	0.000	0.000	0.000	0.001	0.001	0.002	IN	0.005	0.002	130.22	43.565	Acceptable
	Line Scan CMM				0.013	0.013	0.013	0.013	0.013	0.013	0.012	0.012	0.012	0.000	IN	0.000	0.000	1730.99	541.266	Acceptable
	Multi-Sensor CMM				0.009	0.008	0.008	0.009	0.008	0.009	0.008	0.008	0.008	0.000	IN	0.000	0.000	2605.06	831.981	Acceptable
LM	Point Scan CMM	0.050		mm	0.047	0.022	0.026	0.021	0.020	0.027	0.021	0.022	0.022	0.025	IN	0.027	0.008	3.094	1.031	Unacceptable
	Line Scan CMM				0.011	0.011	0.011	0.011	0.010	0.011	0.011	0.011	0.012	0.011	IN	0.002	0.000	79.112	26.371	Acceptable
	Multi-Sensor CMM		-0.050		0.005	0.006	0.006	0.006	0.006	0.006	0.006	0.005	0.006	0.006	IN	0.001	0.000	219.773	73.258	Acceptable
	Optic Measuring Machine				0.017	0.019	0.015	0.020	0.023	0.026	0.021	0.021	0.016	0.020	IN	0.011	0.003	9.078	3.026	Acceptable
	Profile Projector				0.025	0.004	0.031	0.004	-0.003	0.006	0.002	-0.018	0.000	0.006	IN	0.049	0.014	3.224	1.075	Unacceptable
DC	Point Scan CMM	0.050		mm	-0.012	-0.027	-0.024	-0.024	-0.023	-0.024	-0.023	-0.023	-0.022	-0.022	IN	0.015	0.004	7.031	2.344	Acceptable
	Line Scan CMM				-0.010	-0.010	-0.010	-0.010	-0.010	-0.011	-0.011	-0.011	-0.011	-0.011	IN	0.002	0.001	73.065	24.355	Acceptable
	Multi-Sensor CMM		-0.050		-0.028	-0.028	-0.028	-0.028	-0.029	-0.029	-0.028	-0.028	-0.028	-0.028	IN	0.001	0.000	83.323	27.774	Acceptable
	Optic Measuring Machine				-0.028	-0.028	-0.028	-0.028	-0.029	-0.029	-0.028	-0.028	-0.028	-0.028	IN	0.001	0.000	83.323	27.774	Acceptable
	Profile Projector				-0.145	-0.147	-0.166	-0.129	-0.135	-0.134	-0.158	-0.145	-0.155	-0.146	OUT	0.037	0.011	-8.377	-2.792	Unacceptable
DS	Point Scan CMM	0.025		mm	-0.002	-0.003	-0.003	-0.003	-0.003	-0.003	-0.003	-0.003	-0.003	-0.003	IN	0.001	0.000	70.357	23.452	Acceptable
	Line Scan CMM				-0.001	-0.001	-0.001	-0.001	-0.002	-0.002	-0.002	-0.001	-0.001	-0.001	IN	0.000	0.000	237.359	79.120	Acceptable
	Multi-Sensor CMM		-0.025		0.000	0.000	0.000	0.000	0.000	0.000	0.000	0.000	0.000	0.000	IN	0.000	0.000	828.674	276.225	Acceptable
	Optic Measuring Machine				-0.002	-0.002	-0.002	-0.002	-0.003	-0.001	-0.003	-0.003	-0.002	-0.002	IN	0.002	0.001	41.214	13.738	Acceptable
	Profile Projector				-0.014	0.008	0.006	-0.003	0.010	0.016	0.006	0.005	0.003	0.004	IN	0.030	0.008	2.605	0.868	Unacceptable
DT	Point Scan CMM	0.100		mm	-0.005	-0.006	-0.005	-0.005	-0.006	-0.005	-0.006	-0.007	-0.006	-0.006	IN	0.002	0.001	141.500	47.167	Acceptable
	Line Scan CMM				-0.012	-0.012	-0.012	-0.012	-0.012	-0.012	-0.012	-0.013	-0.013	-0.012	IN	0.001	0.000	282.289	94.096	Acceptable
	Optic Measuring Machine		-0.100		-0.016	-0.017	-0.015	-0.014	-0.016	-0.018	-0.015	-0.017	-0.017	-0.016	IN	0.004	0.001	68.674	22.891	Acceptable
	Profile Projector				-0.009	-0.009	-0.006	-0.005	-0.005	-0.005	-0.007	-0.008	-0.007	-0.007	IN	0.004	0.002	60.237	20.079	Acceptable
DL	Point Scan CMM	0.100		mm	-0.027	-0.029	-0.029	-0.029	-0.029	-0.028	-0.029	-0.029	-0.029	-0.029	IN	0.002	0.001	107.000	35.667	Acceptable
	Line Scan CMM				-0.022	-0.021	-0.021	-0.021	-0.020	-0.021	-0.021	-0.021	-0.022	-0.021	IN	0.001	0.000	189.488	63.163	Acceptable
	Multi-Sensor CMM		-0.100		-0.014	-0.014	-0.014	-0.014	-0.014	-0.014	-0.014	-0.014	-0.014	-0.014	IN	0.000	0.000	1784.506	594.835	Acceptable
	Optic Measuring Machine				-0.015	-0.015	-0.015	-0.015	-0.015	-0.015	-0.015	-0.016	-0.016	-0.015	IN	0.001	0.000	236.815	78.938	Acceptable
	Profile Projector				-0.028	-0.009	-0.008	-0.011	-0.005	-0.003	-0.011	-0.016	-0.009	-0.011	IN	0.025	0.007	12.847	4.282	Acceptable
RT1	Multi-Sensor CMM	0.100		mm	-0.089	-0.088	-0.088	-0.089	-0.087	-0.087	-0.087	-0.087	-0.088	-0.088	IN	0.003	0.001	14.451	4.817	Acceptable
	Profile Projector	-0.100			-0.100	-0.080	-0.080	-0.080	-0.080	-0.080	-0.080	-0.080	-0.100	-0.084	IN	0.020	0.008	1.871	0.624	Unacceptable
RT2	Line Scan CMM	0.100		mm	0.090	0.105	0.088	0.083	0.081	0.095	0.107	0.085	0.097	0.092	IN	0.026	0.009	0.890	0.297	Unacceptable
	Multi-Sensor CMM		-0.100		-0.042	-0.034	-0.032	-0.040	-0.045	-0.048	-0.043	-0.060	-0.044	-0.043	IN	0.027	0.008	7.478	2.493	Acceptable
	Profile Projector				-0.100	-0.100	-0.100	-0.080	-0.100	-0.100	-0.080	-0.080	-0.080	-0.091	IN	0.020	0.010	0.894	0.298	Unacceptable
AT	Point Scan CMM	0.500		Degrees	0.102	0.057	0.299	0.436	0.229	0.166	0.446	0.165	0.043	0.216	IN	0.403	0.142	2.000	0.667	Unacceptable
	Line Scan CMM				0.275	0.263	0.256	0.262	0.253	0.249	0.256	0.240	0.257	0.257	IN	0.035	0.009	26.541	8.847	Acceptable
	Multi-Sensor CMM		-0.500		0.259	0.242	0.248	0.267	0.238	0.272	0.259	0.247	0.256	0.254	IN	0.033	0.011	23.297	7.766	Acceptable
	Profile Projector				0.400	0.133	0.267	0.033	0.083	0.333	0.333	0.083	0.050	0.191	IN	0.367	0.134	2.311	0.770	Unacceptable
AE	Point Scan CMM	0.500		Degrees	0.160	0.410	0.360	0.305	0.423	0.452	0.342	0.267	0.323	0.338	IN	0.292	0.084	1.922	0.641	Unacceptable
	Line Scan CMM				-0.337	-0.350	-0.347	-0.348	-0.349	-0.308	-0.328	-0.312	-0.341	-0.335	IN	0.042	0.015	10.834	3.611	Acceptable
	Multi-Sensor CMM		-0.500		-0.010	-0.008	-0.019	-0.016	0.005	0.001	-0.002	-0.016	-0.012	-0.008	IN	0.024	0.008	62.825	20.942	Acceptable
	Profile Projector				0.667	0.067	0.017	0.467	0.067	-0.350	0.150	0.133	0.050	0.141	IN	1.017	0.270	1.328	0.443	Unacceptable
CM	Point Scan CMM	0.500		Degrees	-0.317	0.033	0.052	0.051	0.006	0.051	0.074	0.021	0.043	0.002	IN	0.391	0.114	4.367	1.456	Acceptable
	Line Scan CMM				-0.041	-0.043	-0.039	-0.043	-0.044	-0.044	-0.050	-0.049	-0.038	-0.043	IN	0.012	0.004	116.083	38.694	Acceptable
	Multi-Sensor CMM		-0.500		-0.015	-0.019	-0.009	-0.010	-0.021	-0.026	-0.012	-0.013	-0.016	-0.016	IN	0.017	0.005	91.862	30.621	Acceptable
	Optic Measuring Machine				-0.037	-0.047	-0.010	-0.026	-0.028	-0.033	-0.023	-0.040	0.011	-0.026	IN	0.058	0.017	28.687	9.562	Acceptable
	Profile Projector				-0.083	-0.067	-0.167	-0.083	-0.150	-0.050	0.083	0.067	0.167	-0.031	IN	0.333	0.106	4.415	1.472	Acceptable
RM	Point Scan CMM	0.100		mm	0.023	0.005	0.009	0.010	0.008	0.009	0.009	0.007	0.006	0.005	IN	0.018	0.005	18.974	6.040	Acceptable
	Line Scan CMM				0.014	0.014	0.014	0.013	0.014	0.014	0.013	0.013	0.014	0.000	IN	0.001	0.000	230.701	66.653	Acceptable
	Multi-Sensor CMM				0.007	0.007	0.006	0.006	0.006	0.007	0.007	0.007	0.007	0.000	IN	0.000	0.000	599.118	186.799	Acceptable
RS	Point Scan CMM	0.020		mm	0.022	0.007	0.004	0.007	0.006	0.005	0.009	0.007	0.008	0.005	IN	0.018	0.005	2.913	0.773	Unacceptable
	Line Scan CMM				0.026	0.026	0.027	0.026	0.027	0.027	0.026	0.026	0.027	0.000	IN	0.001	0.000	42.017	-4.547	Unacceptable
	Multi-Sensor CMM				0.012	0.012	0.012	0.012	0.011	0.011	0.011	0.012	0.012	0.000	IN	0.001	0.000	43.378	6.142	Acceptable
RL	Point Scan CMM	0.100		mm	0.035	0.020	0.021	0.019	0.020	0.019	0.018	0.019	0.018	0.005	IN	0.017	0.005	18.807	5.232	Acceptable
	Line Scan CMM				0.017	0.017	0.017	0.016	0.017	0.017	0.017	0.017	0.018	0.001	IN	0.002	0.001	198.398	55.080	Acceptable
	Multi-Sensor CMM				0.005	0.003	0.003	0.003	0.003	0.004	0.003	0.004	0.004	0.001	IN	0.002	0.001	180.987	58.451	Acceptable

APPENDIX D. TOP-ENDCAPS MEASUREMENT RESULTS

Table XL – Measurement results of the 50 batch TEC production run using a CMM and PP (part 1)

Position Name	Method of Inspection	Machining Tolerance Upper Tolerance Lower Tolerence	Unit	1	2	3	4	5	6	7	8	9	10	11	12	13	14	15	16	17	18	19	20	21	22	23	24	25
L1	CMM	0.100	mm	0.271	0.008	0.013	-0.011	0.004	0.001	-0.001	-0.005	-0.006	-0.001	-0.003	0.003	0.003	-0.010	-0.013	-0.005	-0.014	-0.014	-0.018	-0.009	-0.008	-0.022	0.000	-0.012	-0.022
	Profile Projector	-0.100		-0.006	-0.004	0.008	-0.009	0.018	0.004	0.000	-0.020	-0.017	-0.014	0.002	-0.009	0.006	-0.014	-0.020	-0.010	-0.015	-0.024	-0.013	-0.022	-0.015	-0.025	-0.001	-0.031	-0.024
L2	CMM	0.050	mm	0.014	0.011	0.012	0.012	0.012	0.011	0.010	0.019	0.012	0.009	0.014	0.017	0.011	0.024	0.015	0.011	0.018	0.017	0.018	0.016	0.019	0.014	0.023	0.022	0.021
	Profile Projector	-0.050		0.003	0.015	-0.008	0.004	0.002	-0.001	-0.007	0.013	0.003	0.003	0.000	0.017	-0.010	0.003	-0.003	0.001	-0.003	0.006	-0.016	0.004	0.011	0.008	0.013	0.004	0.019
L3	CMM	0.050	mm	0.033	0.049	0.075	0.047	0.142	0.092	0.087	0.063	0.111	0.063	0.095	0.094	0.103	0.077	0.075	0.050	0.076	0.062	0.060	0.086	0.065	0.067	0.064	0.066	0.067
	Profile Projector	-0.050		0.076	0.077	0.072	0.067	0.074	0.072	0.073	0.063	0.065	0.065	0.075	0.071	0.074	0.076	0.072	0.071	0.081	0.073	0.054	0.081	0.062	0.070	0.070	0.067	0.067
LM	CMM	0.050	mm	-0.026	-0.014	-0.008	-0.011	-0.018	-0.012	-0.018	-0.015	-0.012	-0.009	-0.015	-0.014	-0.014	-0.014	-0.017	-0.011	-0.015	-0.010	-0.011	-0.008	-0.011	-0.005	-0.017	-0.009	-0.013
	Profile Projector	-0.050		-0.050	-0.040	-0.053	-0.038	-0.047	-0.041	-0.041	-0.057	-0.032	-0.046	-0.037	-0.042	-0.042	-0.047	-0.058	-0.056	-0.048	-0.055	-0.050	-0.054	-0.050	-0.067	-0.055	-0.049	-0.048
DC	CMM	0.050	mm	-0.026	-0.027	-0.029	-0.030	-0.032	-0.026	-0.030	-0.041	-0.028	-0.028	-0.035	-0.037	-0.031	-0.046	-0.038	-0.036	-0.037	-0.037	-0.034	-0.031	-0.039	-0.032	-0.040	-0.042	-0.042
	Profile Projector	-0.050		-0.037	-0.028	-0.019	-0.028	-0.045	-0.034	-0.018	0.002	-0.037	-0.023	-0.039	-0.031	-0.042	-0.036	-0.028	-0.021	-0.025	-0.041	-0.055	-0.042	-0.052	-0.035	-0.036	-0.032	-0.052
DS	CMM	0.025	mm	-0.013	-0.012	-0.010	-0.009	-0.012	-0.006	-0.005	-0.006	-0.003	-0.005	-0.010	-0.008	-0.006	-0.003	-0.004	-0.003	-0.002	-0.002	0.002	0.003	-0.001	0.002	0.001	0.003	0.003
	Profile Projector	-0.025		-0.006	-0.005	-0.001	-0.011	-0.001	-0.004	0.001	-0.005	0.001	-0.005	-0.014	-0.004	-0.005	0.004	0.003	-0.002	0.003	-0.007	0.001	0.000	0.000	-0.004	-0.009	-0.009	-0.010
DT	CMM	0.100	mm	-0.005	-0.004	0.000	-0.002	0.064	0.002	0.000	0.002	0.002	0.003	0.000	-0.002	-0.002	0.002	0.002	0.002	0.005	0.006	0.006	0.005	0.004	0.005	0.005	0.007	0.005
	Profile Projector	-0.100		-0.011	-0.011	-0.005	-0.011	-0.021	-0.006	-0.007	-0.005	-0.004	-0.016	-0.013	-0.010	-0.011	-0.012	-0.009	-0.005	-0.015	-0.003	-0.004	-0.010	-0.016	-0.008	-0.006	-0.009	-0.006
DL	CMM	0.100	mm	0.003	-0.018	-0.015	-0.022	-0.020	-0.017	-0.015	-0.014	-0.014	-0.019	-0.017	-0.017	-0.013	-0.016	-0.017	-0.015	-0.017	-0.019	-0.012	-0.017	-0.016	-0.019	-0.009	-0.018	-0.023
	Profile Projector	-0.100		0.000	0.010	0.010	0.010	0.010	0.010	0.020	0.010	0.020	0.020	0.010	0.020	0.020	0.020	0.020	0.020	0.020	0.020	0.020	0.020	0.020	0.020	0.020	0.020	0.020
RT1	Profile Projector	0.100	mm	0.500	0.500	0.500	0.500	0.500	0.500	0.500	0.500	0.500	0.500	0.500	0.500	0.500	0.500	0.500	0.500	0.500	0.500	0.500	0.500	0.500	0.500	0.500	0.500	0.500
		-0.100		0.000	0.000	0.000	0.000	0.000	0.000	0.000	0.000	0.000	0.000	0.000	0.000	0.000	0.000	0.000	0.000	0.000	0.000	0.000	0.000	0.000	0.000	0.000	0.000	0.000
RT2	Profile Projector	0.100	mm	0.480	0.480	0.480	0.480	0.460	0.480	0.460	0.460	0.460	0.460	0.460	0.460	0.480	0.460	0.460	0.460	0.460	0.460	0.460	0.480	0.480	0.480	0.440	0.460	0.480
		-0.100		-0.020	-0.020	-0.020	-0.020	-0.040	-0.020	-0.040	-0.040	-0.040	-0.040	-0.040	-0.040	-0.020	-0.040	-0.040	-0.040	-0.040	-0.040	-0.040	-0.020	-0.020	-0.020	-0.060	-0.040	-0.020
AT	CMM	0.500	deg	59.796	59.978	59.835	60.427	60.052	59.941	60.013	59.925	59.997	59.628	59.377	59.459	59.528	60.293	59.975	59.974	59.719	59.751	60.181	60.399	59.706	59.915	60.026	60.152	59.967
				-0.204	-0.022	-0.165	0.427	0.052	-0.059	0.013	-0.075	-0.003	-0.372	-0.623	-0.541	-0.472	0.293	-0.025	-0.026	-0.281	-0.249	0.181	0.399	-0.294	-0.085	0.026	0.152	-0.033
	Profile Projector	-0.500		59.933	59.867	59.650	59.800	60.167	59.850	60.000	59.833	59.900	60.000	60.000	60.000	59.733	60.217	59.833	60.000	60.083	60.000	60.000	59.667	59.867	59.800	60.133	59.700	60.000
				-0.067	-0.133	-0.350	-0.200	0.167	-0.150	0.000	-0.167	-0.100	0.000	0.000	0.000	-0.267	0.217	-0.167	0.000	0.083	0.000	0.000	-0.333	-0.133	-0.200	0.133	-0.300	0.000
AE	CMM	0.500	deg	30.154	29.793	29.916	30.385	30.015	30.097	30.073	30.186	30.040	30.194	30.457	30.163	30.118	30.212	29.848	30.328	29.854	30.230	29.955	30.201	30.190	30.041	30.150	29.925	30.052
				0.154	-0.207	-0.084	0.385	0.015	0.097	0.073	0.186	0.040	0.194	0.457	0.163	0.118	0.212	-0.152	0.328	-0.146	0.230	-0.045	0.201	0.190	0.041	0.150	-0.075	0.052
	Profile Projector	-0.500		30.133	30.200	30.267	30.233	30.333	30.167	30.250	30.167	30.133	30.400	30.333	30.333	30.167	30.250	30.283	30.200	30.333	30.267	30.333	30.417	30.267	30.333	30.267	30.333	29.900
				0.133	0.200	0.267	0.233	0.333	0.167	0.250	0.167	0.133	0.400	0.333	0.333	0.167	0.250	0.283	0.200	0.333	0.267	0.333	0.417	0.267	0.333	0.267	0.333	-0.100
CM	CMM	0.500	deg	45.092	44.961	45.034	45.022	45.029	44.931	44.934	45.026	45.056	45.057	45.111	45.123	45.030	45.084	45.036	45.179	45.117	45.120	45.005	45.026	45.051	45.064	45.165	44.959	45.081
				0.092	-0.039	0.034	0.022	0.029	-0.069	-0.066	0.026	0.056	0.057	0.111	0.123	0.030	0.084	0.036	0.179	0.117	0.120	0.005	0.026	0.051	0.064	0.165	-0.041	0.081
	Profile Projector	-0.500		45.200	45.133	45.267	45.050	45.167	45.000	45.167	45.167	45.000	45.217	45.050	45.200	45.167	45.167	44.850	45.033	45.333	45.167	45.167	45.067	45.000	45.133	45.150	45.167	45.167
				0.200	0.133	0.267	0.050	0.167	0.000	0.167	0.167	0.000	0.217	0.050	0.200	0.167	0.167	-0.150	0.033	0.333	0.167	0.167	0.067	0.000	0.133	0.150	0.167	0.167
F	CMM	0.200	mm	0.001	0.001	0.002	0.000	0.003	0.000	0.000	0.000	0.001	0.001	0.000	0.001	0.000	0.000	0.001	0.000	0.000	0.000	0.000	0.001	0.000	0.001	0.000	0.001	0.000
RM	CMM	0.100	mm	0.014	0.023	0.011	0.014	0.015	0.014	0.017	0.008	0.009	0.010	0.014	0.016	0.033	0.000	0.025	0.014	0.009	0.016	0.027	0.007	0.011	0.015	0.009	0.008	0.013
RS	CMM	0.020	mm	0.007	0.011	0.008	0.001	0.016	0.006	0.012	0.012	0.011	0.010	0.001	0.004	0.023	0.000	0.011	0.003	0.008	0.005	0.017	0.011	0.004	0.009	0.009	0.017	0.015
RL	CMM	0.100	mm	0.025	0.058	0.067	0.055	0.042	0.044	0.050	0.054	0.047	0.051	0.043	0.063	0.062	0.000	0.105	0.045	0.047	0.060	0.062	0.050	0.047	0.077	0.047	0.059	0.058

Table XLI – Measurement results of the 50 batch TEC production run using a CMM and PP (part 2)

Position Name	Method of Inspection	Machining Tolerance Upper Tolerance / Lower Tolerence	Unit	26	27	28	29	30	31	32	33	34	35	36	37	38	39	40	41	42	43	44	45	46	47	48	49	50	Average Difference	IN/OUT	Range	Process Standard Deviation	Q_min	CPk	Acceptable/ Unacceptable
L1	CMM	0.100	mm	-0.009	-0.033	-0.015	-0.010	-0.017	-0.008	-0.024	-0.003	-0.013	-0.001	-0.008	-0.043	-0.019	-0.022	-0.053	0.053	0.046	0.044	0.066	0.065	0.067	0.018	0.045	0.023	0.014	0.006	IN	0.324	0.046	2.028	0.676	Unacceptable
	Profile Projector	-0.100		-0.029	-0.038	-0.003	-0.008	-0.024	-0.013	-0.021	-0.028	-0.013	0.004	-0.005	-0.050	-0.034	0.019	-0.049	0.067	0.035	0.058	0.062	0.062	0.064	0.013	0.051	0.016	-0.014	-0.003	IN	0.117	0.029	3.375	1.125	Unacceptable
L2	CMM	0.050	mm	0.021	0.022	0.023	0.014	0.034	0.012	0.024	0.020	0.025	0.015	0.025	0.030	0.025	0.024	0.026	0.026	0.024	0.024	0.021	0.021	0.026	0.026	0.016	0.024	0.028	0.019	IN	0.025	0.006	5.104	1.701	Acceptable
	Profile Projector	-0.050		0.003	0.019	0.005	0.010	0.021	0.003	0.024	0.006	0.012	-0.004	0.011	0.006	-0.019	0.015	0.020	0.008	0.018	0.017	0.019	-0.015	-0.014	0.018	0.015	0.012	0.006	0.006	IN	0.043	0.010	4.239	1.413	Acceptable
L3	CMM	0.050	mm	0.066	0.075	0.102	0.152	0.069	0.059	0.097	0.062	0.067	0.059	0.071	0.085	0.093	0.062	0.072	0.078	0.069	0.072	0.060	0.072	0.066	0.103	0.066	0.067	0.068	0.076	OUT	0.119	0.022	-1.188	-0.396	Unacceptable
	Profile Projector	-0.050		0.084	0.103	0.087	0.076	0.080	0.088	0.081	0.087	0.079	0.079	0.099	0.098	0.066	0.100	0.093	0.086	0.091	0.091	0.079	0.092	0.085	0.089	0.094	0.077	0.091	0.079	OUT	0.049	0.011	-2.607	-0.869	Unacceptable
LM	CMM	0.050	mm	-0.009	-0.017	-0.010	-0.015	-0.019	-0.006	-0.006	-0.011	-0.017	-0.003	-0.017	-0.012	-0.011	-0.012	-0.010	-0.021	-0.032	-0.025	-0.024	-0.029	-0.031	-0.023	-0.021	-0.017	-0.018	-0.015	IN	0.029	0.007	5.404	1.801	Acceptable
	Profile Projector	-0.050		-0.052	-0.040	-0.047	-0.066	-0.044	-0.046	-0.037	-0.042	-0.049	-0.035	-0.047	-0.050	-0.061	-0.060	-0.042	-0.031	-0.044	-0.036	-0.047	-0.067	-0.046	-0.052	-0.042	-0.064	-0.047	-0.048	IN	0.036	0.009	0.236	0.079	Unacceptable
DC	CMM	0.050	mm	-0.040	-0.041	-0.039	-0.036	-0.053	-0.047	-0.042	-0.042	-0.049	-0.048	-0.054	-0.056	-0.052	-0.041	-0.052	-0.051	-0.041	-0.043	-0.041	-0.042	-0.041	-0.044	-0.040	-0.047	-0.049	-0.040	IN	0.030	0.008	1.311	0.437	Unacceptable
	Profile Projector	-0.050		-0.066	-0.044	-0.050	-0.052	-0.062	-0.063	-0.085	-0.051	-0.063	-0.067	-0.066	-0.062	-0.053	-0.050	-0.058	-0.067	-0.065	-0.063	-0.050	-0.060	-0.054	-0.054	-0.046	-0.053	-0.047	-0.046	IN	0.087	0.016	0.261	0.087	Unacceptable
DS	CMM	0.025	mm	0.003	0.003	0.002	0.004	0.001	-0.001	-0.001	0.000	0.002	0.001	0.002	0.002	0.002	0.018	0.003	0.003	0.021	0.021	0.020	0.020	0.021	0.020	0.021	0.021	0.020	0.002	IN	0.034	0.010	2.242	0.747	Unacceptable
	Profile Projector	-0.025		0.004	-0.001	-0.009	-0.003	-0.002	-0.004	-0.003	-0.012	-0.003	-0.004	-0.002	0.002	0.003	-0.001	-0.006	0.000	-0.002	0.005	0.006	0.003	0.001	0.001	0.005	-0.003	0.005	-0.002	IN	0.020	0.005	4.792	1.597	Acceptable
DT	CMM	0.100	mm	0.005	0.009	0.006	0.005	0.007	-0.001	0.005	0.001	0.003	0.001	0.004	0.005	0.005	0.005	0.005	0.005	0.005	0.004	0.003	0.009	0.008	0.007	-0.001	0.006	0.002	0.005	IN	0.069	0.009	10.427	3.476	Acceptable
	Profile Projector	-0.100		-0.005	-0.004	-0.003	-0.020	-0.010	-0.030	-0.011	-0.010	-0.014	-0.020	-0.011	-0.011	-0.005	-0.011	-0.011	-0.006	-0.006	-0.006	-0.009	-0.006	-0.010	-0.006	-0.022	-0.008	-0.010	-0.010	IN	0.027	0.005	16.385	5.462	Acceptable
DL	CMM	0.100	mm	-0.019	-0.014	-0.015	-0.013	-0.016	-0.021	-0.035	-0.015	-0.019	-0.033	-0.013	-0.028	-0.018	-0.025	-0.039	0.003	0.004	0.003	0.004	0.007	0.008	-0.004	0.003	-0.005	-0.005	-0.014	IN	0.047	0.010	8.314	2.771	Acceptable
	Profile Projector	-0.100		0.020	0.020	0.020	0.020	0.020	0.020	0.020	0.020	0.020	0.020	0.020	0.020	0.020	0.020	0.020	0.020	0.020	0.020	0.020	0.020	0.020	0.020	0.020	0.020	0.020	0.018	IN	0.020	0.004	18.696	6.232	Acceptable
RT1	Profile Projector	0.100	mm	0.500	0.500	0.500	0.500	0.500	0.500	0.500	0.500	0.500	0.500	0.500	0.500	0.500	0.500	0.500	0.500	0.500	0.500	0.500	0.500	0.500	0.500	0.500	0.500	0.500	0.000	IN	0.000	0.000	#DIV/0!	#DIV/0!	Acceptable
		-0.100		0.000	0.000	0.000	0.000	0.000	0.000	0.000	0.000	0.000	0.000	0.000	0.000	0.000	0.000	0.000	0.000	0.000	0.000	0.000	0.000	0.000	0.000	0.000	0.000	0.000							
RT2	Profile Projector	0.100	mm	0.480	0.460	0.460	0.460	0.440	0.440	0.440	0.440	0.460	0.440	0.440	0.460	0.460	0.460	0.460	0.460	0.460	0.460	0.460	0.460	0.460	0.460	0.480	0.460	0.460	-0.038	IN	0.040	0.012	9.137	1.682	Acceptable
		-0.100		-0.020	-0.040	-0.040	-0.040	-0.060	-0.060	-0.060	-0.060	-0.040	-0.060	-0.060	-0.040	-0.040	-0.040	-0.040	-0.040	-0.040	-0.040	-0.040	-0.040	-0.040	-0.040	-0.020	-0.040	-0.040							
AT	CMM	0.500	deg	59.122	60.192	59.559	59.858	59.605	59.799	59.961	59.337	59.949	59.771	60.470	59.640	59.608	60.175	59.645	60.007	60.065	60.156	59.838	60.403	60.008	59.951	59.759	60.080	60.275	-0.095	IN	1.348	0.290	1.395	0.465	Unacceptable
				-0.878	0.192	-0.441	-0.142	-0.395	-0.201	-0.039	-0.663	-0.051	-0.229	0.470	-0.360	-0.392	0.175	-0.355	0.007	0.065	0.156	-0.162	0.403	0.008	-0.049	-0.241	0.080	0.275							
	Profile Projector	-0.500		59.917	60.000	59.933	60.000	59.767	59.833	60.000	60.000	60.100	60.167	60.167	60.000	59.733	60.000	60.000	60.017	60.000	60.117	60.083	59.817	59.917	60.000	60.333	59.750	60.100	-0.044	IN	0.683	0.148	3.070	1.023	Unacceptable
				-0.083	0.000	-0.067	0.000	-0.233	-0.167	0.000	0.000	0.100	0.167	0.167	0.000	-0.267	0.000	0.000	0.017	0.000	0.117	0.083	-0.183	-0.083	0.000	0.333	-0.250	0.100							
AE	CMM	0.500	deg	30.177	30.058	30.235	30.191	30.014	30.288	29.559	30.378	30.240	30.113	30.161	30.375	30.194	30.088	30.338	30.392	30.569	30.191	30.431	30.328	30.260	30.102	30.215	30.278	30.491	0.165	IN	1.010	0.189	1.771	0.590	Unacceptable
				0.177	0.058	0.235	0.191	0.014	0.288	-0.441	0.378	0.240	0.113	0.161	0.375	0.194	0.088	0.338	0.392	0.569	0.191	0.431	0.328	0.260	0.102	0.215	0.278	0.491							
	Profile Projector	-0.500		30.383	30.100	30.367	30.233	30.467	30.283	30.417	30.333	30.283	30.217	30.183	30.283	30.383	30.250	30.333	30.400	30.283	30.233	30.283	30.250	30.300	30.250	30.367	30.133	30.250	0.271	IN	0.567	0.099	2.314	0.771	Unacceptable
				0.383	0.100	0.367	0.233	0.467	0.283	0.417	0.333	0.283	0.217	0.183	0.283	0.383	0.250	0.333	0.400	0.283	0.233	0.283	0.250	0.300	0.250	0.367	0.133	0.250							
CM	CMM	0.500	deg	45.041	45.125	45.127	45.040	45.135	45.070	45.255	45.340	44.985	45.039	44.944	45.140	45.110	44.973	44.975	45.073	45.074	44.997	44.926	44.916	45.057	45.117	45.143	45.061	45.065	0.060	IN	0.424	0.082	5.347	1.782	Acceptable
				0.041	0.125	0.127	0.040	0.135	0.070	0.255	0.340	-0.015	0.039	-0.056	0.140	0.110	-0.027	-0.025	0.073	0.074	-0.003	-0.074	-0.084	0.057	0.117	0.143	0.061	0.065							
	Profile Projector	-0.500		45.083	45.083	45.167	45.167	45.167	45.167	45.267	45.050	45.233	45.233	45.150	45.017	45.167	45.200	45.333	44.917	45.000	45.250	45.333	44.950	45.233	45.100	45.283	45.167	45.333	0.145	IN	0.483	0.109	3.267	1.089	Unacceptable
				0.083	0.083	0.167	0.167	0.167	0.167	0.267	0.050	0.233	0.233	0.150	0.017	0.167	0.200	0.333	-0.083	0.000	0.250	0.333	-0.050	0.233	0.100	0.283	0.167	0.333							
F	CMM	0.200	mm	0.000	0.001	0.001	0.000	0.002	0.000	0.001	0.000	0.000	0.001	0.001	0.001	0.000	0.001	0.000	0.000	0.000	0.001	0.000	0.001	0.001	0.001	0.001	0.000	0.000	0.199	IN	0.003	0.001	295.504	98.501	Acceptable
RM	CMM	0.100	mm	0.010	0.017	0.011	0.013	0.010	0.011	0.026	0.019	0.015	0.014	0.012	0.011	0.012	0.011	0.014	0.009	0.023	0.017	0.012	0.016	0.017	0.013	0.017	0.013	0.017	0.086	IN	0.033	0.006	15.088	5.029	Acceptable
RS	CMM	0.020	mm	0.012	0.012	0.006	0.012	0.014	0.002	0.010	0.003	0.015	0.002	0.012	0.003	0.011	0.019	0.010	0.008	0.007	0.003	0.011	0.005	0.004	0.010	0.002	0.010	0.002	0.011	IN	0.023	0.005	2.162	0.721	Unacceptable
RL	CMM	0.100	mm	0.054	0.086	0.058	0.048	0.056	0.051	0.180	0.060	0.054	0.091	0.049	0.059	0.115	0.046	0.080	0.032	0.035	0.027	0.026	0.023	0.020	0.032	0.032	0.031	0.035	0.046	IN	0.180	0.028	1.670	0.557	Unacceptable